

Augmented Tensor Decomposition with Stochastic Alternating Optimization

¹Chaoqi Yang, ²Cheng Qian, ¹Navjot Singh, ³Cao Xiao, ^{4,5}M Brandon Westover

¹Edgar Solomonik, ¹Jimeng Sun

¹University of Illinois Urbana-Champaign, ²IQVIA, ³Amplitude

⁴Massachusetts General Hospital, ⁵Harvard Medical School

{chaoqi2,navjot2,solomon2,jimeng}@illinois.edu, ²alextoqc@gmail.com

³danica.xiao@amplitude.com, ^{4,5}mwestover@mgh.harvard.edu

Abstract

Tensor decompositions are powerful tools for dimensionality reduction and feature interpretation of multidimensional data such as signals. Existing tensor decomposition objectives (e.g., Frobenius norm) are designed for fitting raw data under statistical assumptions, which may not align with downstream classification tasks. Also, real-world tensor data are usually high-ordered and have large dimensions with millions or billions of entries. Thus, it is expensive to decompose the whole tensor with traditional algorithms. In practice, raw tensor data also contains redundant information while data augmentation techniques may be used to smooth out noise in samples. This paper addresses the above challenges by proposing augmented tensor decomposition (ATD), which effectively incorporates data augmentations to boost downstream classification. To reduce the memory footprint of the decomposition, we propose a stochastic algorithm that updates the factor matrices in a batch fashion. We evaluate ATD on multiple signal datasets. It shows comparable or better performance (e.g., up to 15% in accuracy) over self-supervised and autoencoder baselines with less than 5% of model parameters, achieves 0.6% \sim 1.3% accuracy gain over other tensor-based baselines, and reduces the memory footprint by 9X when compared to standard tensor decomposition algorithms.

1 Introduction

Extracting unsupervised features from high-dimensional data is essential in various scenarios, such as physiological signals (Cong et al., 2015), hyperspectral images (Wang et al., 2017) and fMRI (Hamdi et al., 2018). Tensor decomposition models are often used for high-order feature extraction (Sidiropoulos et al., 2017). Among these, CANDECOMP/PARAFAC (CP) decomposition is one of the most popular models. These low-rank tensor decompositions (Kolda and Bader, 2009), such as CP decomposition, assume the input data is composited by a small set of components, while the reduced features are the coefficients that quantify the importance of each basis component.

Existing tensor decomposition objectives aim to *fit individual data samples* under statistical assumptions (Hong et al., 2020; Singh et al., 2021), e.g., Gaussian noise. Though *fitness* is an essential principle for feature reduction, common objective functions do not account for downstream tasks, e.g., classification. Another line of research for feature reduction is self-supervised contrastive learning (He et al., 2020), which utilizes the class-preserving property of data augmentations (Dao et al., 2019) and encodes low-dimensional embeddings by *enforcing alignments*: maximizing embedding similarity of samples from the same latent class while minimizing embedding similarity of samples from different latent classes (Chen et al., 2020; Wang and Isola, 2020). However, these models are mostly built on deep neural networks, which are often black-box models with many parameters.

This paper aims to learn tensor bases from large scale unlabeled tensors, following both *fitness* and *alignment* principles, and then uses the learned bases to produce better features for downstream tasks. Our main contributions are summarized below.

- We propose **augmented tensor decomposition**, named ATD, which learns an unsupervised CP structure decomposition by extending the original fitness objective with a self-supervised loss on the contrastiveness of similar and dissimilar data samples.
- We propose **stochastic alternating optimization** for the new objective, which can refine the tensor bases effectively in batches, while standard optimization algorithms, e.g., CP alternating least squares (CP-ALS), mostly work on the whole tensor and require to load all data at once.
- Enabled by this stochastic optimization algorithm, our ATD can provide $\sim 3.8\%$ accuracy gain over standard CP-ALS with **asymptotically the same complexity** of each optimization sweep and **less memory consumption** (e.g., a reduction on GPU memory load by 90%).
- We provide **extensive evaluations on four real-world datasets** and compare to recent tensor decomposition models, self-supervised models, autoencoder models, and supervised models. Our model shows better or comparable prediction performance in various downstream classifications while requiring fewer (e.g., less than 5% of) parameters than that of deep learning baselines.

2 Background

Notation. We use plain letters for scalars, such as x or X , boldface uppercase letters for matrices, e.g., \mathbf{X} , boldface lowercase letters for vectors, e.g., \mathbf{x} , and Euler script letters for tensors, random variables of tensors, and probability distributions, e.g., \mathcal{X} . Tensors are multidimensional arrays indexed by three or more indices (modes). For example, an N -mode tensor \mathcal{X} is an N -dimensional array of size $I_1 \times \cdots \times I_N$, where x_{i_1, \dots, i_N} is the element at the (i_1, \dots, i_N) -th position. For matrix \mathbf{X} , the r -th row and column are $\mathbf{x}^{(r)}$ and \mathbf{x}_r respectively, while x_{ij} is for the (i, j) -th element. For vector \mathbf{x} , the r -th element is x_r , and we use $\|\mathbf{x}\|_2$ to denote the vector 2-norm, $\langle \cdot, \cdot \rangle$ for the vector inner product, \circ for the outer product, and $\llbracket \cdot \rrbracket$ for the Kruskal product. Indices in the paper typically start from 1, e.g., \mathbf{x}_1 is the first column of the matrix.

2.1 Tensor Modeling and Motivations

This paper aims to learn tensor bases from unlabeled data and then use the bases to build a feature extractor for downstream classification. Without loss of generality (w.r.t. tensor order), we consider the fourth-order tensor, e.g., a collection of multi-channel Electroencephalography (EEG) signals,

$$\mathcal{T} = [\mathcal{T}^{(1)}, \mathcal{T}^{(2)}, \dots, \mathcal{T}^{(N)}] \in \mathbb{R}^{N \times I \times J \times K}, \quad \text{where } \mathcal{T}^{(n)} \in \mathbb{R}^{I \times J \times K}.$$

The first dimension of \mathcal{T} corresponds to data/signal samples (e.g., one for each patient), while the other three are feature dimensions (e.g., *channel by frequency by timestamp* in this example).

Data Model. Following previous CP decomposition works (Kolda and Bader, 2009), we assume the tensor data admits a low-rank structure and is generated by R rank-one tensor components $\{\mathcal{E}_1, \dots, \mathcal{E}_R\}$, which are parameterized by the bases $\{\mathbf{A} \in \mathbb{R}^{I \times R}, \mathbf{B} \in \mathbb{R}^{J \times R}, \mathbf{C} \in \mathbb{R}^{K \times R}\}$,

$$\mathcal{E}_r = \mathbf{a}_r \circ \mathbf{b}_r \circ \mathbf{c}_r, \quad r \in [1, \dots, R].$$

Each data sample/slice $\mathcal{T}^{(n)}$ is represented as a weighted sum of the R rank-one components, where the n -th coefficient vector is defined as $\mathbf{x}^{(n)}$. Further, element-wise i.i.d. Gaussian noise is super-imposed to model the real-world distortion (e.g., physical noise in signal measurements),

$$\begin{aligned} \mathcal{T}^{(n)} &= \sum_{r=1}^R x_r^{(n)} \cdot \mathcal{E}_r + \epsilon^{(n)} \sim \mathcal{D}_m, \quad m \in \{1, \dots, M\}, \\ \epsilon^{(n)} &\sim_{\text{i.i.d.}} \mathcal{N}(0, \sigma), \quad \text{where } \sigma \text{ is generally small.} \end{aligned} \tag{1}$$

where by the setting of downstream classification, each sample $\mathcal{T}^{(n)}$ is semantically associated to one of the latent classes $m \in \{1, \dots, M\}$, and we let \mathcal{D}_m be the sample distribution of class- m .

CANDECOMP/PARAFAC Decomposition (CPD). Standard CPD only models the i.i.d. Gaussian noise (more details in Appendix A), which results in the following standard loss,

$$\mathcal{L}_{cpd} = \sum_{n=1}^N \left\| \mathcal{T}^{(n)} - \llbracket \mathbf{x}^{(n)}, \mathbf{A}, \mathbf{B}, \mathbf{C} \rrbracket \right\|_F^2 = \left\| \mathcal{T} - \llbracket \mathbf{X}, \mathbf{A}, \mathbf{B}, \mathbf{C} \rrbracket \right\|_F^2.$$

Here, the Kruskal product $\llbracket \cdot \rrbracket$ outputs a fourth-order reconstructed tensor from four input factor matrices. For consistency, if the first input is a vector, the output is considered as a third-order tensor.

2.2 Problem Formulation

CP decomposition seeks a low-rank reconstruction, without special consideration for the downstream classification. In this paper, we are motivated to improve the CPD model by exploiting the latent classes and learn good bases (i.e., rank-one components) to provide better features for classification.

What are Good Bases? This paper considers two design principles for good bases. The first principle is *fitness*, which requires a low-rank tensor reconstruction with the bases. Second, data samples associated with the same latent class should be decomposed into similar coefficient vectors, with the bases, while the vectors should be dissimilar if the samples are from different latent classes. This principle is called *alignment*, which is important for classification but not considered in the standard tensor decomposition. In this paper, we assess the quality of the learned bases by the performance of downstream classification, where the coefficient vectors are the feature inputs.

To put it succinctly, the paper tackles an unsupervised learning problem while using downstream supervised classification for evaluation. The learning and evaluation pipelines are briefly outlined:

- First, we **learn** the bases $\{\mathbf{A}, \mathbf{B}, \mathbf{C}\}$ from a large set of unlabeled data. The loss function is developed in consideration of the *fitness* (i.e., the standard low-rank reconstruction loss) and *alignment* (i.e., our self-supervised loss, defined in the next section) principles.
- Then, we **construct** the following feature extractor given the learned bases $\{\mathbf{A}, \mathbf{B}, \mathbf{C}\}$. The feature vector of a new sample is obtained by the closed-form solution of the least squares problem ($\alpha > 0$),

$$\mathbf{f}(\mathcal{T}^{(new)}; \mathbf{A}, \mathbf{B}, \mathbf{C}) = \arg \min_{\mathbf{x} \in \mathbb{R}^{1 \times R}} \left(\left\| \mathcal{T}^{(new)} - \llbracket \mathbf{x}, \mathbf{A}, \mathbf{B}, \mathbf{C} \rrbracket \right\|_F^2 + \alpha \|\mathbf{x}\|_2^2 \right). \quad (2)$$

Note that, when $\mathbf{f}(\cdot)$ is applied to a batch of samples, e.g., \mathcal{T} , it outputs a coefficient matrix.

- Next, we **evaluate** the feature extractor with a small amount of labeled data. We train an additional logistic regression model on top of the extracted features, so that the result of classifications will implicitly reflect how good the bases are.

3 Augmented Tensor Decomposition (ATD)

We show our model in Figure 1. The design is inspired by the recent popularity of self-supervised learning. To exploit the latent class assignment, we introduce data augmentation into CPD model and design self-supervised loss to constrain the learned low-rank features (i.e., the coefficient vectors).

Data Augmentation.¹ Given a tensor sample $\mathcal{T}^{(n)}$, we assume that the augmentation methods, $\text{aug}(\cdot) : \mathcal{T}^{(n)} \rightarrow \tilde{\mathcal{T}}^{(n)}$, obey the following *class-invariance property*: $\tilde{\mathcal{T}}^{(n)}$ preserves the same class label and admits a component-based representation, specified in Eqn. (1).

3.1 Self-supervised Loss

The design of our self-supervised loss corresponds to the *alignment* principle, which is based on pairwise feature similarity and dissimilarity.

Let $\mathcal{X}_p, \mathcal{Y}_p$ be discrete random variables (of tensor samples) distributed as \mathcal{D}_p , $p \in \{1, \dots, M\}$, which is the sample distribution of class- p . We want to minimize the following objectives when *no class labels are given*,

$$\begin{aligned} \mathcal{L}_{pos} &= -\mathbb{E} [\text{sim}(\mathbf{f}(\mathcal{X}_p), \mathbf{f}(\mathcal{Y}_q)) \mid p = q], \\ \mathcal{L}_{neg} &= \mathbb{E} [\text{sim}(\mathbf{f}(\mathcal{X}_p), \mathbf{f}(\mathcal{Y}_q)) \mid p \neq q], \end{aligned}$$

¹In practice, augmentation methods are chosen based on the input format and application background.

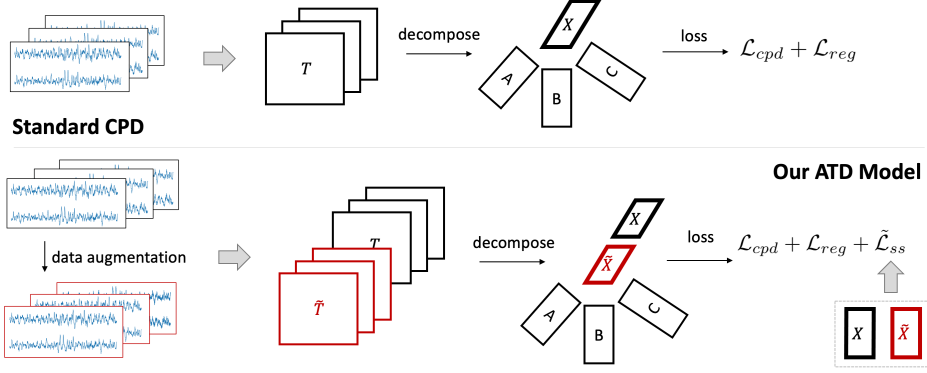


Figure 1: Standard CPD vs Our ATD Model

where $\mathbf{f}(\cdot)$ is the feature extractor, defined in Eqn. (2), and the similarity measure is given by cosine distance, parameterized by two random variables,

$$\text{sim}(\mathbf{f}(\mathcal{X}_p), \mathbf{f}(\mathcal{Y}_q)) = \left\langle \frac{\mathbf{f}(\mathcal{X}_p)}{\|\mathbf{f}(\mathcal{X}_p)\|_2}, \frac{\mathbf{f}(\mathcal{Y}_q)}{\|\mathbf{f}(\mathcal{Y}_q)\|_2} \right\rangle.$$

We call a pair of samples from the same latent class as *positive pair*, a pair of samples from different latent classes as *negative pair* and a pair of independent samples (from the dataset) as *random pair*. Here, \mathcal{L}_{pos} maximizes the feature similarity between positive pairs, and \mathcal{L}_{neg} minimizes that between negative pairs. To this end, the key of the paper is to find positive pairs and negative pairs in an unsupervised setting, since our learning process deals with unlabeled data only.

Construction of Samplers. The sampler of positive pairs can be easily approximated by data augmentation techniques, which provides "surrogate" positive pairs. The sampler of random pairs can be achieved by picking two independent samples from the dataset. However, the sampler of negative pairs is infeasible to construct without labels, and thus we consider using the *law of total probability* (Arora et al., 2019; Chuang et al., 2020). Assume $\mathcal{T}^{(n)}$ is an instance of random variable \mathcal{X}_p and $c(\mathcal{T}^{(n)})$ is the label rate of $\mathcal{T}^{(n)}$'s latent class- p . By law of total probability, the following holds,

$$\begin{aligned} \mathbb{E} [\text{sim}(\mathbf{f}(\mathcal{X}_p), \mathbf{f}(\mathcal{Y}_q)) \mid \mathcal{X}_p = \mathcal{T}^{(n)}] &= c(\mathcal{T}^{(n)}) \mathbb{E} [\text{sim}(\mathbf{f}(\mathcal{X}_p), \mathbf{f}(\mathcal{Y}_q)) \mid \mathcal{X}_p = \mathcal{T}^{(n)}, p = q] \\ &\quad + (1 - c(\mathcal{T}^{(n)})) \mathbb{E} [\text{sim}(\mathbf{f}(\mathcal{X}_p), \mathbf{f}(\mathcal{Y}_q)) \mid \mathcal{X}_p = \mathcal{T}^{(n)}, p \neq q]. \end{aligned}$$

While we do not have access to $c(\mathcal{T}^{(n)})$ with unlabeled data, this issue is dealt with later. By re-arranging the equation, we show that given $\mathcal{X}_p = \mathcal{T}^{(n)}$, the marginal sampler of negative pairs can be replaced by a combination of the marginal samplers of random pairs and positive pairs,

$$\begin{aligned} \mathbb{E} [\text{sim}(\mathbf{f}(\mathcal{X}_p), \mathbf{f}(\mathcal{Y}_q)) \mid \mathcal{X}_p = \mathcal{T}^{(n)}, p \neq q] &= \frac{1}{1 - c(\mathcal{T}^{(n)})} \mathbb{E} [\text{sim}(\mathbf{f}(\mathcal{X}_p), \mathbf{f}(\mathcal{Y}_q)) \mid \mathcal{X}_p = \mathcal{T}^{(n)}] \\ &\quad - \frac{c(\mathcal{T}^{(n)})}{1 - c(\mathcal{T}^{(n)})} \mathbb{E} [\text{sim}(\mathbf{f}(\mathcal{X}_p), \mathbf{f}(\mathcal{Y}_q)) \mid \mathcal{X}_p = \mathcal{T}^{(n)}, p = q]. \end{aligned} \quad (3)$$

Self-supervised Loss. Consequently, we define our self-supervised loss as (let $\lambda \geq 1$),

$$\begin{aligned} \mathcal{L}_{ss} &= \mathcal{L}_{pos} + \lambda \mathcal{L}_{neg} \\ &= -\mathbb{E} [\text{sim}(\mathbf{f}(\mathcal{X}_p), \mathbf{f}(\mathcal{Y}_q)) \mid p = q] + \lambda \mathbb{E} [\text{sim}(\mathbf{f}(\mathcal{X}_p), \mathbf{f}(\mathcal{Y}_q)) \mid p \neq q] \end{aligned} \quad (4)$$

$$= \mathbb{E} \left[\frac{\lambda}{1 - c(\mathcal{X}_p)} \text{sim}(\mathbf{f}(\mathcal{X}_p), \mathbf{f}(\mathcal{Y}_q)) \right] - \mathbb{E} \left[\left(\frac{\lambda c(\mathcal{X}_p)}{1 - c(\mathcal{X}_p)} + 1 \right) \text{sim}(\mathbf{f}(\mathcal{X}_p), \mathbf{f}(\mathcal{Y}_q)) \mid p = q \right]. \quad (5)$$

From Eqn. (4) to Eqn. (5), we use the results in Eqn. (3) (see details in Appendix B). Specifically, $\mathbb{E} [\text{sim}(\mathbf{f}(\mathcal{X}_p), \mathbf{f}(\mathcal{Y}_q)) \mid p \neq q]$ can be replaced by taking expectation over $\mathcal{T}^{(n)}$ in Eqn. (3).

Two-sided Bound. The above result still requires label information, i.e., $c(\mathcal{X}_p)$, we therefore consider using the following approximation to the above loss \mathcal{L}_{ss} ,

$$\mathcal{L}_{ss}^{\Theta}(\gamma) = (\gamma + 1) \mathbb{E} [\text{sim}(\mathbf{f}(\mathcal{X}_p), \mathbf{f}(\mathcal{Y}_q))] - \mathbb{E} [\text{sim}(\mathbf{f}(\mathcal{X}_p), \mathbf{f}(\mathcal{Y}_q)) \mid p = q]. \quad (6)$$

Here, $\gamma \geq 0$ is a hyperparameter, while \mathcal{L}_{ss} is bounded as (more detail in Appendix B),

$$C_1 \mathcal{L}_{ss}^\Theta \left(\frac{\lambda - 1}{C_1} \right) \leq \mathcal{L}_{ss} \leq C_2 \mathcal{L}_{ss}^\Theta \left(\frac{\lambda - 1}{C_2} \right), C_1 = 1 + \max_{\mathcal{X}_p} \frac{\lambda c(\mathcal{X}_p)}{1 - c(\mathcal{X}_p)}, C_2 = 1 + \min_{\mathcal{X}_p} \frac{\lambda c(\mathcal{X}_p)}{1 - c(\mathcal{X}_p)}. \quad (7)$$

The equivalence is established when $C_1 = C_2$, i.e., the class labels are balanced. To simplify the derivation, we ignore λ in the following and directly let γ be a new hyperparameter. Also, the constants C_1 and C_2 are absorbed into a weight hyperparameter β , given in the next section. Therefore, this bound implies that, an easy-to-compute $\beta \mathcal{L}_{ss}^\Theta(\gamma)$ is often a good approximation of \mathcal{L}_{ss} for some β . The next section specifies how to compute $\beta \mathcal{L}_{ss}^\Theta(\gamma)$ in an unsupervised setting.

3.2 The Objective of ATD Model

Empirical Estimator. To obtain an empirical estimator of \mathcal{L}_{ss} , we first estimate the above bound \mathcal{L}_{ss}^Θ with Monte Carlo method. Suppose \mathcal{T} and $\tilde{\mathcal{T}}$ are the input tensor and the augmented tensor respectively, and $\mathbf{X} = \mathbf{f}(\mathcal{T})$, $\tilde{\mathbf{X}} = \mathbf{f}(\tilde{\mathcal{T}}) \in \mathbb{R}^{N \times R}$ are the coefficient/feature matrices. We use the row vectors of $\mathbf{X}, \tilde{\mathbf{X}}$ to estimate Eqn. (6). The first term $\mathbb{E}[\text{sim}(\mathbf{f}(\mathcal{X}_p), \mathbf{f}(\mathcal{Y}_q))]$ is approximated by the average cosine similarity of a pair of non-corresponding row vectors, while the second term $\mathbb{E}[\text{sim}(\mathbf{f}(\mathcal{X}_p), \mathbf{f}(\mathcal{Y}_q)) \mid p = q]$ is estimated by the average cosine similarity of pairs of corresponding row vectors,

$$\begin{aligned} \tilde{\mathcal{L}}_{ss}^\Theta(\gamma) &= \frac{\gamma + 1}{N(N-1)} \sum_{n=1}^N \sum_{s \neq n}^N \left\langle \frac{\mathbf{x}^{(n)}}{\|\mathbf{x}^{(n)}\|_2}, \frac{\tilde{\mathbf{x}}^{(s)}}{\|\tilde{\mathbf{x}}^{(s)}\|_2} \right\rangle - \frac{1}{N} \sum_{n=1}^N \left\langle \frac{\mathbf{x}^{(n)}}{\|\mathbf{x}^{(n)}\|_2}, \frac{\tilde{\mathbf{x}}^{(n)}}{\|\tilde{\mathbf{x}}^{(n)}\|_2} \right\rangle \\ &= \text{Tr} \left(\mathbf{X}^\top D(\mathbf{X}) \mathbf{G}(\gamma) D(\tilde{\mathbf{X}}) \tilde{\mathbf{X}} \right), \end{aligned}$$

where $D(\mathbf{X}) = \text{diag} \left(\frac{1}{\|\mathbf{x}^{(1)}\|_2}, \dots, \frac{1}{\|\mathbf{x}^{(N)}\|_2} \right)$ is the row-wise scaling matrix and

$$\mathbf{G}(\gamma) = \begin{bmatrix} -\frac{1}{N} & \frac{\gamma+1}{N(N-1)} & \dots & \frac{\gamma+1}{N(N-1)} \\ \frac{\gamma+1}{N(N-1)} & -\frac{1}{N} & \dots & \frac{\gamma+1}{N(N-1)} \\ \dots & \dots & \dots & \dots \\ \frac{\gamma+1}{N(N-1)} & \frac{\gamma+1}{N(N-1)} & \dots & -\frac{1}{N} \end{bmatrix}.$$

Objective. According to Eqn. (7), the self supervised loss \mathcal{L}_{ss} is bounded by $\mathcal{L}_{ss}^\Theta(\gamma)$, while the constants can be absorbed into a weight hyperparameter β . We let the empirical self-supervised loss, $\tilde{\mathcal{L}}_{ss} = \beta \tilde{\mathcal{L}}_{ss}^\Theta(\gamma)$. Our objective follows both the *fitness* (i.e., CPD reconstruction loss) and *alignment* (i.e., self-supervised loss) principles, while also considering Tikhonov regularization (Golub and Von Matt, 1997) to constrain the scale of all parameters,

$$\mathcal{L} = \mathcal{L}_{cpd} + \mathcal{L}_{reg} + \tilde{\mathcal{L}}_{ss}, \quad (8)$$

where

$$\begin{aligned} \mathcal{L}_{cpd} &= \|\mathcal{T} - \llbracket \mathbf{X}, \mathbf{A}, \mathbf{B}, \mathbf{C} \rrbracket\|_F^2 + \|\tilde{\mathcal{T}} - \llbracket \tilde{\mathbf{X}}, \mathbf{A}, \mathbf{B}, \mathbf{C} \rrbracket\|_F^2, \\ \mathcal{L}_{reg} &= \alpha \left(\|\mathbf{X}\|_F^2 + \|\tilde{\mathbf{X}}\|_F^2 + \|\mathbf{A}\|_F^2 + \|\mathbf{B}\|_F^2 + \|\mathbf{C}\|_F^2 \right), \\ \tilde{\mathcal{L}}_{ss} &= \beta \tilde{\mathcal{L}}_{ss}^\Theta(\gamma) = \beta \text{Tr} \left(\mathbf{X}^\top D(\mathbf{X}) \mathbf{G}(\gamma) D(\tilde{\mathbf{X}}) \tilde{\mathbf{X}} \right). \end{aligned} \quad (9)$$

In sum, the objective has (i) three hyperparameters, i.e., $\gamma, \alpha, \beta > 0$; (ii) three basis parameter matrices, i.e., $\{\mathbf{A}, \mathbf{B}, \mathbf{C}\}$; (iii) two coefficient matrices, i.e., $\mathbf{X}, \tilde{\mathbf{X}}$.

Theorem 1. Suppose N is the number of data samples. We have with probability $1 - \delta$,

$$|\mathcal{L}_{ss}^\Theta - \tilde{\mathcal{L}}_{ss}^\Theta| < \sqrt{\left(1 + \frac{(\gamma+1)^2}{N-1}\right) \frac{2}{N} \log \frac{2}{\delta}}. \quad (10)$$

A proof of this theorem is provided in Appendix C. Theorem 1 implies that with sufficiently large sample size N , $\tilde{\mathcal{L}}_{ss}^\Theta$ can accurately approximate \mathcal{L}_{ss}^Θ . Further, from Eqn. (7), we know that \mathcal{L}_{ss}^Θ can bound \mathcal{L}_{ss} on both sides. Therefore, to minimize \mathcal{L}_{ss} , it is sufficient to minimize the empirical estimator $\tilde{\mathcal{L}}_{ss}$, defined in Eqn. (9).

3.3 Stochastic Alternating Optimization

If the input tensor \mathcal{T} is small, we can update the parameters in a sequence by using full alternating optimization, e.g., a second-order derivative method (Maehara et al., 2016). However, it can be difficult to optimize on large input tensors directly due to memory constraints.

Optimization by Tensor Batches. This section proposes stochastic alternating optimization (SAO) for the objective in Eqn. (8). Our algorithm optimizes smaller scale objectives in batches: for the l -th data batch, we first use the input bases $\{\mathbf{A}^l, \mathbf{B}^l, \mathbf{C}^l\}$ to obtain \mathbf{X}^l and $\tilde{\mathbf{X}}^l$, which are the coefficient matrices in the l -th batch, and then we use these two matrices to refine the bases to be $\{\mathbf{A}^{l+1}, \mathbf{B}^{l+1}, \mathbf{C}^{l+1}\}$ for the next batch. Note that, \mathbf{X}^l and $\tilde{\mathbf{X}}^l$ will be totally new between batches, since tensor samples will change in the next batch, while the bases are shared and refined gradually. We specify the optimization flow for the l -th data batch.

Given the up-to-date bases $\{\mathbf{A}^l, \mathbf{B}^l, \mathbf{C}^l\}$ and a new size- b data batch $\mathcal{T}^l \in \mathbb{R}^{b \times I \times J \times K}$ (i.e., a subset of slices from \mathcal{T}), our algorithm consists of the following steps:

- *Cold Start:* First, we apply the augmentation methods and obtain an augmented data batch, $\tilde{\mathcal{T}}^l = \text{aug}(\mathcal{T}^l) \in \mathbb{R}^{b \times I \times J \times K}$. At this time, both \mathbf{X}^l and $\tilde{\mathbf{X}}^l$ are unknown, and the batch objective (a small scale form of Eqn. (8)) is non-convex with respect to either of the tensor variables. As a cold start, we use standard CP decomposition with Tikhonov regularizers to obtain an initial guess. The initial guess can be explicitly computed by least squares optimization:

$$\mathbf{X}_{\text{init}}^l \leftarrow \arg \min_{\mathbf{X}} \left(\left\| \mathcal{T}^l - \llbracket \mathbf{X}, \mathbf{A}^l, \mathbf{B}^l, \mathbf{C}^l \rrbracket \right\|_F^2 + \alpha \|\mathbf{X}\|_F^2 \right), \quad (11)$$

$$\tilde{\mathbf{X}}_{\text{init}}^l \leftarrow \arg \min_{\tilde{\mathbf{X}}} \left(\left\| \tilde{\mathcal{T}}^l - \llbracket \tilde{\mathbf{X}}, \mathbf{A}^l, \mathbf{B}^l, \mathbf{C}^l \rrbracket \right\|_F^2 + \alpha \|\tilde{\mathbf{X}}\|_F^2 \right). \quad (12)$$

Next, we show that with the initial guess, we can iteratively find the stationary point of the non-convex problem by formulating independent least squares problems for \mathbf{X}^l and $\tilde{\mathbf{X}}^l$.

- *Auxiliary Step (for \mathbf{X}^l and $\tilde{\mathbf{X}}^l$):* Given $\mathbf{A}^l, \mathbf{B}^l, \mathbf{C}^l, \mathbf{X}_{\text{init}}^l, \tilde{\mathbf{X}}_{\text{init}}^l$, we want to solve the following non-convex problem for \mathbf{X}^l (and similar for $\tilde{\mathbf{X}}^l$),

$$\mathbf{X}^{*l} \leftarrow \arg \min_{\mathbf{X}} \left(\left\| \mathcal{T}^l - \llbracket \mathbf{X}, \mathbf{A}^l, \mathbf{B}^l, \mathbf{C}^l \rrbracket \right\|_F^2 + \alpha \|\mathbf{X}\|_F^2 + \beta \text{Tr} \left(\mathbf{X}^\top D(\mathbf{X}) \mathbf{G} D(\tilde{\mathbf{X}}_{\text{init}}^l) \tilde{\mathbf{X}}_{\text{init}}^l \right) \right). \quad (13)$$

- 1) To solve Eqn. (13), we first solve the following least squares problem,

$$\mathbf{X}_{\text{impr}}^l \leftarrow \arg \min_{\mathbf{X}} \left(\left\| \mathcal{T}^l - \llbracket \mathbf{X}, \mathbf{A}^l, \mathbf{B}^l, \mathbf{C}^l \rrbracket \right\|_F^2 + \alpha \|\mathbf{X}\|_F^2 + \beta \text{Tr} \left(\mathbf{X}^\top D(\mathbf{X}_{\text{init}}^l) \mathbf{G} D(\tilde{\mathbf{X}}_{\text{init}}^l) \tilde{\mathbf{X}}_{\text{init}}^l \right) \right). \quad (14)$$

- 2) Let the improved guess be the initial guess, $\mathbf{X}_{\text{init}}^l \leftarrow \mathbf{X}_{\text{impr}}^l$, and re-run Eqn. (14).
- 3) Repeat 2) to iteratively improve the guess.

Theorem 2 shows that in vector form, the iterative rule in Eqn. (14) converges linearly to the stationary point of Eqn. (13) if β is chosen to be sufficiently small. In Appendix D, we empirically show that one round of Eqn. (14) is sufficient. For this paper, the iterative rules of \mathbf{X}^l and $\tilde{\mathbf{X}}^l$ are conducted independently, while alternating them may be possible, we do not consider it in this paper. Without loss of generality, the *Auxiliary Step* will finally output $\mathbf{X}^{*l}, \tilde{\mathbf{X}}^{*l}$.

- *Main Steps (for $\mathbf{A}, \mathbf{B}, \mathbf{C}$):* Then, we update the basis parameters using \mathbf{X}^{*l} and $\tilde{\mathbf{X}}^{*l}$. The objective function is a least squares problem for each of the basis parameter, e.g., \mathbf{A} , if we fix other factors. Therefore, to obtain a new \mathbf{A}^{l+1} , we use the following closed-form update,

$$\mathbf{A}^* \leftarrow \arg \min_{\mathbf{A}} \left(\left\| \mathcal{T}^l - \llbracket \mathbf{X}^{*l}, \mathbf{A}, \mathbf{B}^l, \mathbf{C}^l \rrbracket \right\|_F^2 + \left\| \tilde{\mathcal{T}}^l - \llbracket \tilde{\mathbf{X}}^{*l}, \mathbf{A}, \mathbf{B}^l, \mathbf{C}^l \rrbracket \right\|_F^2 + \alpha \|\mathbf{A}\|_F^2 \right), \quad (15)$$

$$\mathbf{A}^{l+1} \leftarrow (1 - \eta) \mathbf{A}^l + \eta \mathbf{A}^*. \quad (16)$$

Theorem 2. Given d -dimensional non-zero vectors, $\mathbf{v}_1, \mathbf{v}_2, \mathbf{u}^0 \in \mathbb{R}^d$, where \mathbf{v}_1 is not parallel to \mathbf{v}_2 and $\beta > 0$. The sequence $\{\mathbf{u}^t\}$, generated by the rule, $\mathbf{u}^{t+1} = \mathbf{v}_1 - \frac{\beta}{\|\mathbf{u}^t\|_2} \mathbf{v}_2$, satisfies,

$$\|\mathbf{u}^{t+1} - \mathbf{u}^*\|_2 \leq \frac{\beta \|\mathbf{v}_2\|_2}{\|\mathbf{v}_1\|_2^2 - \langle \mathbf{v}_1, \frac{\mathbf{v}_2}{\|\mathbf{v}_2\|_2} \rangle^2} \|\mathbf{u}^t - \mathbf{u}^*\|_2,$$

where \mathbf{u}^* is the stationary point, i.e., $\mathbf{u}^* = \mathbf{v}_1 - \frac{\beta}{\|\mathbf{u}^*\|_2} \mathbf{v}_2$.

Algorithm 1: Stochastic Alternating Optimization (SAO)

```

1 Input: Data tensor  $\mathcal{T} \in \mathbb{R}^{N \times I \times J \times K}$ ; initialized  $\{\mathbf{A}^1, \mathbf{B}^1, \mathbf{C}^1\}$ ; batch size  $b$ ; learning rate  $\eta$ ; other
  hyperparameters  $\alpha, \beta, \gamma$ ; initial counter  $l = 1$ ;
2 repeat
3   shuffle the data tensor  $\mathcal{T}$ ; /* start a new sweep */
4   for a tensor batch  $\mathcal{T}^l \in \mathbb{R}^{b \times I \times J \times K}$  and its augmented tensor  $\tilde{\mathcal{T}}^l = \text{aug}(\mathcal{T}^l)$  do
5     Cold Start: use  $\{\mathbf{A}^l, \mathbf{B}^l, \mathbf{C}^l\}$  to obtain  $\mathbf{X}_{\text{init}}^l$  and  $\tilde{\mathbf{X}}_{\text{init}}^l$  by Eqn. (11)(12);
6     Auxiliary Step: use  $\{\mathbf{A}^l, \mathbf{B}^l, \mathbf{C}^l, \mathbf{X}_{\text{init}}^l, \tilde{\mathbf{X}}_{\text{init}}^l\}$  to obtain  $\mathbf{X}^{*l}$  by Eqn. (14) and similar for  $\tilde{\mathbf{X}}^{*l}$ ;
7     Main Step 1: use  $\{\mathbf{X}^{*l}, \tilde{\mathbf{X}}^{*l}, \mathbf{B}^l, \mathbf{C}^l\}$  to update  $\mathbf{A}^{l+1}$  by Eqn. (15)(16);
8     Main Step 2: use  $\{\mathbf{X}^{*l}, \tilde{\mathbf{X}}^{*l}, \mathbf{A}^{l+1}, \mathbf{C}^l\}$  to update  $\mathbf{B}^{l+1}$  by Eqn. (15)(16);
9     Main Step 3: use  $\{\mathbf{X}^{*l}, \tilde{\mathbf{X}}^{*l}, \mathbf{A}^{l+1}, \mathbf{B}^{l+1}\}$  to update  $\mathbf{C}^{l+1}$  by Eqn. (15)(16);
10     $l = l + 1$  /* increment the counter */;
11  end
12 until max sweep exceeds or change of average loss  $< 0.1\%$  within 3 consecutive sweeps;
13 Output: the learned bases  $\{\mathbf{A}^L, \mathbf{B}^L, \mathbf{C}^L\}$ .

```

Complexity. The procedures are summarized in Algorithm 1. Each iteration is decomposed into five sub-iterations (cold start, auxiliary step and three main steps), where each sub-iteration involves solving least squares problems. Thus, the computation head of the algorithm is matricized tensor times Khatri-Rao product (MTTKRP). The complexity of our algorithm is asymptotically the same as applying CP-ALS, which costs $O(N I J K R)$ to sweep over the whole dense tensor once.

4 Experiments

This section presents the experimental evaluations. Due to space limitation, additional details, including data augmentations and baseline implementation, are presented in Appendix E.

Data Preparation. We use four real-world datasets: (i) *Sleep-EDF* (Kemp et al., 2000), which contains EOG, EMG and EEG Polysomnography recordings; (ii) human activity recognition (*HAR*) (Anguita et al., 2013) with smartphone accelerometer and gyroscope data; (iii) Physikalisch Technische Bundesanstalt large scale cardiology database (*PTB-XL*) (Alday et al., 2020) with 12-lead ECG signals; (iv) Massachusetts General Hospital (*MGH*) (Biswal et al., 2018) datasets with multi-channel EEG waves. All datasets are split into three disjoint sets (i.e., unlabeled, training and test) by subjects, while training and test sets have labels. Basic statistics are shown in Table 1. All models use the same augmentation techniques: (a) jittering, (b) bandpass filtering, (c) time rotation, and (d) 3D position rotation. We provide an ablation study on the augmentation methods in Appendix E.4.

Table 1: Dataset Statistics

Name	Data Sample Format	Augmentations	# Unlabeled (N)	# Training	# Test	Task	# Class
Sleep-EDF	$I \times J \times K: 14 \times 129 \times 86$	(a), (b), (c)	331,208	42,803	41,078	Sleep Staging	5
HAR	$I \times J \times K: 18 \times 33 \times 33$	(a), (b), (c), (d)	7,352	1,473	1,474	Activity Recognition	6
PTB-XL	$I \times J \times K: 24 \times 129 \times 75$	(a), (b), (c)	17,469	2,183	2,185	Gender Identification	2
MGH	$I \times J \times K: 12 \times 257 \times 43$	(a), (b), (c)	4,377,170	238,312	248,041	Sleep Staging	5

Baseline Methods. We add model variant, ATD_{ss-} , which removes the self-supervised loss from the objective in Eqn. (8). We consider the state-of-the-art CPD algorithm with *dimension trees* (Phan et al., 2013), called *Fast CPD*. Dimension trees accelerate CP decomposition by reusing intermediate MTTKRP results. However, *Fast CPD* model requires to load the full data into memory, and thus it is expensive for large tensors. We also consider the stochastic alternating least square (*SALS*) (Maehara et al., 2016) for the CPD objective, which works on large tensors.

In addition, we consider the following deep learning models: (i) two supervised models: a convolutional neural network (CNN) model, *Supervised* (Biswal et al., 2018), and the same model with augmented training set, *Supervised_{Aug}*; (ii) two self-supervised models: *SimCLR-r* (Chen et al., 2020), *BYOL-r* (Grill et al., 2020); (iii) two autoencoder models: CNN based autoencoder, *AE-r*, and autoencoder model with self-supervised loss in bottleneck layer, *AE_{ss-r}*, where r is the size of the representation. The supervised model only use the training and test sets, and we include them as a

reference. Other baselines use the unlabeled set to train a feature encoder and use training and test sets to evaluate. Note that, deep neural network models use the same CNN backbone.

Experimental Settings. We evaluate model performance mainly based on *classification accuracy* through the common linear evaluation (He et al., 2020). Also, for different models, we compare their *number of learnable parameters*. The experiments are implemented by *Python 3.8.5*, *Torch 1.8.0+cu111* on a Linux workstation with 256 GB memory, 32 core CPUs (3.70 GHz, 128 MB cache), two RTX 3090 GPUs (24 GB memory each). All training is performed on the GPU. For tensor based models, we use $R = 32$ and implement the pipeline in CUDA manually, instead of using *torch-autograd*.

4.1 Results on Small Unlabeled Data: Our ATD vs Fast CPD Model

The first experiment is conduct with a small set of data on MGH dataset. We randomly pick 8,000 unlabeled samples to form the objective and use 5,000 training samples and all test data for downstream classification. For our ATD, we consider 32, 64, 128, 256, 512 as the batch sizes. The metrics are (i) peak GPU memory, (ii) time consumption for sweeping over the data once (for ATD, it includes all batches), (iii) classification accuracy. The experiment runs with five random seeds. We provide similar results for other datasets in Appendix E.2.

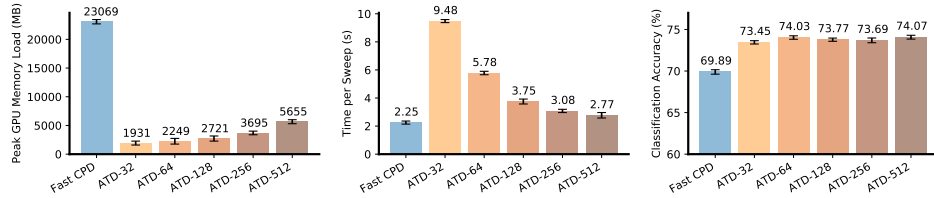


Figure 2: Performance Comparison between Our ATD Method and the *Fast CPD* Method

Result Analysis. Figure 2 (left) shows that our model can greatly reduce the memory footprint. For example, when using 128 as batch size on the $8,000 \times 12 \times 257 \times 43$ tensor, we can reduce the memory load by a factor of about $\frac{1}{9}$. Figure 2 (middle) shows that our ATD provides comparable efficiency compared to Fast CPD. We observe that ATD with large batches (e.g., 256, 512) can achieve relatively small per-sweep time consumption (though cannot beat Fast CPD), while our ATD is more memory efficient. Figure 2 (right) shows that ATD gives better predictive performance. Clearly, our ATD improves the accuracy by around 3.8% over the Fast CPD. We also observe that the classification performance of our ATD is not sensitive to batch size, which enables the customization of our ATD for different computational environments.

4.2 Results on All Unlabeled Data: Our ATD vs Other Baselines

Table 2: Downstream Classification (%). The table shows that our ATD can provide comparable or better performance over all baselines, especially deep learning models (with fewer parameters). It also shows the usefulness of considering both *fitness* and *alignment* as part of the objective function.

	Sleep-EDF (5,000)		HAR (1,473)		PTB-XL (2,183)		MGH (5,000)	
	Accuracy	# of Params.	Accuracy	# of Params.	Accuracy	# of Params.	Accuracy	# of Params.
Supervised	87.62 \pm 0.619	206,256	94.96 \pm 0.695	49,158	68.72 \pm 1.240	188,640	72.99 \pm 0.935	205,392
Supervised _{Aug}	88.16 \pm 0.281	206,256	93.84 \pm 0.415	49,158	67.98 \pm 1.302	188,640	73.17 \pm 0.821	205,392
Self-sup models:								
SimCLR-32	87.82 \pm 0.364	210,384	77.60 \pm 0.668	53,286	69.30 \pm 0.362	200,960	67.88 \pm 0.958	212,624
SimCLR-128	88.18 \pm 0.356	222,768	75.58 \pm 0.675	65,670	69.14 \pm 0.781	237,920	66.40 \pm 1.332	246,608
BYOL-32	87.96 \pm 0.412	211,440	74.16 \pm 2.833	54,342	65.19 \pm 1.472	202,016	68.37 \pm 1.120	214,736
BYOL-128	88.15 \pm 0.327	239,280	72.85 \pm 1.840	82,182	66.03 \pm 0.591	254,432	68.09 \pm 1.362	279,632
Auto-encoders:								
AE-32	79.28 \pm 0.725	217,216	63.13 \pm 0.775	62,940	59.01 \pm 0.896	224,528	68.58 \pm 0.427	220,088
AE-128	78.63 \pm 0.884	241,888	60.52 \pm 1.604	87,612	58.29 \pm 0.412	298,352	67.05 \pm 1.375	257,048
AE _{ss} -32	86.53 \pm 0.331	217,216	71.99 \pm 2.052	62,940	69.69 \pm 0.215	224,528	71.52 \pm 0.371	220,088
AE _{ss} -128	86.64 \pm 0.261	241,888	69.50 \pm 1.495	87,612	69.40 \pm 0.596	298,352	70.25 \pm 0.618	257,048
Tensor models:								
SALS	86.54 \pm 0.496	7,328	92.54 \pm 0.281	2,688	68.98 \pm 0.487	7,296	73.16 \pm 0.366	9,984
ATD _{ss} -	86.87 \pm 0.227	7,328	92.48 \pm 0.357	2,688	69.08 \pm 0.612	7,296	72.93 \pm 0.543	9,984
ATD	87.47 \pm 0.215	7,328	93.40 \pm 0.395	2,688	70.02 \pm 0.546	7,296	74.19 \pm 0.413	9,984

In this experiment, we compare our ATD with other baseline models on all unlabeled data. For the classification, we randomly select a subset of training data (specified in parentheses) and use all test data. Each experiment is conducted with five different random seeds and the mean and standard deviations are reported. The metrics used are the accuracy and the number of learnable parameters. The number of parameters only count for the feature extractors, so it does not include the final prediction layer in supervised model. All models have 32-dim features in the end, except that for two self-supervised baselines and autoencoder models, which have 128-dim options. We show the comparison results in Table 2. On the MGH dataset, we also show the effect of varying the amount of training data in Figure 3.

Result Analysis. From Table 2, ATD shows comparable or better performance over the unsupervised baselines and sometimes can even beat the supervised models. Compared to the variant ATD_{ss-} , our ATD can improve the accuracy by 0.6% \sim 1.3%, which shows the benefit of the inclusion of self-supervised loss. SALS and ATD_{ss-} have similar performance, while their objectives differ in that ATD_{ss-} considers the Frobenius norm of the augmented data. Thus, their accuracy gap is caused by the use of data augmentation. Also, the experiments show that the *fitness* and *alignment* principles are both important. We observe that with a self-supervised loss (i.e., *alignment*), AE_{ss} can give significant improvement over AE, while ATD shows \sim 5% accuracy gain over the self-supervised models on MGH dataset, since we can better preserve the data with a reconstruction loss (i.e., *fitness*).

Moreover, the table shows that tensor based models require fewer parameters, i.e., less than 5% of parameters compared to deep learning models. On HAR, the deep unsupervised models show poor performance due to (i) they may not optimize a large number of parameters on middle-scale dataset; (ii) movement signals in HAR might have few degrees of freedom, which matches well with the low-rank assumption of tensor methods. On large-scale Sleep-EDF, self-supervised models outperforms ATD marginally since they have more parameters thus can capture more information. Of course, with a large rank R , our ATD can further improve the performance as we show in Appendix E.5. In practice, we also find that tensor based methods can quickly achieve high accuracy with only a few iterations. In Figure 3, we observe that with more training data, the performance of all models is improved, especially the supervised model, which outperforms our ATD when more training samples is available.

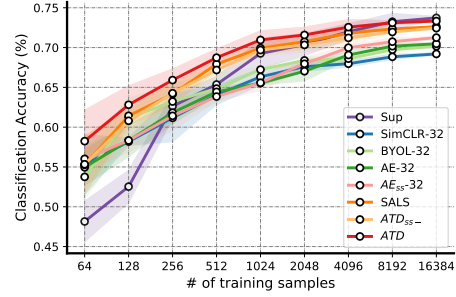


Figure 3: Varying the # of Training Data

5 Related Work

Data augmentation and Self-supervised Learning. Data augmentation exploits class-preserving perturbations to encode prior knowledge and task-invariances (Dao et al., 2019). It has been widely used in various data formats, such as images (Cireřan et al., 2010), text (Lu et al., 2006), audio (Uhlich et al., 2017), and time series (Wen et al., 2020). Data augmentation also benefits the recent development of self-supervised contrastive learning (He et al., 2020; Chen et al., 2020), which extracts feature representations by optimizing a deep neural network encoder to achieve agreements between semantically similar samples and disagreements on dissimilar samples. This paper shows that the concept of "learning to contrast" can also be useful in tensor decomposition.

Stochastic Algorithms for Tensors. With the rapid growth in data volume, efficient stochastic tensor methods become increasingly important for higher-order data structures to boost scalability. These methods are largely based on sampling (Ma and Solomonik, 2021; Yang et al., 2021; Kolda and Hong, 2020), which accelerates the computation of over-determined least square problems (Battaglino et al., 2018; Larsen and Kolda, 2020) in ALS for dense (Ailon and Chazelle, 2006) and sparse (Eshragh et al., 2019) tensors by effective strategies, such as Fast Johnson-Lindenstrauss Transform (Ailon and Chazelle, 2006), leverage-based sampling (Eshragh et al., 2019), and sketching (Zhou et al., 2014). However, these algorithms only focus on making ALS steps less costly and require to load the full data into memory. Thus, we do not consider them in our setting. This paper integrates augmentation techniques and self-supervised loss into tensor decomposition, and we also propose an effective stochastic alternating optimization to handle large scale optimization with less memory consumption.

6 Conclusion

This paper introduces the concept of self-supervised learning for tensors and proposes *Augmented Tensor Decomposition* (ATD). We show that by explicitly contrasting similar and dissimilar samples, the decomposition results are more aligned with downstream classification. Computation-wise, we propose stochastic alternating optimization to decompose large-scale tensor in batch fashion, which shows improved classification performance with less computational burden. On four real-world datasets, we show the advantages of our model over supervised and various unsupervised models.

Compared to deep learning methods, tensor based models are linear and require well-structured data, which is not as flexible in processing multimodal and diverse inputs, such as natural images. However, applying tensor decomposition on the outputs of earlier layers of pre-trained deep neural networks may be a feasible way to address the weaknesses. This direction would be interesting for future work.

References

- Ailon, N. and Chazelle, B. (2006). Approximate nearest neighbors and the fast Johnson-Lindenstrauss transform. In *STOC*, pages 557–563.
- Alday, E. A. P., Gu, A., Shah, A. J., Robichaux, C., Wong, A.-K. I., Liu, C., Liu, F., Rad, A. B., Elola, A., Seyedi, S., et al. (2020). Classification of 12-lead eegs: the physionet/computing in cardiology challenge 2020. *Physiological measurement*, 41(12):124003.
- Anguita, D., Ghio, A., Oneto, L., Parra, X., and Reyes-Ortiz, J. L. (2013). A public domain dataset for human activity recognition using smartphones. In *Esann*, volume 3, page 3.
- Arora, S., Khandeparkar, H., Khodak, M., Plevrakis, O., and Saunshi, N. (2019). A theoretical analysis of contrastive unsupervised representation learning. *arXiv preprint arXiv:1902.09229*.
- Battaglino, C., Ballard, G., and Kolda, T. G. (2018). A practical randomized CP tensor decomposition. *SIAM Journal on Matrix Analysis and Applications*, 39(2):876–901.
- Biswal, S., Sun, H., Goparaju, B., Westover, M. B., Sun, J., and Bianchi, M. T. (2018). Expert-level sleep scoring with deep neural networks. *Journal of the American Medical Informatics Association*, 25(12):1643–1650.
- Cao, Y., Das, S., Oeding, L., and van Wyk, H.-W. (2020). Analysis of the stochastic alternating least squares method for the decomposition of random tensors. *arXiv preprint arXiv:2004.12530*.
- Chen, T., Kornblith, S., Norouzi, M., and Hinton, G. (2020). A simple framework for contrastive learning of visual representations. In *International conference on machine learning*, pages 1597–1607. PMLR.
- Cheng, J. Y., Goh, H., Dogrusoz, K., Tuzel, O., and Azemi, E. (2020). Subject-aware contrastive learning for biosignals. *arXiv preprint arXiv:2007.04871*.
- Chuang, C.-Y., Robinson, J., Yen-Chen, L., Torralba, A., and Jegelka, S. (2020). Debiased contrastive learning. *arXiv preprint arXiv:2007.00224*.
- Cireřan, D. C., Meier, U., Gambardella, L. M., and Schmidhuber, J. (2010). Deep, big, simple neural nets for handwritten digit recognition. *Neural computation*, 22(12):3207–3220.
- Cong, F., Lin, Q.-H., Kuang, L.-D., Gong, X.-F., Astikainen, P., and Ristaniemi, T. (2015). Tensor decomposition of EEG signals: a brief review. *Journal of neuroscience methods*, 248:59–69.
- Dao, T., Gu, A., Ratner, A., Smith, V., De Sa, C., and Ré, C. (2019). A kernel theory of modern data augmentation. In *International Conference on Machine Learning*, pages 1528–1537. PMLR.
- Eshragh, A., Roosta, F., Nazari, A., and Mahoney, M. (2019). Lsar: Efficient leverage score sampling algorithm for the analysis of big time series data. *arXiv*.
- Golub, G. H. and Von Matt, U. (1997). *Tikhonov regularization for large scale problems*. Citeseer.

- Grill, J.-B., Strub, F., Altché, F., Tallec, C., Richemond, P. H., Buchatskaya, E., Doersch, C., Pires, B. A., Guo, Z. D., Azar, M. G., et al. (2020). Bootstrap your own latent: A new approach to self-supervised learning. *arXiv preprint arXiv:2006.07733*.
- Hamdi, S. M., Wu, Y., Boubrahimi, S. F., Angryk, R., Krishnamurthy, L. C., and Morris, R. (2018). Tensor decomposition for neurodevelopmental disorder prediction. In *International Conference on Brain Informatics*, pages 339–348. Springer.
- He, K., Fan, H., Wu, Y., Xie, S., and Girshick, R. (2020). Momentum contrast for unsupervised visual representation learning. In *Proceedings of the IEEE/CVF Conference on Computer Vision and Pattern Recognition*, pages 9729–9738.
- Hong, D., Kolda, T. G., and Dueresch, J. A. (2020). Generalized canonical polyadic tensor decomposition. *SIAM Review*, 62(1):133–163.
- Kemp, B., Zwinderman, A. H., Tuk, B., Kamphuisen, H. A., and Obery, J. J. (2000). Analysis of a sleep-dependent neuronal feedback loop: the slow-wave microcontinuity of the eeg. *IEEE Transactions on Biomedical Engineering*, 47(9):1185–1194.
- Kolda, T. G. and Bader, B. W. (2009). Tensor decompositions and applications. *SIAM review*, 51(3):455–500.
- Kolda, T. G. and Hong, D. (2020). Stochastic gradients for large-scale tensor decomposition. *SIAM Journal on Mathematics of Data Science*, 2(4):1066–1095.
- Larsen, B. W. and Kolda, T. G. (2020). Practical leverage-based sampling for low-rank tensor decomposition. *arXiv preprint arXiv:2006.16438*.
- Lu, X., Zheng, B., Velivelli, A., and Zhai, C. (2006). Enhancing text categorization with semantic-enriched representation and training data augmentation. *Journal of the American Medical Informatics Association*, 13(5):526–535.
- Ma, L. and Solomonik, E. (2021). Fast and accurate randomized algorithms for low-rank tensor decompositions. *arXiv preprint arXiv:2104.01101*.
- Maehara, T., Hayashi, K., and Kawarabayashi, K.-i. (2016). Expected tensor decomposition with stochastic gradient descent. In *Proceedings of the AAAI Conference on Artificial Intelligence*, volume 30.
- Mairal, J. (2013). Stochastic majorization-minimization algorithms for large-scale optimization. *arXiv preprint arXiv:1306.4650*.
- Phan, A.-H., Tichavský, P., and Cichocki, A. (2013). Fast alternating ls algorithms for high order CANDECOMP/PARAFAC tensor factorizations. *IEEE Transactions on Signal Processing*, 61(19):4834–4846.
- Sidiropoulos, N. D., De Lathauwer, L., Fu, X., Huang, K., Papalexakis, E. E., and Faloutsos, C. (2017). Tensor decomposition for signal processing and machine learning. *IEEE Transactions on Signal Processing*, 65(13):3551–3582.
- Singh, N., Zhang, Z., Wu, X., Zhang, N., Zhang, S., and Solomonik, E. (2021). Distributed-memory tensor completion for generalized loss functions in python using new sparse tensor kernels and randomized algorithms for low-rank tensor decompositions. *arXiv preprint arXiv:1910.02371*.
- Uhlich, S., Porcu, M., Giron, F., Enenkl, M., Kemp, T., Takahashi, N., and Mitsufuji, Y. (2017). Improving music source separation based on deep neural networks through data augmentation and network blending. In *2017 IEEE International Conference on Acoustics, Speech and Signal Processing (ICASSP)*, pages 261–265. IEEE.
- Van der Maaten, L. and Hinton, G. (2008). Visualizing data using t-SNE. *Journal of machine learning research*, 9(11).
- Wang, T. and Isola, P. (2020). Understanding contrastive representation learning through alignment and uniformity on the hypersphere. In *International Conference on Machine Learning*, pages 9929–9939. PMLR.

- Wang, Y., Peng, J., Zhao, Q., Leung, Y., Zhao, X.-L., and Meng, D. (2017). Hyperspectral image restoration via total variation regularized low-rank tensor decomposition. *IEEE Journal of Selected Topics in Applied Earth Observations and Remote Sensing*, 11(4):1227–1243.
- Wen, Q., Sun, L., Song, X., Gao, J., Wang, X., and Xu, H. (2020). Time series data augmentation for deep learning: A survey. *arXiv preprint arXiv:2002.12478*.
- Yang, C., Singh, N., Xiao, C., Qian, C., Solomonik, E., and Sun, J. (2021). MTC: Multiresolution tensor completion from partial and coarse observations.
- Zhou, G., Cichocki, A., and Xie, S. (2014). Decomposition of big tensors with low multilinear rank. *arXiv preprint arXiv:1412.1885*.

Contents

1	Introduction	1
2	Background	2
2.1	Tensor Modeling and Motivations	2
2.2	Problem Formulation	3
3	Augmented Tensor Decomposition (ATD)	3
3.1	Self-supervised Loss	3
3.2	The Objective of ATD Model	5
3.3	Stochastic Alternating Optimization	6
4	Experiments	7
4.1	Results on Small Unlabeled Data: Our ATD vs Fast CPD Model	8
4.2	Results on All Unlabeled Data: Our ATD vs Other Baselines	8
5	Related Work	9
6	Conclusion	10
A	Derivation of Frobenius Norm in CPD model	14
B	The Two-sided Bound in Section 3.1	14
C	Proof of Theorem 1	15
D	Proof and Experimental Insights of Theorem 2	17
D.1	Proof and Application of the Theorem	17
D.2	One Round of the Iterative Rule is Sufficient	18
E	Additional Information for Experiments	19
E.1	Data Processing and Implementations	19
E.2	Comparison Between ATD and Fast CPD on Other Datasets	21
E.3	Representation Structure in 2D: Our ATD vs Fast CPD Model	21
E.4	Effect of Data Augmentation	22
E.5	Effect of the Decomposition Rank R and Hyperparameters	23
F	Convergence Analysis With Moving Average Setting	23
F.1	Convergence Theorem	23
F.2	Proof Sketch	24
F.3	Assumptions and Lemmas	26
F.4	Proof of the Main Theorem	35

A Derivation of Frobenius Norm in CPD model

The standard CPD model employs maximum likelihood estimation (MLE) on the Gaussian noise assumption ϵ , which maximizes the likelihood of observing all tensor samples. In the model, the likelihood of observing one tensor sample $\mathcal{T}^{(n)}$ is given by the product of probabilities for each tensor element,

$$\begin{aligned} p(\mathcal{T}^{(n)}; \mathbf{x}^{(n)}, \mathbf{A}, \mathbf{B}, \mathbf{C}, \sigma) &= \prod_{ijk} p(t_{ijk}^{(n)}; \mathbf{x}^{(n)}, \mathbf{a}^{(i)}, \mathbf{b}^{(j)}, \mathbf{c}^{(k)}, \sigma) \\ &= \prod_{ijk} \frac{1}{\sqrt{2\pi}\sigma} \exp\left(-\frac{(t_{ijk}^{(n)} - \sum_r x_r^{(n)} a_r^{(i)} b_r^{(j)} c_r^{(k)})^2}{2\sigma^2}\right) \\ &= \left(\frac{1}{\sqrt{2\pi}\sigma}\right)^{IJK} \exp\left(-\frac{\sum_{ijk} (t_{ijk}^{(n)} - \sum_r x_r^{(n)} a_{ir} b_{jr} c_{kr})^2}{2\sigma^2}\right). \end{aligned}$$

Then, the likelihood of observing all tensor samples are given by the product of their individual likelihoods,

$$\prod_{n=1}^N p(\mathcal{T}^{(n)}; \mathbf{x}^{(n)}, \mathbf{A}, \mathbf{B}, \mathbf{C}, \sigma) = \left(\frac{1}{\sqrt{2\pi}\sigma}\right)^{NIJK} \exp\left(-\frac{\sum_n \sum_{ijk} (t_{ijk}^{(n)} - \sum_r x_r^{(n)} a_{ir} b_{jr} c_{kr})^2}{2\sigma^2}\right).$$

To maximize the above is equivalent to minimizing the negative log-likelihood,

$$\begin{aligned} \mathcal{L}_{cpd} &= \sum_n \sum_{ijk} (t_{ijk}^{(n)} - \sum_r x_r^{(n)} a_{ir} b_{jr} c_{kr})^2 \\ &= \sum_n \|\mathcal{T}^{(n)} - \sum_r x_r^{(n)} (\mathbf{a}_r \odot \mathbf{b}_r \odot \mathbf{c}_r)\|_F^2 \\ &= \sum_n \|\mathcal{T}^{(n)} - \llbracket \mathbf{x}^{(n)}, \mathbf{A}, \mathbf{B}, \mathbf{C} \rrbracket\|_F^2 \\ &= \|\mathcal{T} - \llbracket \mathbf{X}, \mathbf{A}, \mathbf{B}, \mathbf{C} \rrbracket\|_F^2. \end{aligned}$$

B The Two-sided Bound in Section 3.1

In Section 3.1 of the main paper, the self-supervised loss is calculated as follows.

$$\begin{aligned} \mathcal{L}_{ss} &= \mathcal{L}_{pos} + \lambda \mathcal{L}_{neg} \\ &= -\mathbb{E}[\text{sim}(\mathbf{f}(\mathcal{X}_p), \mathbf{f}(\mathcal{Y}_q)) \mid p = q] + \lambda \mathbb{E}[\text{sim}(\mathbf{f}(\mathcal{X}_p), \mathbf{f}(\mathcal{Y}_q)) \mid p \neq q] \\ &= \mathbb{E}\left[\frac{\lambda}{1 - c(\mathcal{X}_p)} \text{sim}(\mathbf{f}(\mathcal{X}_p), \mathbf{f}(\mathcal{Y}_q))\right] - \mathbb{E}\left[\left(\frac{\lambda c(\mathcal{X}_p)}{1 - c(\mathcal{X}_p)} + 1\right) \text{sim}(\mathbf{f}(\mathcal{X}_p), \mathbf{f}(\mathcal{Y}_q)) \mid p = q\right], \end{aligned}$$

where $\mathcal{X}_p, \mathcal{Y}_p$ are discrete random variables (of tensor samples) distributed as \mathcal{D}_p , $p \in \{1, \dots, M\}$, which is the sample distribution of class- p , and $c(\cdot)$ is a function over the tensor sample or the random variables, which outputs the class label rate (i.e., the probability of the latent class). Note that, if the input of $c(\cdot)$ is a tensor sample $\mathcal{T}^{(n)}$ or the input is \mathcal{X}_p , and p is fixed, then $c(\mathcal{T}^{(n)})$ or $c(\mathcal{X}_p)$ is fixed, otherwise, $c(\mathcal{X}_p)$ is also a random variable over p .

This section presents the details of how we transform the second term, $\mathbb{E}[\text{sim}(\mathbf{f}(\mathcal{X}_p), \mathbf{f}(\mathcal{Y}_q)) \mid p \neq q]$. Specifically, the expectation is taken over four different random variables, $p, q, \mathcal{X}_p, \mathcal{Y}_q$ (first we have two class indicator random variable: p and q , then we have two random variable $\mathcal{X}_p, \mathcal{Y}_q$ for samples in that specific class). Without loss of generality, we will remove the subscript under the expectation if it is taken over all random variables, otherwise, we specify the random variables in expectation subscript.

In the main paper, we use the results from the law of total probability, which states that if $\mathcal{T}^{(n)}$ is an arbitrary instance of random variable \mathcal{X}_p (where p is not given yet), then the law of total probability

will gives (according to the marginal probability),

$$\begin{aligned} \mathbb{E}_{q, \mathcal{Y}_q} [\text{sim}(\mathbf{f}(\mathcal{X}_p), \mathbf{f}(\mathcal{Y}_q)) \mid \mathcal{X}_p = \mathcal{T}^{(n)}, p \neq q] &= \frac{1}{1 - c(\mathcal{T}^{(n)})} \mathbb{E}_{q, \mathcal{Y}_q} [\text{sim}(\mathbf{f}(\mathcal{X}_p), \mathbf{f}(\mathcal{Y}_q)) \mid \mathcal{X}_p = \mathcal{T}^{(n)}] \\ &\quad - \frac{c(\mathcal{T}^{(n)})}{1 - c(\mathcal{T}^{(n)})} \mathbb{E}_{q, \mathcal{Y}_q} [\text{sim}(\mathbf{f}(\mathcal{X}_p), \mathbf{f}(\mathcal{Y}_q)) \mid \mathcal{X}_p = \mathcal{T}^{(n)}, p = q]. \end{aligned}$$

Then, we take expectation over the instance $\mathcal{T}^{(n)}$, which is equivalent to taking expectation over p and \mathcal{X}_p , yielding the result,

$$\begin{aligned} &\mathbb{E} [\text{sim}(\mathbf{f}(\mathcal{X}_p), \mathbf{f}(\mathcal{Y}_q)) \mid p \neq q] \\ &= -\mathbb{E} \left[\frac{c(\mathcal{X}_p)}{1 - c(\mathcal{X}_p)} \text{sim}(\mathbf{f}(\mathcal{X}_p), \mathbf{f}(\mathcal{Y}_q)) \mid p = q \right] + \mathbb{E} \left[\frac{1}{1 - c(\mathcal{X}_p)} \text{sim}(\mathbf{f}(\mathcal{X}_p), \mathbf{f}(\mathcal{Y}_q)) \right]. \end{aligned} \quad (17)$$

We substitute this result into the self-supervised loss, which yields the results (of Equation (5) in the main paper).

$$\begin{aligned} \mathcal{L}_{ss} &= -\mathbb{E} [\text{sim}(\mathbf{f}(\mathcal{X}_p), \mathbf{f}(\mathcal{Y}_q)) \mid p = q] + \lambda \mathbb{E} [\text{sim}(\mathbf{f}(\mathcal{X}_p), \mathbf{f}(\mathcal{Y}_q)) \mid p \neq q] \\ &= -\mathbb{E} [\text{sim}(\mathbf{f}(\mathcal{X}_p), \mathbf{f}(\mathcal{Y}_q)) \mid p = q] + \lambda \mathbb{E} \left[\frac{1}{1 - c(\mathcal{X}_p)} \text{sim}(\mathbf{f}(\mathcal{X}_p), \mathbf{f}(\mathcal{Y}_q)) \right] \\ &\quad - \lambda \mathbb{E} \left[\frac{c(\mathcal{X}_p)}{1 - c(\mathcal{X}_p)} \text{sim}(\mathbf{f}(\mathcal{X}_p), \mathbf{f}(\mathcal{Y}_q)) \mid p = q \right] \\ &= \mathbb{E} \left[\frac{\lambda}{1 - c(\mathcal{X}_p)} \text{sim}(\mathbf{f}(\mathcal{X}_p), \mathbf{f}(\mathcal{Y}_q)) \right] - \mathbb{E} \left[\left(\frac{\lambda c(\mathcal{X}_p)}{1 - c(\mathcal{X}_p)} + 1 \right) \text{sim}(\mathbf{f}(\mathcal{X}_p), \mathbf{f}(\mathcal{Y}_q)) \mid p = q \right]. \end{aligned} \quad (18)$$

Then, we let,

$$\mathcal{L}_{ss}^\Theta(\gamma) = (\gamma + 1) \mathbb{E} [\text{sim}(\mathbf{f}(\mathcal{X}_p), \mathbf{f}(\mathcal{Y}_q))] - \mathbb{E} [\text{sim}(\mathbf{f}(\mathcal{X}_p), \mathbf{f}(\mathcal{Y}_q)) \mid p = q]. \quad (19)$$

then, the following term can be bounded by

$$C_1 \mathcal{L}_{ss}^\Theta(0) \leq \mathbb{E} \left[\left(\frac{\lambda c(\mathcal{X}_p)}{1 - c(\mathcal{X}_p)} + 1 \right) \text{sim}(\mathbf{f}(\mathcal{X}_p), \mathbf{f}(\mathcal{Y}_q)) \right] - \mathbb{E} \left[\left(\frac{\lambda c(\mathcal{X}_p)}{1 - c(\mathcal{X}_p)} + 1 \right) \text{sim}(\mathbf{f}(\mathcal{X}_p), \mathbf{f}(\mathcal{Y}_q)) \mid p = q \right] \leq C_2 \mathcal{L}_{ss}^\Theta(0). \quad (20)$$

which is equivalent to

$$C_1 \mathcal{L}_{ss}^\Theta \left(\frac{\lambda - 1}{C_1} \right) \leq \mathcal{L}_{ss} \leq C_2 \mathcal{L}_{ss}^\Theta \left(\frac{\lambda - 1}{C_2} \right), C_1 = 1 + \max_{\mathcal{X}_p} \frac{\lambda c(\mathcal{X}_p)}{1 - c(\mathcal{X}_p)}, C_2 = 1 + \min_{\mathcal{X}_p} \frac{\lambda c(\mathcal{X}_p)}{1 - c(\mathcal{X}_p)},$$

since generally $\mathcal{L}_{ss}^\Theta(\gamma) \leq 0$ (otherwise, we can flip C_1 and C_2). It is easy to verify that when class labels are balanced, i.e., $c(\cdot) \equiv \frac{1}{M}$, where M is the number of latent classes, then $C_1 = C_2$ and the inequality in Equation (20) becomes an equality.

Alternative Proof. For the result in Equation (17), we provide an alternative (simpler) proof here.

$$\begin{aligned} &\mathbb{E} [\text{sim}(\mathbf{f}(\mathcal{X}_p), \mathbf{f}(\mathcal{Y}_q)) \mid p \neq q] \\ &= \sum_{p=1}^M c(\mathcal{X}_p) \sum_{q \neq p} \frac{c(\mathcal{Y}_q)}{1 - c(\mathcal{X}_p)} \mathbb{E}_{\mathcal{X}_p, \mathcal{Y}_q} [\text{sim}(\mathbf{f}(\mathcal{X}_p), \mathbf{f}(\mathcal{Y}_q))] \\ &= -\sum_{p=1}^M \frac{c(\mathcal{X}_p)c(\mathcal{Y}_p)}{1 - c(\mathcal{X}_p)} \mathbb{E}_{\mathcal{X}_p, \mathcal{Y}_p} [\text{sim}(\mathbf{f}(\mathcal{X}_p), \mathbf{f}(\mathcal{Y}_q))] + \sum_{p=1}^M \sum_{q=1}^M \frac{c(\mathcal{X}_p)c(\mathcal{Y}_q)}{1 - c(\mathcal{X}_p)} \mathbb{E}_{\mathcal{X}_p, \mathcal{Y}_q} [\text{sim}(\mathbf{f}(\mathcal{X}_p), \mathbf{f}(\mathcal{Y}_q))] \\ &= -\mathbb{E} \left[\frac{c(\mathcal{X}_p)}{1 - c(\mathcal{X}_p)} \text{sim}(\mathbf{f}(\mathcal{X}_p), \mathbf{f}(\mathcal{Y}_q)) \mid p = q \right] + \mathbb{E} \left[\frac{1}{1 - c(\mathcal{X}_p)} \text{sim}(\mathbf{f}(\mathcal{X}_p), \mathbf{f}(\mathcal{Y}_q)) \right]. \end{aligned}$$

C Proof of Theorem 1

We first state the well-known Hoeffding inequality.

Lemma 1 (Hoeffding Inequality). *Suppose Y_1, \dots, Y_n are n independent random variables such that*

$$P(Y_i \in [a_i, b_i]) = 1, \quad i \in [1, \dots, n].$$

Let $S_n = \sum_{i=1}^n Y_i$. Then for $t > 0$, we have,

$$P(|S_n - \mathbb{E}[S_n]| \geq t) \leq 2 \exp \left(-\frac{2t^2}{\sum_{i=1}^n (b_i - a_i)^2} \right).$$

Theorem 3. *Suppose N is the number of data samples. We have with probability $1 - \delta$,*

$$|\mathcal{L}_{ss}^\Theta - \tilde{\mathcal{L}}_{ss}^\Theta| < \sqrt{\left(1 + \frac{(\gamma+1)^2}{N-1}\right) \frac{2}{N} \log \frac{2}{\delta}}.$$

Proof. The proof for the Theorem is built on Lemma 1. Let

$$\begin{aligned} \{Y_i\}_{i \in [1, \dots, N(N-1)]} : & \left\{ \frac{\gamma+1}{N(N-1)} \left\langle \frac{\mathbf{x}^{(n)}}{\|\mathbf{x}^{(n)}\|_2}, \frac{\tilde{\mathbf{x}}^{(s)}}{\|\tilde{\mathbf{x}}^{(s)}\|_2} \right\rangle \right\}_{n \in [1, \dots, N], s \in [1, \dots, n-1, n+1, \dots, N]}, \\ \{Y_i\}_{i \in [N(N-1)+1, \dots, N^2]} : & \left\{ -\frac{1}{N} \left\langle \frac{\mathbf{x}^{(n)}}{\|\mathbf{x}^{(n)}\|_2}, \frac{\tilde{\mathbf{x}}^{(n)}}{\|\tilde{\mathbf{x}}^{(n)}\|_2} \right\rangle \right\}_{n \in [1, \dots, N]}. \end{aligned}$$

Then,

$$S_n = \tilde{\mathcal{L}}_{ss}^\Theta = \sum_{i=1}^{N^2} Y_i, \quad \mathbb{E}[S_n] = \mathcal{L}_{ss}^\Theta = \mathbb{E} \left[\sum_i^{N^2} Y_i \right],$$

$$\begin{aligned} \frac{\gamma+1}{N(N-1)} \min_n \left\langle \frac{\mathbf{x}^{(n)}}{\|\mathbf{x}^{(n)}\|_2}, \frac{\tilde{\mathbf{x}}^{(s)}}{\|\tilde{\mathbf{x}}^{(s)}\|_2} \right\rangle \leq Y_i \leq \frac{\gamma+1}{N(N-1)} \max_n \left\langle \frac{\mathbf{x}^{(n)}}{\|\mathbf{x}^{(n)}\|_2}, \frac{\tilde{\mathbf{x}}^{(s)}}{\|\tilde{\mathbf{x}}^{(s)}\|_2} \right\rangle, \quad i \in [1, \dots, N(N-1)], \\ -\frac{1}{N} \max_n \left\langle \frac{\mathbf{x}^{(n)}}{\|\mathbf{x}^{(n)}\|_2}, \frac{\tilde{\mathbf{x}}^{(n)}}{\|\tilde{\mathbf{x}}^{(n)}\|_2} \right\rangle \leq Y_i \leq -\frac{1}{N} \min_n \left\langle \frac{\mathbf{x}^{(n)}}{\|\mathbf{x}^{(n)}\|_2}, \frac{\tilde{\mathbf{x}}^{(n)}}{\|\tilde{\mathbf{x}}^{(n)}\|_2} \right\rangle, \quad i \in [N(N-1)+1, \dots, N^2]. \end{aligned}$$

According to Lemma 1,

$$P(|\mathcal{L}_{ss}^\Theta - \tilde{\mathcal{L}}_{ss}^\Theta| \geq t) \leq 2 \exp \left(-\frac{2t^2}{\sum_{i=1}^{N(N-1)} \left(\frac{(\gamma+1)D_2}{N(N-1)} \right)^2 + \sum_{i=N(N-1)+1}^{N^2} \left(\frac{D_1}{N} \right)^2} \right), \quad \forall t > 0, \quad (21)$$

where

$$\begin{aligned} D_1 &= \max_n \left\langle \frac{\mathbf{x}^{(n)}}{\|\mathbf{x}^{(n)}\|_2}, \frac{\tilde{\mathbf{x}}^{(n)}}{\|\tilde{\mathbf{x}}^{(n)}\|_2} \right\rangle - \min_n \left\langle \frac{\mathbf{x}^{(n)}}{\|\mathbf{x}^{(n)}\|_2}, \frac{\tilde{\mathbf{x}}^{(n)}}{\|\tilde{\mathbf{x}}^{(n)}\|_2} \right\rangle, \\ D_2 &= \max_{n \neq s} \left\langle \frac{\mathbf{x}^{(n)}}{\|\mathbf{x}^{(n)}\|_2}, \frac{\tilde{\mathbf{x}}^{(s)}}{\|\tilde{\mathbf{x}}^{(s)}\|_2} \right\rangle - \min_{n \neq s} \left\langle \frac{\mathbf{x}^{(n)}}{\|\mathbf{x}^{(n)}\|_2}, \frac{\tilde{\mathbf{x}}^{(s)}}{\|\tilde{\mathbf{x}}^{(s)}\|_2} \right\rangle. \end{aligned}$$

Using the choice,

$$t = \sqrt{D_1^2 + \frac{(\gamma+1)^2 D_2^2}{N-1}} \sqrt{\frac{1}{2N} \log \frac{2}{\delta}},$$

Equation (21) yields that with probability $1 - \delta$,

$$|\mathcal{L}_{ss}^\Theta - \tilde{\mathcal{L}}_{ss}^\Theta| < \sqrt{D_1^2 + \frac{(\gamma+1)^2 D_2^2}{N-1}} \sqrt{\frac{1}{2N} \log \frac{2}{\delta}}.$$

Further, we provide a looser but more succinct upper bound. Using $0 \leq D_1, D_2 \leq 2$, we obtain,

$$\sqrt{D_1^2 + \frac{(\gamma+1)^2 D_2^2}{N-1}} \sqrt{\frac{1}{2N} \log \frac{2}{\delta}} < \sqrt{\left(1 + \frac{(\gamma+1)^2}{N-1}\right) \frac{2}{N} \log \frac{2}{\delta}}, \quad (22)$$

which completes the proof. \square

D Proof and Experimental Insights of Theorem 2

D.1 Proof and Application of the Theorem

We first prove the following theorem and then explain how to apply it to the iterative rule.

Theorem 4. *Given non-zero vectors, $\mathbf{v}_1, \mathbf{v}_2, \mathbf{u}^0 \in \mathbb{R}^d$, where \mathbf{v}_1 is not parallel to \mathbf{v}_2 and $\beta > 0$. The sequence $\{\mathbf{u}^t\}$, generated by the recursion, $\mathbf{u}^{t+1} = \mathbf{v}_1 - \frac{\beta}{\|\mathbf{u}^t\|_2} \mathbf{v}_2$, satisfies,*

$$\|\mathbf{u}^{t+1} - \mathbf{u}^*\|_2 \leq \frac{\beta \|\mathbf{v}_2\|_2}{\|\mathbf{v}_1\|_2^2 - \langle \mathbf{v}_1, \frac{\mathbf{v}_2}{\|\mathbf{v}_2\|_2} \rangle^2} \|\mathbf{u}^t - \mathbf{u}^*\|_2, \quad (23)$$

where $\mathbf{u}^* = \mathbf{v}_1 - \frac{\beta}{\|\mathbf{u}^*\|_2} \mathbf{v}_2$, is the stationary point.

Proof.

$$\begin{aligned} \|\mathbf{u}^{t+1} - \mathbf{u}^*\|_2 &= \left\| \left(\mathbf{v}_1 - \frac{\beta}{\|\mathbf{u}^t\|_2} \mathbf{v}_2 \right) - \left(\mathbf{v}_1 - \frac{\beta}{\|\mathbf{u}^*\|_2} \mathbf{v}_2 \right) \right\|_2 \\ &= \left\| \beta \mathbf{v}_2 \frac{\|\mathbf{u}^t\|_2 - \|\mathbf{u}^*\|_2}{\|\mathbf{u}^*\|_2 \|\mathbf{u}^t\|_2} \right\|_2 \leq \frac{\beta \|\mathbf{v}_2\|_2}{\|\mathbf{u}^*\|_2 \|\mathbf{u}^t\|_2} \|\mathbf{u}^t - \mathbf{u}^*\|_2. \end{aligned}$$

The proof is complete, since

$$\frac{1}{\|\mathbf{u}^*\|_2 \|\mathbf{u}^t\|_2} \leq \frac{1}{\min_t \left\| \mathbf{v}_1 - \frac{\beta}{\|\mathbf{u}^t\|_2} \mathbf{v}_2 \right\|_2^2} \leq \frac{1}{\min_{h \in \mathbb{R}} \|\mathbf{v}_1 - h \mathbf{v}_2\|_2^2} = \frac{1}{\|\mathbf{v}_1\|_2^2 - \langle \mathbf{v}_1, \frac{\mathbf{v}_2}{\|\mathbf{v}_2\|_2} \rangle^2}. \quad (24)$$

□

Now, let us write down the closed-form solution of the least squares problem in Equation (14) of the main text,

$$\mathbf{X}_{\text{impr}}^l = \mathbf{V}_1 - \beta D(\mathbf{X}_{\text{init}}^l) \mathbf{V}_2, \quad (25)$$

where (the iterative rule is for one size- b data batch),

$$D(\mathbf{X}_{\text{init}}^l) = \text{diag} \left(\frac{1}{\|\mathbf{x}_{\text{init}}^{l(1)}\|_2}, \dots, \frac{1}{\|\mathbf{x}_{\text{init}}^{l(b)}\|_2} \right), \quad (26)$$

$$\mathbf{V}_1 = \mathbf{T}_1^l (\mathbf{A}^l \odot \mathbf{B}^l \odot \mathbf{C}^l) (\mathbf{A}^{l\top} \mathbf{A}^l * \mathbf{B}^{l\top} \mathbf{B}^l * \mathbf{C}^{l\top} \mathbf{C}^l + \alpha \mathbf{I})^{-1}, \quad (27)$$

$$\mathbf{V}_2 = \mathbf{G} D(\tilde{\mathbf{X}}_{\text{init}}^l) \tilde{\mathbf{X}}_{\text{init}}^l (\mathbf{A}^{l\top} \mathbf{A}^l * \mathbf{B}^{l\top} \mathbf{B}^l * \mathbf{C}^{l\top} \mathbf{C}^l + \alpha \mathbf{I})^{-1}. \quad (28)$$

\mathbf{V}_1 and \mathbf{V}_2 are fixed matrices. We can decompose the matrix iterative rule in Equation (25) into a row-wise version, since the iterative rule of each row is independent. Specifically, for the n -th row vector of Equation (25), we have

$$\mathbf{x}_{\text{impr}}^{l(n)} = \mathbf{v}_1^{(n)} - \frac{\beta}{\|\mathbf{x}_{\text{init}}^{l(n)}\|_2} \mathbf{v}_2^{(n)},$$

where $\mathbf{x}_{\text{impr}}^{l(n)}, \mathbf{v}_1^{(n)}, \mathbf{x}_{\text{init}}^{l(n)}, \mathbf{v}_2^{(n)}$ are the n -th row vector of $\mathbf{X}_{\text{impr}}^l, \mathbf{V}_1, \mathbf{X}_{\text{init}}^l, \mathbf{V}_2$, respectively. Then, the original iterative rule reduces to the vector iterative rule in the theorem.

Remark. As for the condition stated in the theorem. First, it is trivial to assume that when applying the iterative rules, $\mathbf{x}_{\text{impr}}^{l(n)}, \mathbf{v}_1^{(n)}, \mathbf{v}_2^{(n)}$ are non-zero vectors, since $\mathcal{T}^l, \tilde{\mathcal{T}}^l$ are dense. Second, it is also trivial to assume that when applying the iterative rules, $\mathbf{v}_1^{(n)}$ and $\mathbf{v}_2^{(n)}$ are not parallel. Even if they are parallel, the L2 norm of $\mathbf{v}_1^{(n)}$ is much larger than the L2 norm of $\mathbf{v}_2^{(n)}$ by definition. Thus, by choosing a suitable β , the denominator of Equation (24) can still be bounded, which completes the theorem without the requirement of " $\mathbf{v}_1^{(n)}$ and $\mathbf{v}_2^{(n)}$ are not parallel". Finally, $\beta > 0$ is naturally satisfied when we define our objective in the main text.

The choice of β . In this theorem, the denominator of the convergence rate of Equation (23) is quadratic to the L2 norm of $\mathbf{v}_1^{(n)}$. As we stated above, the L2 norm of $\mathbf{v}_1^{(n)}$ can be obviously much larger than L2 norm of $\mathbf{v}_2^{(n)}$. Thus, to ensure the linear convergence, β should be chosen from a large range, e.g., $\left(0, \frac{\|\mathbf{v}_1\|_2^2 - \langle \mathbf{v}_1, \frac{\mathbf{v}_2}{\|\mathbf{v}_2\|_2} \rangle^2}{\|\mathbf{v}_2\|_2^2}\right)$ (see the effect of β in Figure 4 when $\beta = 2$). We show an ablation study on β in Appendix E.

D.2 One Round of the Iterative Rule is Sufficient

Settings of the Study. Now, we study how many rounds of the iterative rules are needed to achieve a good classification result.

We first clarify that the "iterative rule" is different from "iteration" in our paper. An "iteration" (e.g., the l -th iteration) means five optimization steps (cold start, auxiliary step, three main steps) for one data batch, while one round of the "iterative rule" means applying Equation (14) in the main paper once, which is part of the auxiliary step.

This study is conducted on HAR with all data and Sleep-EDF with 50,000 random unlabeled data, 5,000 random training samples, and all test samples. The experiments are taken over five random seeds.

First, we study the convergence speed (when $\beta = 2$). We consider two scenarios: (i) before the iteration, when the bases $\{\mathbf{A}, \mathbf{B}, \mathbf{C}\}$ are initialized as random matrices; (ii) after the iteration, when the good based $\{\mathbf{A}, \mathbf{B}, \mathbf{C}\}$ are already learned. We use the average relative difference (of the F-norm) as the convergence measure, i.e., $\frac{1}{N} \sum_{n=1}^N \frac{\|\mathbf{x}_{t+1}^{l(n)} - \mathbf{x}_t^{l(n)}\|_2}{\|\mathbf{x}_t^{l(n)}\|} = \frac{1}{N} \sum_{n=1}^N \frac{\|\mathbf{x}_{\text{impr}}^{l(n)} - \mathbf{x}_{\text{init}}^{l(n)}\|}{\|\mathbf{x}_{\text{init}}^{l(n)}\|}$, where t means the number of rounds of the iterative rule. We test on $t = 1, 2, 3, 4, 8$. The comparison is shown in Figure 4. Both scenarios verify the linear convergence speed (when the difference values are too small, it may not change, like in Scenario 2 on HAR, or exceed the minimum precision and go to zero (like Scenario 2 on Sleep-EDF)).

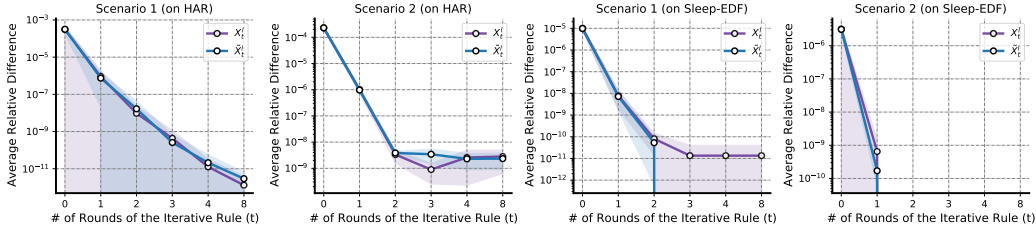


Figure 4: Verification of Convergence Speed. When t becomes larger, the difference could be unchanged (like in Scenario 2 on HAR) or exceed the minimum precision and go to zero (like Scenario 2 on Sleep-EDF).

Next, we consider the performance of downstream classification with different rounds of iterative rules, i.e., the accuracy and time per sweep (including the computation of metrics). The results are shown in Table 3 and 4.

Table 3: Performance with Different Rounds of Iterative Rules (on HAR)

# of rounds (t)	1	2	3	4	8
time per sweep	8.608s	10.121s	11.012s	12.540s	17.073s
accuracy (%)	93.45 ± 0.395	93.49 ± 0.169	93.46 ± 0.146	93.46 ± 0.115	93.46 ± 0.115

We observe that with an increasing number of # of rounds of iterative rule, the classification results will not improve further (in fact, we find 4 rounds of iterative rules give the same results as 8 rounds of iterative rules if the batch order is the same, which means it already converges), however, the time consumption increases. Thus, we use only one round of the iterative rule in our experiments.

Table 4: Performance with Different Rounds of Iterative Rules (on Sleep-EDF)

# of rounds (t)	1	2	3	4	8
time per sweep	45.698s	48.925s	52.361s	56.193s	71.386s
accuracy (%)	87.47 \pm 0.209	87.43 \pm 0.173	87.38 \pm 0.178	87.39 \pm 0.177	87.39 \pm 0.177

E Additional Information for Experiments

E.1 Data Processing and Implementations

Dataset Processing. *Sleep-EDF* is collected during an age effect study on sleep healthy Caucasians performed in 1987-1991. The age of the patients ranges from 25 to 101, and the patient was taking non sleep-related medications. The dataset contains 153 full-night EEG (from Fpz-Cz and Pz-Oz electrode locations), EOG (horizontal), and submental chin EMG recordings. This dataset is under Open Data Commons Attribution License v1.0; *MGH Sleep* is provided by (Biswal et al., 2018) and sleep laboratory at Massachusetts General Hospital (MGH), where six EEG channels (i.e., F3-M2, F4-M1, C3-M2, C4-M1, O1-M2, O2-M1) are used for sleep staging recorded at 200.0 Hz frequency. After filtering out mismatched signals and missing labels, we finally get 6,478 recordings. These two datasets are processed in a similar way. First, the raw data are (long) recordings of each subject. On subject-level, these recordings are categorized into unlabeled and labeled sets by 90% : 10%. Then the labeled sets are further separated into training and test by 5% : 5%. Next, within each set (unlabeled, training, test), recordings are further segmented into disjoint 30-second-long periods, called *epochs* (note that the "epoch" has different meanings here, not the same as in deep learning), which are the data samples in our study. Here, for a fair comparison, we do not consider the dependency between epochs, and they are assumed i.i.d. samples. Each signal epoch is a matrix, *channel by timestamp*, and they have the same size. Every epoch is associated with one of five sleep stages, Awake (W), Non-REM stage 1 (N1), Non-REM stage 2 (N2), Non-REM stage 3 (N3), and REM stage (R). The stage assignments obtained by clinicians are published along with the datasets, and we use them as class labels.

Human Activity Recognition (HAR) is carried out with a group of volunteers within an age bracket of 19-48 years. Each person performed six activities (walking, walking upstairs, walking downstairs, sitting, standing, laying) wearing a smartphone on the waist. The data is collected as 3-axial linear acceleration and 3-axial angular velocity at a constant rate of 50Hz by the embedded accelerometer and gyroscope. The action labels are published along with the dataset. The obtained dataset has been randomly partitioned into 70% and 30%. We use 70% as the unlabeled data (we remove their labels) and split the other part: 15% as training data and 15% as the test data. The license of this dataset is included in their citation. *PTB-XL* is a large publicly available electrocardiography dataset from Physikalisch Technische Bundesanstalt (PTB). It contains 21,837 clinical 12-lead ECGs (male: 11,379 and female: 10,458) of 10-second length with a sampling frequency of 500 Hz. We randomly split the dataset into unlabeled (remove the labels) and labeled sets by 90% : 10%; then the labeled sets are further separated into training and test by 5% : 5%. This dataset is under Open BSD 3.0.

All datasets are de-identified (e.g., no names, no locations), and there is no offensive content. All the labels are also provided along with the datasets. The label distributions are shown below.

Table 5: Class Label Distribution

Name	Label Distribution
Sleep-EDF	W: 68.8%, N1: 5.2%, N2: 16.6%, N3: 3.2%, R: 6.2%
HAR	Walk: 16.72%, Walk upstairs: 14.99%, Walk downstairs: 13.65%, Sit: 17.25%, Stand: 18.51%, Lay: 18.88%
PTB-XL	Male: 52.11%, Female: 47.89%
MGH Sleep	W: 44.3%, N1: 9.9%, N2: 14.4%, N3: 17.6%, R: 13.8%

STFT Transform. We find that directly using the spatial information does not provide good results, even for the deep learning models. Thus, we consider extracting information from the frequency domain as one step of data preprocessing. We take Short-Time Fourier Transforms (STFT) for each input data sample. From a single channel, we can extract both the amplitude and phase information, which is then stacked together as two different channels. After STFT, each data sample becomes a three-order tensor, *channel by frequency by timestamp*. The FFT size is 256 and hop length is 32 for

Sleep-EDF, data sample format: $14 \times 129 \times 86$; the FFT size is 64 and hop length is 2 for HAR, data sample format: $18 \times 33 \times 33$; the FFT size is 256 and hop length is 64 for PTB-XL, data sample format: $24 \times 129 \times 75$; and the FFT size is 512 and hop length is 128 for MGH, data sample format: $12 \times 257 \times 43$. We use these third-order tensors as final input data samples for all models.

Data Augmentation. As mentioned in the main text, we consider four different augmentation methods: (i) *Jittering* adds additional perturbations to each sample as one step of data processing. We consider both high and low-frequency noise on each channel independently. For high-frequency noise, we first generate a noisy sequence s , which has the same length as the signal channel, and each element of s is i.i.d. sampled from a uniform distribution $U[-1, 1]$. We then control the amplitude of the noisy sequence by the noisy degree $d \in \mathbb{R}$. Finally, we add the scaled noisy sequence ds to the channel. In the experiment, $d = 0.05$ for Sleep-EDF, $d = 0.002$ for HAR, $d = 0.001$ for PTB-XL and $d = 0.01$ for MGH. For low-frequency noise, we generate a short noisy sequence ($\frac{1}{100}$ length of the channel) in the same way and then use `scipy.interpolate.interp1d` to interpolate the noisy sequence to be at the same length as the channel. The choice of high-frequency noise or low-frequency noise, or both are coin-tossed with equal probability. (ii) *Bandpass filtering* reduces signal noise. We use the order-1 Butterworth filter by `scipy.signal.butter` to preserve only the within-band frequency information. The high-pass and low-pass are $(1Hz, 30Hz)$ and $(10Hz, 49Hz)$ for Sleep-EDF, $(1Hz, 20Hz)$ and $(5Hz, 24.5Hz)$ for HAR, $(1Hz, 30Hz)$ and $(10Hz, 50Hz)$ for PTB-XL, $(1Hz, 30Hz)$ and $(10Hz, 50Hz)$ for MGH. Low-pass or high-pass or both are selected with equal probability. Also, the bandpass filtering is applied to each channel independently. (iii) *time rotation*. We split one epoch (i.e., data sample) randomly into two pieces and then resemble two pieces in reverse order. The time rotation is conducted for each channel simultaneously. (iv) *3D position rotation* is an augmentation technique used only for HAR datasets, which have x-y-z axis information from accelerometer and gyroscope sensors. We apply a 3D x-y-z coordinate system rotation by a rotation matrix to mimic different cellphone positions. The first three augmentation techniques are shown in Figure 5, and the 3D position rotation example is borrowed from ² in Figure 6.

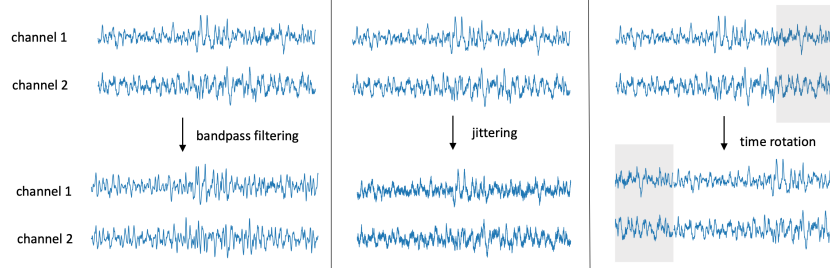


Figure 5: The First Three Augmentation Methods. The upper figures are the original multi-channel signals, while the lower figures are the transformed data.

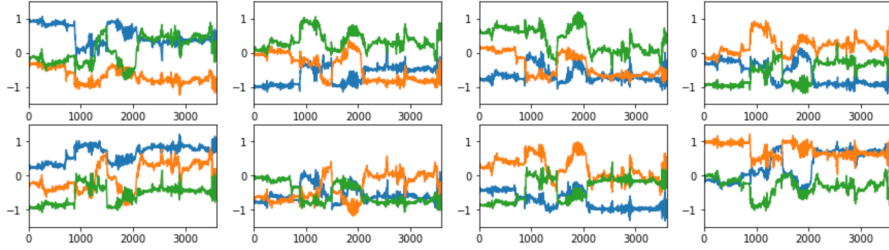


Figure 6: 3D Position Rotation (Examples). Four upper figures are the original x-y-z signal data, while the lower figures are the transformed channel data by some random rotation matrices.

Note that the data augmentations are applied to signal epochs, and the augmentation methods are selected with equal probability. The STFT is performed after the data augmentation.

²<https://github.com/terryum/Data-Augmentation-For-Wearable-Sensor-Data>

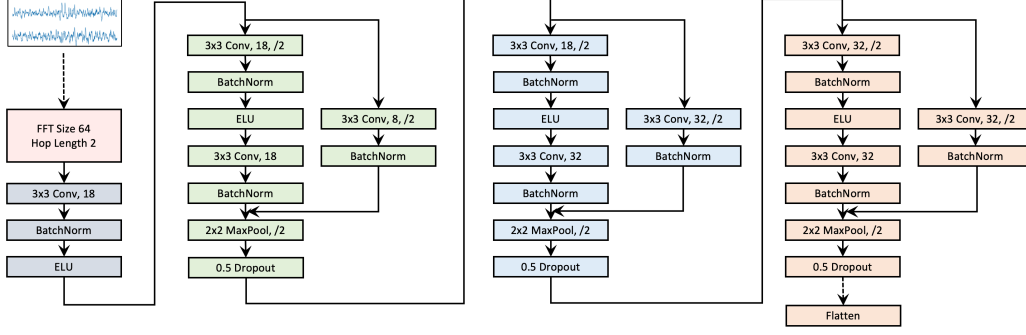


Figure 7: Backbone CNN Architecture. This is the backbone model for HAR, the backbone architecture of other three datasets are very similar with different configurations, e.g., FFT size, hop length, channel numbers.

Implementation. Since all deep learning baselines are based on CNN, we use the same backbone model, shown in Figure 7. The model is adopted from (Cheng et al., 2020). Based on the backbone model, we add a fully connected layer for a supervised model, add non-linear layers for self-supervised models (they also have their respective loss), and add corresponding deconvolutional layers for autoencoder models. The supervised models map raw signal epochs directly to the labels, and they are trained on the training set; other baselines learn a low-dimensional feature extractor from an unlabeled set, and then a logistic classifier is trained on the training set, on top of the feature extractor. Without loss of generality, we use 128 as batch size. For supervised models, we set max sweep/epoch 100, and for unsupervised models, we set max sweep/epoch 50. For deep learning models, we use Adam optimizer with a learning rate 1×10^{-3} and weight decaying 5×10^{-4} . We use 2×10^{-3} as the learning rate for our ATD. Since the paper deals with unsupervised learning and uses standard logistic regression (*sklearn.linear_model.LogisticRegression*) to evaluate, the hyperparameters of all models (except supervised model) are chosen based on the classification performance on the training data. If the unsupervised feature extractor learns well (i.e., train logistic regression model on training data and test also on training data and get high accuracy score), then the set of hyperparameters are considered good. The hyperparameters of the supervised models are the same as self-supervised models since they share the same backbone. For our ATD model, by default, we use $R = 32$, $\alpha = 1 \times 10^{-3}$, $\beta = 2$, $\gamma = b$, which is batch size, and the reference configurations (i.e., command line arguments) for each experiments are listed in code appendix.

E.2 Comparison Between ATD and Fast CPD on Other Datasets

The main paper shows the comparison between our ATD with the Fast CPD model on MGH. This section shows the results on the other three datasets: Sleep-EDF, HAR, and PTB-XL. To allow the GPU to hold the whole tensor, for Sleep-EDF, we use 7,000 unlabeled samples to form the objective, and use 5,000 training samples and all test data for classification. For HAR, we use all data. For PTB-XL, we use 4,000 unlabeled samples to form the objective, and use all training samples and all test data for classification. We provide the results in Figure 8, Figure 9, and Figure 10.

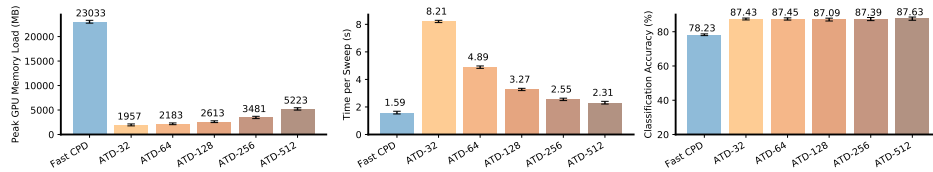


Figure 8: Performance Comparison on Sleep-EDF (7,000 Unlabeled Samples)

E.3 Representation Structure in 2D: Our ATD vs Fast CPD Model

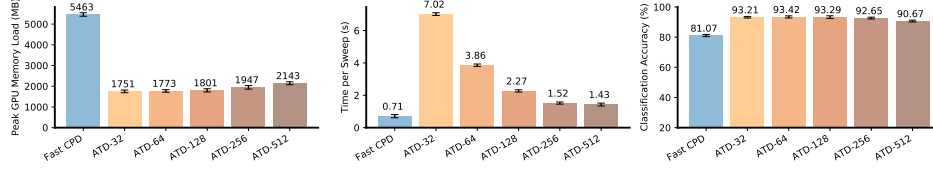


Figure 9: Performance Comparison on HAR (7,352 Unlabeled Samples)

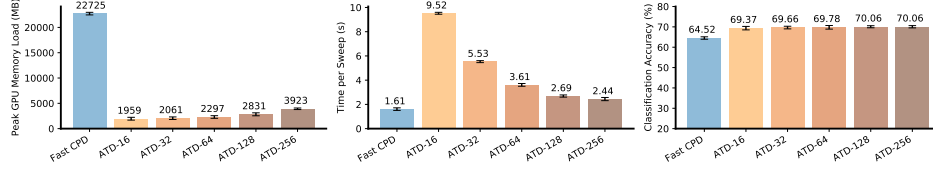


Figure 10: Performance Comparison on PTB-XL (4,000 Unlabeled Samples)

To provide a qualitative evaluation of the representation structure generated by the CPD model and our ATD, we project the learned coefficient vectors to 2D space by the TSNE (Van der Maaten and Hinton, 2008). These experiments are done with MGH dataset. Specifically, we load the learned bases $\{A, B, C\}$ from the Fast CPD model and our ATD-128 in Section 4.1. Then, we randomly picked 2,500 samples from the test set for each class (5 in total) and extract their low-rank features. After TSNE projection, we further color each point by the class label for visualization purposes.

From Figure 11, we find that the two models give similar representation structures, e.g., class W and R are far away, while N1, N2, N3 stages are gathered. This phenomenon accords with the transition patterns of human sleep: between the awake stage (W) and deep sleep (R), individuals will go through the transition stages (N1, N2, N3). This means that both models learned meaningful information. By comparison, our ATD clearly presents a more separable pattern, while for the Fast CPD model, we find that N1, N2, N3, and R stages are largely mixed, which explains its poor classification results.

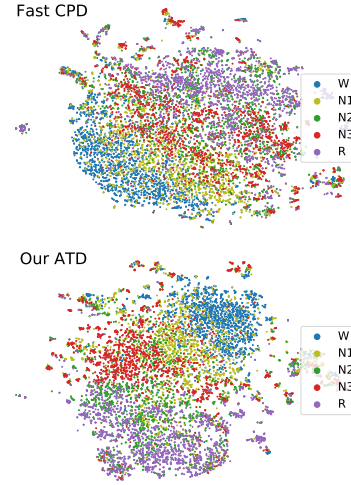


Figure 11: 2D Representation

E.4 Effect of Data Augmentation

We also study the effects of data augmentation methods. Let us assume (a): *jittering*, (b): *bandpass filtering*, (c): *time rotation*, (d): *3D position rotation*. We test on different combinations of the augmentation methods. The experiments are conducted on two datasets: (i) for the MGH dataset, we use 50,000 unlabeled data, 5,000 training samples, and all test samples; (ii) for the HAR dataset, we use all data. We use 128 as the batch size for MGH Sleep, 64 for SHHS, and $R = 32$ as the tensor rank.

Table 6: Ablation Studies on Data Augmentation (MGH Sleep)

Method	Acc (%)	Method	Acc (%)	Method	Acc (%)
A	72.53 \pm 0.652	A+B	73.60 \pm 0.270	A+B+C	73.98 \pm 0.203
B	72.24 \pm 0.267	A+C	73.69 \pm 0.581	/	/
C	73.50 \pm 0.319	B+C	73.60 \pm 0.460	/	/

Table 7: Ablation Studies on Data Augmentation (HAR)

Method	Acc (%)	Method	Acc (%)	Method	Acc (%)	Method	Acc (%)
A	91.84 ± 0.465	A+B	92.74 ± 0.166	B+D	92.99 ± 0.423	A+C+D	93.03 ± 0.671
B	92.94 ± 0.387	A+C	92.29 ± 0.210	C+D	92.36 ± 0.279	B+C+D	92.78 ± 0.139
C	91.77 ± 0.315	A+D	92.70 ± 0.164	A+B+C	92.74 ± 0.453	A+B+C+D	93.31 ± 0.149
D	92.18 ± 0.195	B+C	92.20 ± 0.528	A+B+D	92.92 ± 0.582	/	/

Table 6 and Table 7 conclude that the augmentation methods influence the final classification results. However, for different datasets, the effects are different. We observe that for the MGH Sleep dataset, time rotation (method C) works better than other methods. In HAR, some individual augmentations work better than their combinations (e.g., applying B solely is better than applying A+B). Overall, we find that with more diverse data augmentation methods, the final results are relatively better. The study of how to choose/design better augmentation techniques will be our future work.

E.5 Effect of the Decomposition Rank R and Hyperparameters

This section conducts ablation studies for decomposition rank R and other hyperparameters, α , β , γ . The experiments are conducted on Sleep-EDF with 50,000 random unlabeled data, 5,000 random training samples, and all test samples, and HAR dataset with all data.

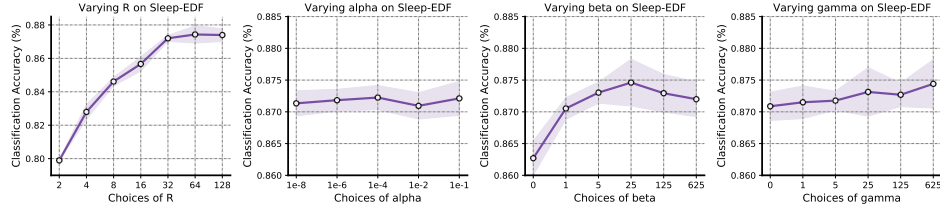


Figure 12: Ablation Studies on Sleep-EDF

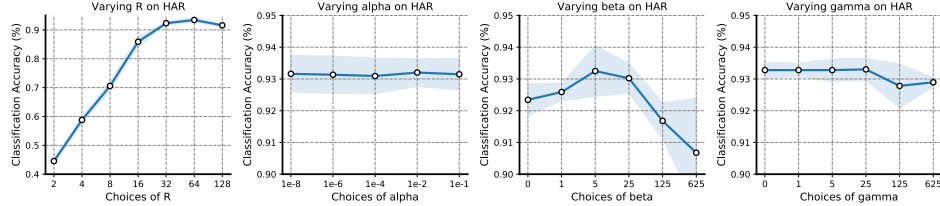


Figure 13: Ablation Studies on HAR.

The results are shown in Figure 12 and Figure 13. First, we can conclude that with a larger decomposition rank R , the performance will be better generally. Though we observe that the performance worsens from $R = 64$ to $R = 128$, with limited training data, if the representation size (equals to R) becomes larger, the logistic regression model can overfit. Also, we find that the choices of α and γ do not affect the final performance a lot. Finally, we find that the accuracy score first increases then decreases with an increasing value of β . The reason might be that a large β will negatively affect the fitness loss.

F Convergence Analysis With Moving Average Setting

F.1 Convergence Theorem

In the appendix, we prove the (in expectation, local) convergence of our optimization algorithm with a moving average setting. This theoretical result is largely adopted from a recent theoretical work on stochastic alternating least squares (Cao et al., 2020). We present the convergence theorem and then

outline a proof sketch first. Note that, to simplify the derivations, we reduce the loss function by $\frac{1}{2}$, which does not affect the algorithm or the proof.

Theorem 5. Assume the learning rate be harmonic, i.e., η^l decreases at the rate of $O(\frac{1}{l})$; (ii) the following moving average step is applied in the beginning of each batch,

$$\mathcal{T}^l \leftarrow \eta^l * \mathcal{T}^l + (1 - \eta^l) * \mathcal{T}^{l-1}, \quad \tilde{\mathcal{T}}^l \leftarrow \eta^l * \tilde{\mathcal{T}}^l + (1 - \eta^l) * \tilde{\mathcal{T}}^{l-1}.$$

Then, the sequence $\{\mathbf{A}^l, \mathbf{B}^l, \mathbf{C}^l\}$ generated by Algorithm 1 satisfies

$$\lim_{l \rightarrow \infty} \mathbb{E} \left[\|\nabla_{\mathbf{A}} \mathcal{L}(\mathcal{T}, \tilde{\mathcal{T}}; \mathbf{A}^l, \mathbf{B}^l, \mathbf{C}^l)\|_F^2 \right] = 0,$$

where \mathcal{L} is defined in Equation (8) in main paper. Symmetrically, the above also holds for $\nabla_{\mathbf{B}}$ and $\nabla_{\mathbf{C}}$.

Definition 1 (Base Sets). We use \mathcal{S} to store the base sets in different scenarios. First, if we only consider two generic sets, then we use

$$\mathcal{S} = \{\mathbf{A}, \mathbf{B}, \mathbf{C}\} \text{ and } \mathcal{S}' = \{\mathbf{A}', \mathbf{B}', \mathbf{C}'\}. \quad (29)$$

If we consider the order and iterations, then we use

$$\mathcal{S}^{l,0} = \{\mathbf{A}^l, \mathbf{B}^l, \mathbf{C}^l\} \text{ and } \mathcal{S}^{l,1} = \{\mathbf{A}^{l+1}, \mathbf{B}^l, \mathbf{C}^l\} \text{ and } \mathcal{S}^{l,2} = \{\mathbf{A}^{l+1}, \mathbf{B}^{l+1}, \mathbf{C}^l\}, \quad (30)$$

where we have $\mathcal{S}^{l+1,0} = \mathcal{S}^{l,3}$.

Definition 2 (Gradient and Hessian). We use the following notation to represent the gradient w.r.t. \mathbf{A} , given the tensor and the augmented tensor $\mathcal{T}, \tilde{\mathcal{T}}$ and the base set $\mathcal{S} = \{\mathbf{A}, \mathbf{B}, \mathbf{C}\}$.

$$\begin{aligned} \mathbf{G}_1(\mathcal{T}; \mathcal{S}) &= \nabla_{\mathbf{A}} \mathcal{L}(\mathcal{T}, \tilde{\mathcal{T}}; \mathcal{S}) = \mathbf{A}[\Pi(\mathbf{X}, \mathbf{B}, \mathbf{C}) + \Pi(\tilde{\mathbf{X}}, \mathbf{B}, \mathbf{C}) + \alpha \mathbf{I}] \\ &\quad - [\mathbf{T}_2 \text{KR}(\mathbf{X}, \mathbf{B}, \mathbf{C}) + \tilde{\mathbf{T}}_2 \text{KR}(\tilde{\mathbf{X}}, \mathbf{B}, \mathbf{C})], \end{aligned}$$

where \mathbf{T}_2 is the unfolding of tensor \mathcal{T} along the second mode, $\{\mathbf{X}, \tilde{\mathbf{X}}\}$ are the outputs of the Auxiliary Step from $\mathcal{T}, \tilde{\mathcal{T}}, \mathcal{S}$.

We use the following notation to represent the Hessian w.r.t. \mathbf{A} , given the tensor and the augmented tensor $\mathcal{T}, \tilde{\mathcal{T}}$ and the base set \mathcal{S} ,

$$\mathbf{H}_1(\mathcal{T}; \mathcal{S}) = \nabla_{\mathbf{A}}^2 \mathcal{L}(\mathcal{T}, \tilde{\mathcal{T}}; \mathcal{S}) = \Pi(\mathbf{X}, \mathbf{B}, \mathbf{C}) + \Pi(\tilde{\mathbf{X}}, \mathbf{B}, \mathbf{C}) + \alpha \mathbf{I}.$$

where $\{\mathbf{X}, \tilde{\mathbf{X}}\}$ are the outputs of the Auxiliary Step from $\mathcal{T}, \tilde{\mathcal{T}}, \mathcal{S}$.

Note that, for both the gradient and the Hessian, $\mathcal{T}, \tilde{\mathcal{T}}$ could be either the whole tensor or for tensor batches, which we use notation $\mathcal{T}^l, \tilde{\mathcal{T}}^l$.

The notational conventions we used are listed in Table 8.

Table 8: Auxiliary symbols used in the proof

Symbols	Definition
$\text{KR}(\mathbf{A}^{(1)}, \dots, \mathbf{A}^{(K)})$	$\mathbf{A}^{(1)} \odot \dots \odot \mathbf{A}^{(K)}$ (Khatra-Rao product)
$\Pi(\mathbf{A}^{(1)}, \dots, \mathbf{A}^{(K)})$	$\text{KR}(\mathbf{A}^{(1)}, \dots, \mathbf{A}^{(K)})^\top \text{KR}(\mathbf{A}^{(1)}, \dots, \mathbf{A}^{(K)})$
$\mathbf{G}_k(\mathcal{T}; \mathcal{S}), k = [1, 2, 3]$	the matrix-formed gradient w.r.t. $\mathbf{A}, \mathbf{B}, \mathbf{C}$, separately, defined in Definition 2
$\mathbf{H}_k(\mathcal{T}; \mathcal{S}), k = [1, 2, 3]$	the matrix-formed Hessian w.r.t. $\mathbf{A}, \mathbf{B}, \mathbf{C}$, separately, defined in Definition 2
$\ \mathbf{A}^{(1)}, \dots, \mathbf{A}^{(K)}\ _F$	$\sqrt{\ \mathbf{A}^{(1)}\ _F^2 + \dots + \ \mathbf{A}^{(K)}\ _F^2}$
$M_i, C_i, i \in [1, 2, \dots]$	they are all real-valued constants
b, N	b is the batch size, N is the size of the dataset

F.2 Proof Sketch

The flow of our proof is based on (Cao et al., 2020). We adopt some lemmas from this work to fit our settings, while we also propose several new lemmas to complete the proof.

(1) Our assumption:

- a. We assume the learning rate at the l -th batch/iteration satisfies $\frac{C_{min}}{l} \leq \eta^l \leq \frac{C_{max}}{l}$, $0 \leq C_{min} < C_{max} < \infty$ and the regularization parameter $\alpha \in \mathbb{R}^+$.
- b. We assume the data batches are i.i.d. sampled from the dataset.
- c. We assume the Frobenius norm of the intermediate factors and the tensor batches are bounded.

$$\max_l \left\{ \|\mathbf{X}\|_F, \|\tilde{\mathbf{X}}\|_F, \|\mathbf{A}\|_F, \|\mathbf{B}\|_F, \|\mathbf{C}\|_F, \|\mathcal{T}^l\|_F, \|\tilde{\mathcal{T}}^l\|_F \right\} < M, \quad \exists 0 < M < +\infty.$$

- (2) (Lemma 3) We prove that the F-norm of Khatri-Rao product is C_3 -Lipschitz continuous to the F-norm of difference of the factors, e.g.,

$$\|\text{KR}(\mathbf{A}, \mathbf{B}, \mathbf{C}) - \text{KR}(\mathbf{A}', \mathbf{B}', \mathbf{C}')\|_F \leq C_3 \|\mathbf{A} - \mathbf{A}', \mathbf{B} - \mathbf{B}', \mathbf{C} - \mathbf{C}'\|_F.$$

- (3) (Lemma 4) We use result (2) to prove that the F-norm of self-product of Khatri-Rao product is C_4 -Lipschitz continuous to the F-norm of the difference of the factors, e.g.,

$$\|\Pi(\mathbf{A}, \mathbf{B}, \mathbf{C}) - \Pi(\mathbf{A}', \mathbf{B}', \mathbf{C}')\|_F \leq C_4 \|\mathbf{A} - \mathbf{A}', \mathbf{B} - \mathbf{B}', \mathbf{C} - \mathbf{C}'\|_F.$$

- (4) (Lemma 5) At the l -th batch/iteration, given the same bases, two different set of tensors $\{\mathcal{T}^j, \tilde{\mathcal{T}}^j\}, \{\mathcal{T}^k, \tilde{\mathcal{T}}^k\}$ would yield two sets of coefficient matrices, separately, denoted as $\{\mathbf{X}^j, \tilde{\mathbf{X}}^j\}, \{\mathbf{X}^k, \tilde{\mathbf{X}}^k\}$. We use result (2) and (3) to prove that they are bounded by the learning rate, e.g.,

$$\|\mathbf{X}^j - \mathbf{X}^k\|_F \leq C_5 \eta^l \quad \text{and} \quad \|\tilde{\mathbf{X}}^j - \tilde{\mathbf{X}}^k\|_F \leq C_6 \eta^l.$$

- (5) (Lemma 6) Given the same tensor batch, two different set of bases, $\{\mathbf{A}, \mathbf{B}, \mathbf{C}\}, \{\mathbf{A}', \mathbf{B}', \mathbf{C}'\}$, would yield two sets of coefficient matrices, separately, denoted as $\{\mathbf{X}, \tilde{\mathbf{X}}\}, \{\mathbf{X}', \tilde{\mathbf{X}}'\}$. We use result (2) and (3) to prove that they are bounded by the F-norm of the difference of the base sets, e.g.,

$$\begin{aligned} \|\mathbf{X} - \mathbf{X}'\|_F &\leq C_7 \|\mathbf{A} - \mathbf{A}', \mathbf{B} - \mathbf{B}', \mathbf{C} - \mathbf{C}'\|_F \\ \|\tilde{\mathbf{X}} - \tilde{\mathbf{X}}'\|_F &\leq C_8 \|\mathbf{A} - \mathbf{A}', \mathbf{B} - \mathbf{B}', \mathbf{C} - \mathbf{C}'\|_F. \end{aligned}$$

- (6) (Lemma 7) For two different base sets, given the same set of tensors (i.e., the batch data and the augmented data), we use the results from (2)(3)(5) to prove that the gradient and the Newton step is bounded by the F-norm of the difference of the base sets, e.g., for the first basis factor \mathbf{A} ,

$$\begin{aligned} \|\mathbf{G}_1 - \mathbf{G}'_1\|_F &\leq C_9 \|\mathbf{A} - \mathbf{A}', \mathbf{B} - \mathbf{B}', \mathbf{C} - \mathbf{C}'\|_F. \\ \|\mathbf{G}_1 \mathbf{H}_1^{-1} - \mathbf{G}'_1 \mathbf{H}_1'^{-1}\|_F &\leq C_{10} \|\mathbf{A} - \mathbf{A}', \mathbf{B} - \mathbf{B}', \mathbf{C} - \mathbf{C}'\|_F. \end{aligned}$$

- (7) (Lemma 8) For the l -th batch, given two different set of tensors $\{\mathcal{T}^j, \tilde{\mathcal{T}}^j\}, \{\mathcal{T}^k, \tilde{\mathcal{T}}^k\}$, we use the results from (2)(3)(4) to prove that the gradient and the Newton step is bounded by the learning rate, e.g., for the first basis factor \mathbf{A} ,

$$\begin{aligned} \|\mathbf{G}_1^j - \mathbf{G}_1^k\|_F &\leq C_{11} \eta^l. \\ \|\mathbf{G}_1^j \mathbf{H}_1^{j-1} - \mathbf{G}_1^k \mathbf{H}_1^{k-1}\|_F &\leq C_{12} \eta^l. \end{aligned}$$

- (8) (Lemma 9) We know that in first-order SGD, the gradient of a batch is equal to the gradient of all data samples, in expectation, given the historical data \mathcal{H}^l , i.e., $\mathbb{E}_j [\mathbf{G}_1(\mathcal{T}^j; \mathcal{S}^{l,0}) - \frac{b}{N} \mathbf{G}_1(\mathcal{T}; \mathcal{S}^{l,0})] = \mathbf{0}$. Since our objective function grows linearly with the number of samples, we use a factor $\frac{b}{N}$ to rescale the gradient, where N is the overall sample size and b is the batch size. In our second-order method, we use (6) to prove that this second-order quantity decreases at the same speed of the learning rate, e.g.,

$$\mathbb{E} \left[\left\| \left(\mathbf{G}_1(\mathcal{T}^j; \mathcal{S}^{l,0}) - \frac{b}{N} \mathbf{G}_1(\mathcal{T}; \mathcal{S}^{l,0}) \right) \mathbf{H}_1^{-1}(\mathcal{T}^j; \mathcal{S}^{l,0}) \right\|_F \right] \leq C_{13} \eta^l.$$

- (9) We consider the following lemma and let $a^l = \eta^l$ be our learning rate and $b^l = \mathbb{E} [\|\nabla_{\mathbf{A}} \mathcal{L}(\mathcal{T}, \tilde{\mathcal{T}}; \mathbf{A}^l, \mathbf{B}^l, \mathbf{C}^l)\|_F^2] = \mathbb{E} [\|\mathbf{G}_1(\mathcal{T}; \mathcal{S}^{l,0})\|_F^2]$ be the expected gradient Frobenius-norm.

Lemma 2. Let $(a^l)_{l \geq 1}$ and $(b^l)_{l \geq 1}$ be two non-negative real sequences such that the series $\sum_{l=1}^{\infty} a^l$ diverges, the series $\sum_{l=1}^{\infty} a^l b^l$ converges, and there exists $K > 0$ such that $|b^{l+1} - b^l| \leq K a^l$. Then, the sequence $(b^l)_{l \geq 1}$ converges to 0.

- (10) If we can show that three conditions in Lemma 2 are all satisfied, then we can complete the convergence proof of our theorem. We will show that
- a. $\sum_l a^l$ diverges (given by that it is a harmonic sequence),
 - b. $\sum_l a^l b^l \leq Q_1 + Q_2 + Q_3$, and Q_i , $i = [1, 2, 3]$ are bounded, among which the bound of Q_1, Q_2 is given by (8),
 - c. $|b^{l+1} - b^l| \leq K a^l$ (by using result (4)).

F.3 Assumptions and Lemmas

Learning Rate Assumption. Let us use $\frac{C_{min}}{l} \leq \eta^l \leq \frac{C_{max}}{l}$, $0 \leq C_{min} < C_{max} < \infty$, as the learning rate for the l -th iteration.

Samples are i.i.d. Let us assume the samples in each data batch are i.i.d. samples from the dataset.

Boundness on Data. We assume the Frobenius norm of the intermediate factors and the tensor batches are bounded.

Lemma 3. (Adopted from Lemma 3.1 in (Cao et al., 2020)) For two factor sets $\{\mathbf{X}, \tilde{\mathbf{X}}, \mathbf{A}, \mathbf{B}, \mathbf{C}\}$ and $\{\mathbf{X}', \tilde{\mathbf{X}}', \mathbf{A}', \mathbf{B}', \mathbf{C}'\}$, there exists a constant, $0 \leq C_3 < \infty$, such that for any three factors, e.g., $\mathbf{A}, \mathbf{B}, \mathbf{C}$, we have

$$\|\text{KR}(\mathbf{A}, \mathbf{B}, \mathbf{C}) - \text{KR}(\mathbf{A}', \mathbf{B}', \mathbf{C}')\|_F \leq C_3 \|\mathbf{A} - \mathbf{A}', \mathbf{B} - \mathbf{B}', \mathbf{C} - \mathbf{C}'\|_F.$$

Proof. By using triangle inequality of Frobenius norm, we have (adding and subtracting terms)

$$\begin{aligned} & \|\text{KR}(\mathbf{A}, \mathbf{B}, \mathbf{C}) - \text{KR}(\mathbf{A}', \mathbf{B}', \mathbf{C}')\|_F \\ &= \|\text{KR}(\mathbf{A}, \mathbf{B}, \mathbf{C}) - \text{KR}(\mathbf{A}', \mathbf{B}, \mathbf{C}) + \text{KR}(\mathbf{A}', \mathbf{B}, \mathbf{C}) - \text{KR}(\mathbf{A}', \mathbf{B}', \mathbf{C}') + \text{KR}(\mathbf{A}', \mathbf{B}', \mathbf{C}') - \text{KR}(\mathbf{A}', \mathbf{B}', \mathbf{C}')\|_F \\ &\leq \|\text{KR}(\mathbf{A}, \mathbf{B}, \mathbf{C}) - \text{KR}(\mathbf{A}', \mathbf{B}, \mathbf{C})\|_F + \|\text{KR}(\mathbf{A}', \mathbf{B}, \mathbf{C}) - \text{KR}(\mathbf{A}', \mathbf{B}', \mathbf{C}')\|_F + \|\text{KR}(\mathbf{A}', \mathbf{B}', \mathbf{C}') - \text{KR}(\mathbf{A}', \mathbf{B}', \mathbf{C}')\|_F. \end{aligned} \quad (31)$$

We show how to bound the first term, the derivations for the last two terms are similar.

$$\begin{aligned} & \|\text{KR}(\mathbf{A}, \mathbf{B}, \mathbf{C}) - \text{KR}(\mathbf{A}', \mathbf{B}, \mathbf{C})\|_F = \|\text{KR}(\mathbf{A} - \mathbf{A}', \mathbf{B}, \mathbf{C})\|_F \\ &= \|[(\mathbf{a}_1 - \mathbf{a}'_1) \odot \mathbf{b}_1 \odot \mathbf{c}_1, \dots, (\mathbf{a}_R - \mathbf{a}'_R) \odot \mathbf{b}_R \odot \mathbf{c}_R]\|_F \\ &= \sqrt{\|(\mathbf{a}_1 - \mathbf{a}'_1) \odot \mathbf{b}_1 \odot \mathbf{c}_1\|_2^2 + \dots + \|(\mathbf{a}_R - \mathbf{a}'_R) \odot \mathbf{b}_R \odot \mathbf{c}_R\|_2^2} \\ &\leq \sum_{r=1}^R \|(\mathbf{a}_r - \mathbf{a}'_r) \odot \mathbf{b}_r \odot \mathbf{c}_r\|_2 = \sum_{r=1}^R \|\mathbf{a}_r - \mathbf{a}'_r\|_2 \|\mathbf{b}_r\|_2 \|\mathbf{c}_r\|_2 \end{aligned} \quad (32)$$

$$\leq \sum_{r=1}^R \|\mathbf{a}_r - \mathbf{a}'_r\|_2 \frac{\|\mathbf{b}_r\|_2^2 + \|\mathbf{c}_r\|_2^2}{2} \leq \sum_{r=1}^R \|\mathbf{a}_r - \mathbf{a}'_r\|_2 \cdot M_1 \leq R \|\mathbf{A} - \mathbf{A}'\|_F \cdot M_1, \quad (33)$$

where $\mathbf{a}_r, \mathbf{b}_r, \mathbf{c}_r$ are column vectors. We use

$$M_1 = \max_r \{\|\mathbf{x}_r\|_2^2, \|\tilde{\mathbf{x}}_r\|_2^2, \|\mathbf{a}_r\|_2^2, \|\mathbf{b}_r\|_2^2, \|\mathbf{c}_r\|_2^2, \|\mathbf{x}'_r\|_2^2, \|\tilde{\mathbf{x}}'_r\|_2^2, \|\mathbf{a}'_r\|_2^2, \|\mathbf{b}'_r\|_2^2, \|\mathbf{c}'_r\|_2^2\}. \quad (34)$$

From Equation (32) to (33), we use geometric-arithmetic inequality, and within Equation (33), we use $\|\mathbf{a}_r - \mathbf{a}'_r\|_2 \leq \|\mathbf{A} - \mathbf{A}'\|_F$, $\forall r$. Similarly, we have.

$$\|\text{KR}(\mathbf{A}', \mathbf{B}, \mathbf{C}) - \text{KR}(\mathbf{A}', \mathbf{B}', \mathbf{C}')\|_F \leq R \|\mathbf{B} - \mathbf{B}'\|_F \cdot M_1 \quad (35)$$

$$\|\text{KR}(\mathbf{A}', \mathbf{B}', \mathbf{C}) - \text{KR}(\mathbf{A}', \mathbf{B}', \mathbf{C}')\|_F \leq R \|\mathbf{C} - \mathbf{C}'\|_F \cdot M_1 \quad (36)$$

Thus, we let $C_3 = 3RM_1$. By summing them up, we get

$$\begin{aligned} \|\text{KR}(\mathbf{A}, \mathbf{B}, \mathbf{C}) - \text{KR}(\mathbf{A}', \mathbf{B}', \mathbf{C}')\|_F &\leq RM_1 (\|\mathbf{A} - \mathbf{A}'\|_F + \|\mathbf{B} - \mathbf{B}'\|_F + \|\mathbf{C} - \mathbf{C}'\|_F) \\ &\leq 3RM_1 \|\mathbf{A} - \mathbf{A}', \mathbf{B} - \mathbf{B}', \mathbf{C} - \mathbf{C}'\|_F. \end{aligned} \quad (37)$$

Here, R is the decomposition rank. \square

Lemma 4. (Adopted from Corollary 3.2 in (Cao et al., 2020)) For two factor sets $\{\mathbf{X}, \tilde{\mathbf{X}}, \mathbf{A}, \mathbf{B}, \mathbf{C}\}$ and $\{\mathbf{X}', \tilde{\mathbf{X}}', \mathbf{A}', \mathbf{B}', \mathbf{C}'\}$, there exists a constant, $0 \leq C_4 < \infty$, such that for any three factors, e.g., $\mathbf{A}, \mathbf{B}, \mathbf{C}$, we have

$$\|\Pi(\mathbf{A}, \mathbf{B}, \mathbf{C}) - \Pi(\mathbf{A}', \mathbf{B}', \mathbf{C}')\|_F \leq C_4 \|\mathbf{A} - \mathbf{A}', \mathbf{B} - \mathbf{B}', \mathbf{C} - \mathbf{C}'\|_F. \quad (38)$$

Proof. We add and subtract terms and use triangular inequality,

$$\begin{aligned} & \|\Pi(\mathbf{A}, \mathbf{B}, \mathbf{C}) - \Pi(\mathbf{A}', \mathbf{B}', \mathbf{C}')\|_F \\ &= \|\text{KR}(\mathbf{A}, \mathbf{B}, \mathbf{C})^\top \text{KR}(\mathbf{A}, \mathbf{B}, \mathbf{C}) - \text{KR}(\mathbf{A}', \mathbf{B}', \mathbf{C}')^\top \text{KR}(\mathbf{A}', \mathbf{B}', \mathbf{C}')\|_F \\ &= \|\text{KR}(\mathbf{A}, \mathbf{B}, \mathbf{C})^\top (\text{KR}(\mathbf{A}, \mathbf{B}, \mathbf{C}) - \text{KR}(\mathbf{A}', \mathbf{B}', \mathbf{C}')) + (\text{KR}(\mathbf{A}, \mathbf{B}, \mathbf{C}) - \text{KR}(\mathbf{A}', \mathbf{B}', \mathbf{C}'))^\top \text{KR}(\mathbf{A}', \mathbf{B}', \mathbf{C}')\|_F \\ &\leq \|\text{KR}(\mathbf{A}, \mathbf{B}, \mathbf{C})\|_F \|\text{KR}(\mathbf{A}, \mathbf{B}, \mathbf{C}) - \text{KR}(\mathbf{A}', \mathbf{B}', \mathbf{C}')\|_F + \|\text{KR}(\mathbf{A}, \mathbf{B}, \mathbf{C}) - \text{KR}(\mathbf{A}', \mathbf{B}', \mathbf{C}')\|_F \|\text{KR}(\mathbf{A}', \mathbf{B}', \mathbf{C}')\|_F. \end{aligned} \quad (39)$$

We show how to bound the first term, the derivations for the last term is similar. The proof is based on Lemma 3,

$$\|\text{KR}(\mathbf{A}, \mathbf{B}, \mathbf{C}) - \text{KR}(\mathbf{A}', \mathbf{B}', \mathbf{C}')\|_F \leq C_3 \|\mathbf{A} - \mathbf{A}', \mathbf{B} - \mathbf{B}', \mathbf{C} - \mathbf{C}'\|_F. \quad (40)$$

In Lemma 3, we let the second factor sets to be the all-zero set, so we have the following result

$$\|\text{KR}(\mathbf{A}, \mathbf{B}, \mathbf{C})\|_F \leq C_3 \|\mathbf{A}, \mathbf{B}, \mathbf{C}\|_F \leq C_3 \|\mathbf{X}, \tilde{\mathbf{X}}, \mathbf{A}, \mathbf{B}, \mathbf{C}\|_F. \quad (41)$$

Thus, by substituting this result into the above inequality, Lemma 4 can be proved with

$$C_4 = (C_3)^2 \max\{\|\mathbf{X}, \tilde{\mathbf{X}}, \mathbf{A}, \mathbf{B}, \mathbf{C}\|_F + \|\mathbf{X}', \tilde{\mathbf{X}}', \mathbf{A}', \mathbf{B}', \mathbf{C}'\|_F\}. \quad (42)$$

□

Lemma 5. For the l -th batch, given the same base set $\{\mathbf{A}^l, \mathbf{B}^l, \mathbf{C}^l\}$, two different pairs of tensor and augmented tensor batch, $\{\mathbf{T}^j, \tilde{\mathbf{T}}^j\}$ and $\{\mathbf{T}^k, \tilde{\mathbf{T}}^k\}$ yield two different coefficient sets $\{\mathbf{X}^j, \tilde{\mathbf{X}}^j\}$, $\{\mathbf{X}^k, \tilde{\mathbf{X}}^k\}$, separately (these correspond to the output of Auxiliary Step). Then, there exist $0 \leq C_5, C_6 < \infty$, such that

$$\|\mathbf{X}^j - \mathbf{X}^k\|_F \leq C_5 \eta^l \quad \text{and} \quad \|\tilde{\mathbf{X}}^j - \tilde{\mathbf{X}}^k\|_F \leq C_6 \eta^l. \quad (43)$$

Proof. This bound states that if the l -th data batch is different, then the difference of the outputs of the *Auxiliary Step* will be bounded by the learning rate. Since the role of \mathbf{X} and $\tilde{\mathbf{X}}$ are identical, we only prove for \mathbf{X} , and similar derivations can be applied to prove for $\tilde{\mathbf{X}}$.

Bounds on Cold Start. First, considering the moving average setting for the *Cold Start*, we have the closed-form solutions (of the least squares problem Equation (11)(12) of the main paper) for the initial guesses. (only the first term is different),

$$\mathbf{X}_{\text{init}}^j = (\eta^l * \mathbf{T}_1^j + (1 - \eta^l) * \mathbf{T}_1^{l-1}) \text{KR}(\mathbf{A}^l, \mathbf{B}^l, \mathbf{C}^l) (\Pi(\mathbf{A}^l, \mathbf{B}^l, \mathbf{C}^l) + \alpha \mathbf{I})^{-1}, \quad (44)$$

$$\mathbf{X}_{\text{init}}^k = (\eta^l * \mathbf{T}_1^k + (1 - \eta^l) * \mathbf{T}_1^{l-1}) \text{KR}(\mathbf{A}^l, \mathbf{B}^l, \mathbf{C}^l) (\Pi(\mathbf{A}^l, \mathbf{B}^l, \mathbf{C}^l) + \alpha \mathbf{I})^{-1}. \quad (45)$$

where \mathbf{T}_i^j is the unfolded tensor of \mathcal{T}^j along the i -th mode. Then, the difference of these two initial guesses are bounded,

$$\|\mathbf{X}_{\text{init}}^j - \mathbf{X}_{\text{init}}^k\|_F = \left\| \eta^l (\mathbf{T}_1^j - \mathbf{T}_1^k) \text{KR}(\mathbf{A}^l, \mathbf{B}^l, \mathbf{C}^l) (\Pi(\mathbf{A}^l, \mathbf{B}^l, \mathbf{C}^l) + \alpha \mathbf{I})^{-1} \right\|_F \quad (46)$$

$$\leq \eta^l \|\mathbf{T}_1^j - \mathbf{T}_1^k\|_F \|\text{KR}(\mathbf{A}^l, \mathbf{B}^l, \mathbf{C}^l)\|_F \left\| (\Pi(\mathbf{A}^l, \mathbf{B}^l, \mathbf{C}^l) + \alpha \mathbf{I})^{-1} \right\|_F. \quad (47)$$

Similarly, the difference of two initial guesses of $\tilde{\mathbf{X}}$ are bounded,

$$\|\tilde{\mathbf{X}}_{\text{init}}^j - \tilde{\mathbf{X}}_{\text{init}}^k\|_F \leq \eta^l \|\tilde{\mathbf{T}}_1^j - \tilde{\mathbf{T}}_1^k\|_F \|\text{KR}(\mathbf{A}^l, \mathbf{B}^l, \mathbf{C}^l)\|_F \left\| (\Pi(\mathbf{A}^l, \mathbf{B}^l, \mathbf{C}^l) + \alpha \mathbf{I})^{-1} \right\|_F. \quad (48)$$

We let,

$$M_2 = \max_{j,k,l} \left\{ \|\mathbf{T}_1^j - \mathbf{T}_1^k\|_F \|\text{KR}(\mathbf{A}^l, \mathbf{B}^l, \mathbf{C}^l)\|_F \left\| (\Pi(\mathbf{A}^l, \mathbf{B}^l, \mathbf{C}^l) + \alpha \mathbf{I})^{-1} \right\|_F \right\},$$

such that,

$$\|\mathbf{X}_{\text{init}}^j - \mathbf{X}_{\text{init}}^k\|_F \leq M_2 \eta^l \quad \text{and} \quad \|\tilde{\mathbf{X}}_{\text{init}}^j - \tilde{\mathbf{X}}_{\text{init}}^k\|_F \leq M_2 \eta^l. \quad (49)$$

Bounds on Auxiliary Step. For now, we derive the bounds for the difference between the outputs of the *Auxiliary Step*. We have the closed-form solutions (of the least squares problem in main text Equation (14)) for the improved guesses,

$$\begin{aligned} \mathbf{X}_{\text{impr}}^j &= \left[(\eta^l * \mathbf{T}_1^j + (1 - \eta^l) * \mathbf{T}_1^{l-1}) \text{KR}(\mathbf{A}^l, \mathbf{B}^l, \mathbf{C}^l) - \beta D(\mathbf{X}_{\text{init}}^j) \mathbf{G} D(\tilde{\mathbf{X}}_{\text{init}}^j) \tilde{\mathbf{X}}_{\text{init}}^j \right] (\Pi(\mathbf{A}^l, \mathbf{B}^l, \mathbf{C}^l) + \alpha \mathbf{I})^{-1}, \\ \mathbf{X}_{\text{impr}}^k &= \left[(\eta^l * \mathbf{T}_1^k + (1 - \eta^l) * \mathbf{T}_1^{l-1}) \text{KR}(\mathbf{A}^l, \mathbf{B}^l, \mathbf{C}^l) - \beta D(\mathbf{X}_{\text{init}}^k) \mathbf{G} D(\tilde{\mathbf{X}}_{\text{init}}^k) \tilde{\mathbf{X}}_{\text{init}}^k \right] (\Pi(\mathbf{A}^l, \mathbf{B}^l, \mathbf{C}^l) + \alpha \mathbf{I})^{-1}. \end{aligned}$$

Thus, the difference of the improved guesses is bounded by

$$\begin{aligned} \|\mathbf{X}_{\text{impr}}^j - \mathbf{X}_{\text{impr}}^k\|_F &\leq \|\mathbf{X}_{\text{init}}^j - \mathbf{X}_{\text{init}}^k\|_F \\ &\quad + \beta \left\| D(\mathbf{X}_{\text{init}}^j) \mathbf{G} D(\tilde{\mathbf{X}}_{\text{init}}^j) \tilde{\mathbf{X}}_{\text{init}}^j - D(\mathbf{X}_{\text{init}}^k) \mathbf{G} D(\tilde{\mathbf{X}}_{\text{init}}^k) \tilde{\mathbf{X}}_{\text{init}}^k \right\|_F \left\| \left(\Pi(\mathbf{A}^l, \mathbf{B}^l, \mathbf{C}^l) + \alpha \mathbf{I} \right)^{-1} \right\|_F \end{aligned} \quad (50)$$

Let us consider the following bound for the second term (we add and subtract terms and apply triangular inequality),

$$\begin{aligned} &\left\| D(\mathbf{X}_{\text{init}}^j) \mathbf{G} D(\tilde{\mathbf{X}}_{\text{init}}^j) \tilde{\mathbf{X}}_{\text{init}}^j - D(\mathbf{X}_{\text{init}}^k) \mathbf{G} D(\tilde{\mathbf{X}}_{\text{init}}^k) \tilde{\mathbf{X}}_{\text{init}}^k \right\|_F \\ &\leq \left\| D(\mathbf{X}_{\text{init}}^j) \mathbf{G} D(\tilde{\mathbf{X}}_{\text{init}}^j) \tilde{\mathbf{X}}_{\text{init}}^j - D(\mathbf{X}_{\text{init}}^k) \mathbf{G} D(\tilde{\mathbf{X}}_{\text{init}}^j) \tilde{\mathbf{X}}_{\text{init}}^j \right\|_F \\ &\quad + \left\| D(\mathbf{X}_{\text{init}}^k) \mathbf{G} D(\tilde{\mathbf{X}}_{\text{init}}^j) \tilde{\mathbf{X}}_{\text{init}}^j - D(\mathbf{X}_{\text{init}}^k) \mathbf{G} D(\tilde{\mathbf{X}}_{\text{init}}^k) \tilde{\mathbf{X}}_{\text{init}}^j \right\|_F \\ &\quad + \left\| D(\mathbf{X}_{\text{init}}^k) \mathbf{G} D(\tilde{\mathbf{X}}_{\text{init}}^k) \tilde{\mathbf{X}}_{\text{init}}^j - D(\mathbf{X}_{\text{init}}^k) \mathbf{G} D(\tilde{\mathbf{X}}_{\text{init}}^k) \tilde{\mathbf{X}}_{\text{init}}^k \right\|_F \\ &\leq \left\| D(\mathbf{X}_{\text{init}}^j) - D(\mathbf{X}_{\text{init}}^k) \right\|_F \|\mathbf{G}\|_F \left\| D(\tilde{\mathbf{X}}_{\text{init}}^j) \right\|_F \left\| \tilde{\mathbf{X}}_{\text{init}}^j \right\|_F \\ &\quad + \left\| D(\tilde{\mathbf{X}}_{\text{init}}^j) - D(\tilde{\mathbf{X}}_{\text{init}}^k) \right\|_F \left\| D(\mathbf{X}_{\text{init}}^k) \right\|_F \|\mathbf{G}\|_F \left\| \tilde{\mathbf{X}}_{\text{init}}^j \right\|_F \\ &\quad + \left\| \tilde{\mathbf{X}}_{\text{init}}^j - \tilde{\mathbf{X}}_{\text{init}}^k \right\|_F \left\| D(\mathbf{X}_{\text{init}}^k) \right\|_F \|\mathbf{G}\|_F \left\| D(\tilde{\mathbf{X}}_{\text{init}}^k) \right\|_F. \end{aligned} \quad (51)$$

where we have

$$\begin{aligned} \left\| D(\mathbf{X}_{\text{init}}^j) - D(\mathbf{X}_{\text{init}}^k) \right\|_F &= \left\| \begin{bmatrix} \frac{1}{\|\mathbf{X}_{\text{init}}^{j(1)}\|_2} & & \\ & \ddots & \\ & & \frac{1}{\|\mathbf{X}_{\text{init}}^{j(b)}\|_2} \end{bmatrix} - \begin{bmatrix} \frac{1}{\|\mathbf{X}_{\text{init}}^{k(1)}\|_2} & & \\ & \ddots & \\ & & \frac{1}{\|\mathbf{X}_{\text{init}}^{k(b)}\|_2} \end{bmatrix} \right\|_F \\ &= \left\| \begin{bmatrix} \frac{\|\mathbf{X}_{\text{init}}^{k(1)}\|_2 - \|\mathbf{X}_{\text{init}}^{j(1)}\|_2}{\|\mathbf{X}_{\text{init}}^{j(1)}\|_2 \|\mathbf{X}_{\text{init}}^{k(1)}\|_2} & & \\ & \ddots & \\ & & \frac{\|\mathbf{X}_{\text{init}}^{k(b)}\|_2 - \|\mathbf{X}_{\text{init}}^{j(b)}\|_2}{\|\mathbf{X}_{\text{init}}^{j(b)}\|_2 \|\mathbf{X}_{\text{init}}^{k(b)}\|_2} \end{bmatrix} \right\|_F \leq \left\| \begin{bmatrix} \frac{\|\mathbf{X}_{\text{init}}^{k(1)} - \mathbf{X}_{\text{init}}^{j(1)}\|_2}{\|\mathbf{X}_{\text{init}}^{j(1)}\|_2 \|\mathbf{X}_{\text{init}}^{k(1)}\|_2} & & \\ & \ddots & \\ & & \frac{\|\mathbf{X}_{\text{init}}^{k(b)} - \mathbf{X}_{\text{init}}^{j(b)}\|_2}{\|\mathbf{X}_{\text{init}}^{j(b)}\|_2 \|\mathbf{X}_{\text{init}}^{k(b)}\|_2} \end{bmatrix} \right\|_F \\ &\leq \left\| \begin{bmatrix} \frac{\|\mathbf{X}^k - \mathbf{X}^j\|_F}{\|\mathbf{X}_{\text{init}}^{j(1)}\|_2 \|\mathbf{X}_{\text{init}}^{k(1)}\|_2} & & \\ & \ddots & \\ & & \frac{\|\mathbf{X}^k - \mathbf{X}^j\|_F}{\|\mathbf{X}_{\text{init}}^{j(b)}\|_2 \|\mathbf{X}_{\text{init}}^{k(b)}\|_2} \end{bmatrix} \right\|_F = \left\| \mathbf{X}_{\text{init}}^j - \mathbf{X}_{\text{init}}^k \right\|_F \left\| D(\mathbf{X}_{\text{init}}^j) * D(\mathbf{X}_{\text{init}}^k) \right\|_F. \end{aligned} \quad (52)$$

We plug the result of Equation (52) into Equation (51) and let

$$\begin{aligned} M_3 &= \max_j \{ \|\mathbf{G}\|_F \|D(\tilde{\mathbf{X}}_{\text{init}}^j)\|_F \|\tilde{\mathbf{X}}_{\text{init}}^j\|_F \|D(\mathbf{X}_{\text{init}}^j) * D(\mathbf{X}_{\text{init}}^k)\|_F \}, \\ M_4 &= \max_{j,k} \{ \|D(\mathbf{X}_{\text{init}}^k)\|_F \|\mathbf{G}\|_F \|\tilde{\mathbf{X}}_{\text{init}}^j\|_F \|D(\tilde{\mathbf{X}}_{\text{init}}^j) * D(\tilde{\mathbf{X}}_{\text{init}}^k)\|_F \}, \\ M_5 &= \max_k \{ \|D(\mathbf{X}_{\text{init}}^k)\|_F \|\mathbf{G}\|_F \|D(\tilde{\mathbf{X}}_{\text{init}}^k)\|_F \}, \end{aligned}$$

and then, we can bound Equation (51),

$$\begin{aligned} & \left\| D(\mathbf{X}_{\text{init}}^j) \mathbf{G} D(\tilde{\mathbf{X}}_{\text{init}}^j) \tilde{\mathbf{X}}_{\text{init}}^j - D(\mathbf{X}_{\text{init}}^k) \mathbf{G} D(\tilde{\mathbf{X}}_{\text{init}}^k) \tilde{\mathbf{X}}_{\text{init}}^k \right\|_F \\ & \leq M_3 \left\| \mathbf{X}_{\text{init}}^j - \mathbf{X}_{\text{init}}^k \right\|_F + (M_4 + M_5) \left\| \tilde{\mathbf{X}}_{\text{init}}^j - \tilde{\mathbf{X}}_{\text{init}}^k \right\|_F. \end{aligned} \quad (53)$$

We plug this result into Equation (50), which yields,

$$\begin{aligned} \|\mathbf{X}_{\text{impr}}^j - \mathbf{X}_{\text{impr}}^k\|_F & \leq \|\mathbf{X}_{\text{init}}^j - \mathbf{X}_{\text{init}}^k\|_F \\ & + \left(M_3 \left\| \mathbf{X}_{\text{init}}^j - \mathbf{X}_{\text{init}}^k \right\|_F + (M_4 + M_5) \left\| \tilde{\mathbf{X}}_{\text{init}}^j - \tilde{\mathbf{X}}_{\text{init}}^k \right\|_F \right) \left\| (\Pi(\mathbf{A}^l, \mathbf{B}^l, \mathbf{C}^l) + \alpha \mathbf{I})^{-1} \right\|_F. \end{aligned}$$

Given the results in Equation (49), we let

$$C_5 = M_2 + M_2(M_3 + M_4 + M_5) \max_l \left\{ \left\| (\Pi(\mathbf{A}^l, \mathbf{B}^l, \mathbf{C}^l) + \alpha \mathbf{I})^{-1} \right\|_F \right\}, \quad (54)$$

which gives,

$$\|\mathbf{X}_{\text{impr}}^j - \mathbf{X}_{\text{impr}}^k\|_F \leq C_5 \eta^l.$$

Here, \mathbf{X}_{impr} is the output of the auxiliary step by definition. It is easy to know that even we run the iterative rules for many times (by letting $\mathbf{X}_{\text{init}}^j \leftarrow \mathbf{X}_{\text{impr}}^j$), the bound still holds. The bound of $\tilde{\mathbf{X}}$ can be derived using the similar derivations with another constant C_6 ,

$$\|\tilde{\mathbf{X}}_{\text{impr}}^j - \tilde{\mathbf{X}}_{\text{impr}}^k\|_F \leq C_6 \eta^l.$$

□

Lemma 6. For two base sets $\{\mathbf{A}, \mathbf{B}, \mathbf{C}\}$ and $\{\mathbf{A}', \mathbf{B}', \mathbf{C}'\}$, given the same tensor and the augmented tensor batch $\mathcal{T}^l, \tilde{\mathcal{T}}^l$, there exist constants, $0 \leq C_7, C_8 < \infty$, such that the Auxiliary Step yields, $\{\mathbf{X}, \tilde{\mathbf{X}}\}$ and $\{\mathbf{X}', \tilde{\mathbf{X}}'\}$, satisfying,

$$\begin{aligned} \|\mathbf{X} - \mathbf{X}'\|_F & \leq C_7 \|\mathbf{A} - \mathbf{A}', \mathbf{B} - \mathbf{B}', \mathbf{C} - \mathbf{C}'\|_F, \\ \|\tilde{\mathbf{X}} - \tilde{\mathbf{X}}'\|_F & \leq C_8 \|\mathbf{A} - \mathbf{A}', \mathbf{B} - \mathbf{B}', \mathbf{C} - \mathbf{C}'\|_F. \end{aligned}$$

Proof. This bound states that given the same data batch, the output of the *Auxiliary Step* will be bounded by the F-norm of the difference of the bases. Since the role of \mathbf{X} and $\tilde{\mathbf{X}}$ are identical, we only prove for \mathbf{X} , and similar derivations can be applied to prove for $\tilde{\mathbf{X}}$.

Bounds on Cold Start. Considering the moving average setting for the *Cold Start*, we have the following closed-form solutions for the initial guesses (the last two terms are different),

$$\begin{aligned} \mathbf{X}_{\text{init}} &= (\eta^l * \mathbf{T}_1^l + (1 - \eta^l) * \mathbf{T}_1^{l-1}) \text{KR}(\mathbf{A}, \mathbf{B}, \mathbf{C}) (\Pi(\mathbf{A}, \mathbf{B}, \mathbf{C}) + \alpha \mathbf{I})^{-1}, \\ \mathbf{X}'_{\text{init}} &= (\eta^l * \mathbf{T}_1^l + (1 - \eta^l) * \mathbf{T}_1^{l-1}) \text{KR}(\mathbf{A}', \mathbf{B}', \mathbf{C}') (\Pi(\mathbf{A}', \mathbf{B}', \mathbf{C}') + \alpha \mathbf{I})^{-1}. \end{aligned}$$

Then, the difference of these two initial guesses are

$$\mathbf{X}_{\text{init}} - \mathbf{X}'_{\text{init}} = \left(\eta^l * \mathbf{T}_1^l + (1 - \eta^l) * \mathbf{T}_1^{l-1} \right) \left(\text{KR}(\mathbf{A}, \mathbf{B}, \mathbf{C}) (\Pi(\mathbf{A}, \mathbf{B}, \mathbf{C}) + \alpha \mathbf{I})^{-1} - \text{KR}(\mathbf{A}', \mathbf{B}', \mathbf{C}') (\Pi(\mathbf{A}', \mathbf{B}', \mathbf{C}') + \alpha \mathbf{I})^{-1} \right). \quad (55)$$

Let us bound the second term of the product (again, we add and subtract terms and use triangular inequality),

$$\begin{aligned}
& \left\| \text{KR}(\mathbf{A}, \mathbf{B}, \mathbf{C})(\Pi(\mathbf{A}, \mathbf{B}, \mathbf{C}) + \alpha \mathbf{I})^{-1} - \text{KR}(\mathbf{A}', \mathbf{B}', \mathbf{C}')(\Pi(\mathbf{A}', \mathbf{B}', \mathbf{C}') + \alpha \mathbf{I})^{-1} \right\|_F \\
&= \left\| (\text{KR}(\mathbf{A}, \mathbf{B}, \mathbf{C}) - \text{KR}(\mathbf{A}', \mathbf{B}', \mathbf{C}')) (\Pi(\mathbf{A}, \mathbf{B}, \mathbf{C}) + \alpha \mathbf{I})^{-1} \right. \\
&\quad \left. + \text{KR}(\mathbf{A}', \mathbf{B}', \mathbf{C}') ((\Pi(\mathbf{A}, \mathbf{B}, \mathbf{C}) + \alpha \mathbf{I})^{-1} - (\Pi(\mathbf{A}', \mathbf{B}', \mathbf{C}') + \alpha \mathbf{I})^{-1}) \right\|_F \\
&= \left\| (\text{KR}(\mathbf{A}, \mathbf{B}, \mathbf{C}) - \text{KR}(\mathbf{A}', \mathbf{B}', \mathbf{C}')) (\Pi(\mathbf{A}, \mathbf{B}, \mathbf{C}) + \alpha \mathbf{I})^{-1} \right. \\
&\quad \left. + \text{KR}(\mathbf{A}', \mathbf{B}', \mathbf{C}') ((\Pi(\mathbf{A}, \mathbf{B}, \mathbf{C}) + \alpha \mathbf{I})^{-1} (\Pi(\mathbf{A}', \mathbf{B}', \mathbf{C}') - \Pi(\mathbf{A}, \mathbf{B}, \mathbf{C})) (\Pi(\mathbf{A}', \mathbf{B}', \mathbf{C}') + \alpha \mathbf{I})^{-1}) \right\|_F \\
&\tag{56}
\end{aligned}$$

$$\begin{aligned}
&\leq \left\| (\text{KR}(\mathbf{A}, \mathbf{B}, \mathbf{C}) - \text{KR}(\mathbf{A}', \mathbf{B}', \mathbf{C}')) \right\|_F \left\| (\Pi(\mathbf{A}, \mathbf{B}, \mathbf{C}) + \alpha \mathbf{I})^{-1} \right\|_F \\
&+ \left\| \text{KR}(\mathbf{A}', \mathbf{B}', \mathbf{C}') \right\|_F \left\| (\Pi(\mathbf{A}, \mathbf{B}, \mathbf{C}) + \alpha \mathbf{I})^{-1} \right\|_F \left\| \Pi(\mathbf{A}', \mathbf{B}', \mathbf{C}') - \Pi(\mathbf{A}, \mathbf{B}, \mathbf{C}) \right\|_F \left\| (\Pi(\mathbf{A}', \mathbf{B}', \mathbf{C}') + \alpha \mathbf{I})^{-1} \right\|_F. \\
&\tag{57}
\end{aligned}$$

From Equation (56) to Equation (57), we use this result

$$\begin{aligned}
& (\Pi(\mathbf{A}, \mathbf{B}, \mathbf{C}) + \alpha \mathbf{I})^{-1} - (\Pi(\mathbf{A}', \mathbf{B}', \mathbf{C}') + \alpha \mathbf{I})^{-1} \\
&= (\Pi(\mathbf{A}, \mathbf{B}, \mathbf{C}) + \alpha \mathbf{I})^{-1} (\Pi(\mathbf{A}, \mathbf{B}, \mathbf{C}) + \alpha \mathbf{I} - \Pi(\mathbf{A}, \mathbf{B}, \mathbf{C}) + \alpha \mathbf{I}) (\Pi(\mathbf{A}', \mathbf{B}', \mathbf{C}') + \alpha \mathbf{I})^{-1} \\
&= (\Pi(\mathbf{A}, \mathbf{B}, \mathbf{C}) + \alpha \mathbf{I})^{-1} (\Pi(\mathbf{A}', \mathbf{B}', \mathbf{C}') - \Pi(\mathbf{A}, \mathbf{B}, \mathbf{C})) (\Pi(\mathbf{A}', \mathbf{B}', \mathbf{C}') + \alpha \mathbf{I})^{-1}. \\
&\tag{58}
\end{aligned}$$

In Equation (58), we can use the results from Lemma 3 and Lemma 4. Let

$$M_6 = C_3 \max \left\{ \left\| (\Pi(\mathbf{A}, \mathbf{B}, \mathbf{C}) + \alpha \mathbf{I})^{-1} \right\|_F \right\} + C_4 \max \left\{ \left\| \text{KR}(\mathbf{A}', \mathbf{B}', \mathbf{C}') \right\|_F \left\| (\Pi(\mathbf{A}, \mathbf{B}, \mathbf{C}) + \alpha \mathbf{I})^{-1} \right\|_F^2 \right\}$$

which makes Equation (58) bounded by

$$\left\| \text{KR}(\mathbf{A}, \mathbf{B}, \mathbf{C})(\Pi(\mathbf{A}, \mathbf{B}, \mathbf{C}) + \alpha \mathbf{I})^{-1} - \text{KR}(\mathbf{A}', \mathbf{B}', \mathbf{C}')(\Pi(\mathbf{A}', \mathbf{B}', \mathbf{C}') + \alpha \mathbf{I})^{-1} \right\|_F \leq M_6 \|\mathbf{A} - \mathbf{A}', \mathbf{B} - \mathbf{B}', \mathbf{C} - \mathbf{C}'\|_F.$$

We let

$$M_7 = M_6 \max_l \left\{ \left\| \eta^l * \mathbf{T}_1^l + (1 - \eta^l) * \mathbf{T}_1^{l-1} \right\|_F \right\},$$

which gives,

$$\left\| \mathbf{X}_{\text{init}} - \mathbf{X}'_{\text{init}} \right\|_F \leq M_7 \|\mathbf{A} - \mathbf{A}', \mathbf{B} - \mathbf{B}', \mathbf{C} - \mathbf{C}'\|_F. \tag{60}$$

Similarly, we have,

$$\left\| \tilde{\mathbf{X}}_{\text{init}} - \tilde{\mathbf{X}}'_{\text{init}} \right\|_F \leq M_7 \|\mathbf{A} - \mathbf{A}', \mathbf{B} - \mathbf{B}', \mathbf{C} - \mathbf{C}'\|_F.$$

Bound on Auxiliary Step. For now, we start to derive the bounds for the output of the *Auxiliary Step*. Given the initial guesses, we use the following closed-form solution,

$$\begin{aligned}
\mathbf{X}_{\text{impr}} &= \left[(\eta^l * \mathbf{T}_1^l + (1 - \eta^l) * \mathbf{T}_1^{l-1}) \text{KR}(\mathbf{A}, \mathbf{B}, \mathbf{C}) - D(\mathbf{X}_{\text{init}}) \mathbf{G} D(\tilde{\mathbf{X}}_{\text{init}}) \tilde{\mathbf{X}}_{\text{init}} \right] (\Pi(\mathbf{A}, \mathbf{B}, \mathbf{C}) + \alpha \mathbf{I})^{-1}, \\
\mathbf{X}'_{\text{impr}} &= \left[(\eta^l * \mathbf{T}_1^l + (1 - \eta^l) * \mathbf{T}_1^{l-1}) \text{KR}(\mathbf{A}', \mathbf{B}', \mathbf{C}') - D(\mathbf{X}'_{\text{init}}) \mathbf{G} D(\tilde{\mathbf{X}}'_{\text{init}}) \tilde{\mathbf{X}}'_{\text{init}} \right] (\Pi(\mathbf{A}', \mathbf{B}', \mathbf{C}') + \alpha \mathbf{I})^{-1}.
\end{aligned}$$

Their difference is bounded by (we add and subtract terms and use triangular inequality)

$$\begin{aligned}
& \left\| \mathbf{X}_{\text{impr}} - \mathbf{X}'_{\text{impr}} \right\|_F \\
&= \left\| (\mathbf{X}_{\text{init}} - \mathbf{X}'_{\text{init}}) + \left(D(\mathbf{X}'_{\text{init}}) \mathbf{G} D(\tilde{\mathbf{X}}'_{\text{init}}) \tilde{\mathbf{X}}'_{\text{init}} - D(\mathbf{X}_{\text{init}}) \mathbf{G} D(\tilde{\mathbf{X}}_{\text{init}}) \tilde{\mathbf{X}}_{\text{init}} \right) (\Pi(\mathbf{A}, \mathbf{B}, \mathbf{C}) + \alpha \mathbf{I})^{-1} \right. \\
&\quad \left. + D(\mathbf{X}'_{\text{init}}) \mathbf{G} D(\tilde{\mathbf{X}}'_{\text{init}}) \tilde{\mathbf{X}}'_{\text{init}} \left[(\Pi(\mathbf{A}', \mathbf{B}', \mathbf{C}') + \alpha \mathbf{I})^{-1} - (\Pi(\mathbf{A}, \mathbf{B}, \mathbf{C}) + \alpha \mathbf{I})^{-1} \right] \right\|_F \\
&\leq \left\| \mathbf{X}_{\text{init}} - \mathbf{X}'_{\text{init}} \right\|_F \\
&\quad + \left\| D(\mathbf{X}'_{\text{init}}) \mathbf{G} D(\tilde{\mathbf{X}}'_{\text{init}}) \tilde{\mathbf{X}}'_{\text{init}} - D(\mathbf{X}_{\text{init}}) \mathbf{G} D(\tilde{\mathbf{X}}_{\text{init}}) \tilde{\mathbf{X}}_{\text{init}} \right\|_F \left\| (\Pi(\mathbf{A}, \mathbf{B}, \mathbf{C}) + \alpha \mathbf{I})^{-1} \right\|_F \\
&\quad + \left\| D(\mathbf{X}'_{\text{init}}) \mathbf{G} D(\tilde{\mathbf{X}}'_{\text{init}}) \tilde{\mathbf{X}}'_{\text{init}} \right\|_F \left\| (\Pi(\mathbf{A}', \mathbf{B}', \mathbf{C}') + \alpha \mathbf{I})^{-1} - (\Pi(\mathbf{A}, \mathbf{B}, \mathbf{C}) + \alpha \mathbf{I})^{-1} \right\|_F
\end{aligned}$$

The bound for the second term is given by Equation (53),

$$\left\| D(\mathbf{X}'_{\text{init}}) \mathbf{G} D(\tilde{\mathbf{X}}'_{\text{init}}) \tilde{\mathbf{X}}'_{\text{init}} - D(\mathbf{X}_{\text{init}}) \mathbf{G} D(\tilde{\mathbf{X}}_{\text{init}}) \tilde{\mathbf{X}}_{\text{init}} \right\|_F \leq M_3 \left\| \mathbf{X}_{\text{init}} - \mathbf{X}'_{\text{init}} \right\|_F + (M_4 + M_5) \left\| \tilde{\mathbf{X}}_{\text{init}} - \tilde{\mathbf{X}}'_{\text{init}} \right\|_F.$$

The bound for the third term is given by Equation (59) and Lemma 4,

$$\begin{aligned} & \left\| (\Pi(\mathbf{A}, \mathbf{B}, \mathbf{C}) + \alpha \mathbf{I})^{-1} - (\Pi(\mathbf{A}', \mathbf{B}', \mathbf{C}') + \alpha \mathbf{I})^{-1} \right\|_F \\ & \leq \max \left\{ \left\| (\Pi(\mathbf{A}, \mathbf{B}, \mathbf{C}) + \alpha \mathbf{I})^{-1} \right\|_F^2 \right\} \left\| \Pi(\mathbf{A}', \mathbf{B}', \mathbf{C}') - \Pi(\mathbf{A}, \mathbf{B}, \mathbf{C}) \right\|_F \\ & \leq \max \left\{ \left\| (\Pi(\mathbf{A}, \mathbf{B}, \mathbf{C}) + \alpha \mathbf{I})^{-1} \right\|_F^2 \right\} C_4 \left\| \mathbf{A} - \mathbf{A}', \mathbf{B} - \mathbf{B}', \mathbf{C} - \mathbf{C}' \right\|_F. \end{aligned}$$

We collect the constants and let

$$C_7 = (1 + M_3 + M_4 + M_5)M_7 + C_4 \max \left\{ \left\| (\Pi(\mathbf{A}, \mathbf{B}, \mathbf{C}) + \alpha \mathbf{I})^{-1} \right\|_F^2 \right\}, \quad (61)$$

which yields,

$$\left\| \mathbf{X}_{\text{impr}} - \mathbf{X}'_{\text{impr}} \right\|_F \leq C_7 \left\| \mathbf{A} - \mathbf{A}', \mathbf{B} - \mathbf{B}', \mathbf{C} - \mathbf{C}' \right\|_F. \quad (62)$$

Here, \mathbf{X}_{impr} is the output of the auxiliary step by definition. It is easy to know that even if we run the iterative rules for many times (by letting $\mathbf{X}_{\text{init}}^j \leftarrow \mathbf{X}_{\text{impr}}^j$), the bound still holds. The bound of $\tilde{\mathbf{X}}$ can be derived using the similar derivations,

$$\left\| \tilde{\mathbf{X}}_{\text{impr}} - \tilde{\mathbf{X}}'_{\text{impr}} \right\|_F \leq C_8 \left\| \mathbf{A} - \mathbf{A}', \mathbf{B} - \mathbf{B}', \mathbf{C} - \mathbf{C}' \right\|_F.$$

□

Lemma 7. (Adopted from Lemma 3.3 in (Cao et al., 2020)) For two factor sets $\mathcal{S} = \{\mathbf{A}, \mathbf{B}, \mathbf{C}\}$ and $\mathcal{S}' = \{\mathbf{A}', \mathbf{B}', \mathbf{C}'\}$, for the same tensor and the augmented tensor batch $\mathcal{T}^l, \tilde{\mathcal{T}}^l$, we first conduct the Cold Start and Auxiliary Step to obtain $\{\mathbf{X}, \tilde{\mathbf{X}}\}$ and $\{\mathbf{X}', \tilde{\mathbf{X}}'\}$. Then, there exist constants, $0 \leq C_9, C_{10} < \infty$, such that the gradient and the Newton step from the batch (e.g., a small scale of the objective in main text Equation (8)) are bounded. We have

$$\begin{aligned} & \left\| \mathbf{G}_1(\mathcal{T}^l; \mathcal{S}) - \mathbf{G}_1(\mathcal{T}^l; \mathcal{S}') \right\|_F \leq C_9 \left\| \mathbf{A} - \mathbf{A}', \mathbf{B} - \mathbf{B}', \mathbf{C} - \mathbf{C}' \right\|_F. \\ & \left\| \mathbf{G}_1(\mathcal{T}^l; \mathcal{S}) \mathbf{H}_1^{-1}(\mathcal{T}^l; \mathcal{S}) - \mathbf{G}_1(\mathcal{T}^l; \mathcal{S}') \mathbf{H}_1^{-1}(\mathcal{T}^l; \mathcal{S}') \right\|_F \leq C_{10} \left\| \mathbf{A} - \mathbf{A}', \mathbf{B} - \mathbf{B}', \mathbf{C} - \mathbf{C}' \right\|_F. \end{aligned}$$

Proof. This bound states that given the same data batch, the gradient and the Newton step will be bounded by the F-norm of the difference of the bases. We only prove for \mathbf{A} . Similar derivations could be mimicked for \mathbf{B}, \mathbf{C} .

Proof for the gradient. Follow Definition 2, the gradients are,

$$\begin{aligned} \mathbf{G}_1(\mathcal{T}^l; \mathcal{S}) &= \mathbf{A} [\Pi(\mathbf{X}, \mathbf{B}, \mathbf{C}) + \Pi(\tilde{\mathbf{X}}, \mathbf{B}, \mathbf{C}) + \alpha \mathbf{I}] - \left[\mathbf{T}_2^l \text{KR}(\mathbf{X}, \mathbf{B}, \mathbf{C}) + \tilde{\mathbf{T}}_2^l \text{KR}(\tilde{\mathbf{X}}, \mathbf{B}, \mathbf{C}) \right], \\ \mathbf{G}_1(\mathcal{T}^l; \mathcal{S}') &= \mathbf{A}' [\Pi(\mathbf{X}', \mathbf{B}', \mathbf{C}') + \Pi(\tilde{\mathbf{X}}', \mathbf{B}', \mathbf{C}') + \alpha \mathbf{I}] - \left[\mathbf{T}_2^l \text{KR}(\mathbf{X}', \mathbf{B}', \mathbf{C}') + \tilde{\mathbf{T}}_2^l \text{KR}(\tilde{\mathbf{X}}', \mathbf{B}', \mathbf{C}') \right]. \end{aligned}$$

where $\{\mathbf{X}, \tilde{\mathbf{X}}\}$ are the outputs of the Auxiliary Step from $\mathcal{T}^l, \tilde{\mathcal{T}}^l, \mathcal{S}$, and $\{\mathbf{X}', \tilde{\mathbf{X}}'\}$ are the outputs of the Auxiliary Step from $\mathcal{T}^l, \tilde{\mathcal{T}}^l, \mathcal{S}'$. Here, the tensor $\mathbf{T}_2^l, \tilde{\mathbf{T}}_2^l$ should be written as moving average form, however, we simplify it this way since they do not affect the bound.

We can bound the difference of the first order derivatives by triangular inequality (we add and subtract terms),

$$\begin{aligned} & \left\| \mathbf{G}_1(\mathcal{T}^l; \mathcal{S}) - \mathbf{G}_1(\mathcal{T}^l; \mathcal{S}') \right\|_F \\ &= \left\| (\mathbf{A} - \mathbf{A}') \left(\Pi(\mathbf{X}', \mathbf{B}', \mathbf{C}') + \Pi(\tilde{\mathbf{X}}', \mathbf{B}', \mathbf{C}') + \alpha \mathbf{I} \right) \right. \\ & \quad + \mathbf{A} (\Pi(\mathbf{X}, \mathbf{B}, \mathbf{C}) - \Pi(\mathbf{X}', \mathbf{B}', \mathbf{C}')) + \mathbf{A} (\Pi(\tilde{\mathbf{X}}, \mathbf{B}, \mathbf{C}) - \Pi(\tilde{\mathbf{X}}', \mathbf{B}', \mathbf{C}')) \\ & \quad \left. - \mathbf{T}_2^l (\text{KR}(\mathbf{X}, \mathbf{B}, \mathbf{C}) - \text{KR}(\mathbf{X}', \mathbf{B}', \mathbf{C}')) - \tilde{\mathbf{T}}_2^l (\text{KR}(\tilde{\mathbf{X}}, \mathbf{B}, \mathbf{C}) - \text{KR}(\tilde{\mathbf{X}}', \mathbf{B}', \mathbf{C}')) \right\|_F \\ &\leq \left\| \mathbf{A} - \mathbf{A}' \right\|_F \left\| \Pi(\mathbf{X}', \mathbf{B}', \mathbf{C}') + \Pi(\tilde{\mathbf{X}}', \mathbf{B}', \mathbf{C}') + \alpha \mathbf{I} \right\|_F \\ & \quad + \left\| \mathbf{A} \right\|_F \left\| \Pi(\mathbf{X}, \mathbf{B}, \mathbf{C}) - \Pi(\mathbf{X}', \mathbf{B}', \mathbf{C}') \right\|_F + \left\| \mathbf{A} \right\|_F \left\| \Pi(\tilde{\mathbf{X}}, \mathbf{B}, \mathbf{C}) - \Pi(\tilde{\mathbf{X}}', \mathbf{B}', \mathbf{C}') \right\|_F \\ & \quad + \left\| \mathcal{T}^l \right\|_F \left\| \text{KR}(\mathbf{X}, \mathbf{B}, \mathbf{C}) - \text{KR}(\mathbf{X}', \mathbf{B}', \mathbf{C}') \right\|_F + \left\| \tilde{\mathcal{T}}^l \right\|_F \left\| \text{KR}(\tilde{\mathbf{X}}, \mathbf{B}, \mathbf{C}) - \text{KR}(\tilde{\mathbf{X}}', \mathbf{B}', \mathbf{C}') \right\|_F. \end{aligned} \quad (63)$$

For the first term, we let

$$M_8 = \max \left\{ \left\| \Pi(\mathbf{X}', \mathbf{B}', \mathbf{C}') + \Pi(\tilde{\mathbf{X}}', \mathbf{B}', \mathbf{C}') + \alpha \mathbf{I} \right\|_F \right\}$$

For the second term, we let

$$M_9 = C_4 \max \{ \|\mathbf{A}\|_F \}$$

For the third term, we let

$$M_{10} = C_3 \max \{ \|\mathcal{T}^l\|_F, \|\mathcal{T}^l\|_F \}$$

Thus, we use the results from Lemma 3 and Lemma 4, which yields that Equation (63) is bounded by

$$\begin{aligned} \|\mathbf{G}_1(\mathcal{T}^l; \mathcal{S}) - \mathbf{G}_1(\mathcal{T}^l; \mathcal{S}')\|_F &\leq M_8 \|\mathbf{A} - \mathbf{A}'\|_F + (M_9 + M_{10}) \|\mathbf{X} - \mathbf{X}', \mathbf{B} - \mathbf{B}', \mathbf{C} - \mathbf{C}'\|_F \\ &\quad + (M_9 + M_{10}) \|\tilde{\mathbf{X}} - \tilde{\mathbf{X}}', \mathbf{B} - \mathbf{B}', \mathbf{C} - \mathbf{C}'\|_F \end{aligned}$$

There, with Lemma 6, we have with some constant,

$$C_9 = M_8 + (M_9 + M_{10}) \left(\sqrt{C_7^2 + 1} + \sqrt{C_8^2 + 1} \right),$$

such that,

$$\|\mathbf{G}_1(\mathcal{T}^l; \mathcal{S}) - \mathbf{G}_1(\mathcal{T}^l; \mathcal{S}')\|_F \leq C_9 \|\mathbf{A} - \mathbf{A}', \mathbf{B} - \mathbf{B}', \mathbf{C} - \mathbf{C}'\|_F. \quad (64)$$

Proof for the Newton Step. The proof of the Newton step is built on the bound of gradient (we add and subtract terms and use triangular inequality),

$$\begin{aligned} &\|\mathbf{G}_1(\mathcal{T}^l; \mathcal{S}) \mathbf{H}_1^{-1}(\mathcal{T}^l; \mathcal{S}) - \mathbf{G}_1(\mathcal{T}^l; \mathcal{S}') \mathbf{H}_1^{-1}(\mathcal{T}^l; \mathcal{S}')\|_F \\ &= \|\mathbf{G}_1(\mathcal{T}^l; \mathcal{S}) \mathbf{H}_1^{-1}(\mathcal{T}^l; \mathcal{S}) - \mathbf{G}_1(\mathcal{T}^l; \mathcal{S}') \mathbf{H}_1^{-1}(\mathcal{T}^l; \mathcal{S}) + \mathbf{G}_1(\mathcal{T}^l; \mathcal{S}') \mathbf{H}_1^{-1}(\mathcal{T}^l; \mathcal{S}) - \mathbf{G}_1(\mathcal{T}^l; \mathcal{S}') \mathbf{H}_1^{-1}(\mathcal{T}^l; \mathcal{S}')\|_F \\ &\leq \|\mathbf{G}_1(\mathcal{T}^l; \mathcal{S}) - \mathbf{G}_1(\mathcal{T}^l; \mathcal{S}')\|_F \|\mathbf{H}_1^{-1}(\mathcal{T}^l; \mathcal{S})\|_F + \|\mathbf{G}_1(\mathcal{T}^l; \mathcal{S}')\|_F \|\mathbf{H}_1^{-1}(\mathcal{T}^l; \mathcal{S}) - \mathbf{H}_1^{-1}(\mathcal{T}^l; \mathcal{S}')\|_F. \end{aligned} \quad (65)$$

The first term is bounded by Equation (64), and as for the second term, we use the result from Equation (59),

$$\begin{aligned} &\|\mathbf{H}_1^{-1}(\mathcal{T}^l; \mathcal{S}) - \mathbf{H}_1^{-1}(\mathcal{T}^l; \mathcal{S}')\|_F \\ &= \|\mathbf{H}_1^{-1}(\mathcal{T}^l; \mathcal{S}) [\mathbf{H}_1(\mathcal{T}^l; \mathcal{S}') - \mathbf{H}_1(\mathcal{T}^l; \mathcal{S})] \mathbf{H}_1^{-1}(\mathcal{T}^l; \mathcal{S}')\|_F \\ &= \left\| \mathbf{H}_1^{-1}(\mathcal{T}^l; \mathcal{S}) \left[\Pi(\mathbf{X}', \mathbf{B}', \mathbf{C}') + \Pi(\tilde{\mathbf{X}}', \mathbf{B}', \mathbf{C}') - \Pi(\mathbf{X}, \mathbf{B}, \mathbf{C}) - \Pi(\tilde{\mathbf{X}}, \mathbf{B}, \mathbf{C}) \right] \mathbf{H}_1^{-1}(\mathcal{T}^l; \mathcal{S}') \right\|_F \\ &\leq \|\mathbf{H}_1^{-1}(\mathcal{T}^l; \mathcal{S})\|_F \left(\|\Pi(\mathbf{X}', \mathbf{B}', \mathbf{C}') - \Pi(\mathbf{X}, \mathbf{B}, \mathbf{C})\|_F + \|\Pi(\tilde{\mathbf{X}}', \mathbf{B}', \mathbf{C}') - \Pi(\tilde{\mathbf{X}}, \mathbf{B}, \mathbf{C})\|_F \right) \|\mathbf{H}_1^{-1}(\mathcal{T}^l; \mathcal{S}')\|_F \end{aligned}$$

By using the results from Lemma 4 and Lemma 6, we have,

$$\begin{aligned} &\|\mathbf{H}_1^{-1}(\mathcal{T}^l; \mathcal{S}) - \mathbf{H}_1^{-1}(\mathcal{T}^l; \mathcal{S}')\|_F \\ &\leq C_4 \max_{\mathcal{S}} \{ \|\mathbf{H}_1^{-1}(\mathcal{T}^l; \mathcal{S})\|_F^2 \} \left(\|\mathbf{X} - \mathbf{X}', \mathbf{B} - \mathbf{B}', \mathbf{C} - \mathbf{C}'\|_F + \|\tilde{\mathbf{X}} - \tilde{\mathbf{X}}', \mathbf{B} - \mathbf{B}', \mathbf{C} - \mathbf{C}'\|_F \right) \\ &\leq C_4 \left(\sqrt{C_7^2 + 1} + \sqrt{C_8^2 + 1} \right) \max_{\mathcal{S}} \{ \|\mathbf{H}_1^{-1}(\mathcal{T}^l; \mathcal{S})\|_F^2 \} \|\mathbf{A} - \mathbf{A}', \mathbf{B} - \mathbf{B}', \mathbf{C} - \mathbf{C}'\|_F. \end{aligned} \quad (66)$$

Therefore, by inserting the results from Equation (64) and Equation (66) into Equation (65), the proof is completed for some constants,

$$C_{10} = C_9 \max_{\mathcal{S}} \{ \|\mathbf{H}_1^{-1}(\mathcal{T}^l; \mathcal{S})\|_F \} + C_4 \left(\sqrt{C_7^2 + 1} + \sqrt{C_8^2 + 1} \right) \max_{\mathcal{S}'} \{ \|\mathbf{G}_1(\mathcal{T}^l; \mathcal{S}')\|_F \} \max_{\mathcal{S}} \{ \|\mathbf{H}_1^{-1}(\mathcal{T}^l; \mathcal{S})\|_F^2 \},$$

such that,

$$\|\mathbf{G}_1(\mathcal{T}^l; \mathcal{S}) \mathbf{H}_1^{-1}(\mathcal{T}^l; \mathcal{S}) - \mathbf{G}_1(\mathcal{T}^l; \mathcal{S}') \mathbf{H}_1^{-1}(\mathcal{T}^l; \mathcal{S}')\|_F \leq C_{10} \|\mathbf{A} - \mathbf{A}', \mathbf{B} - \mathbf{B}', \mathbf{C} - \mathbf{C}'\|_F.$$

□

Lemma 8. For a up-to-date factor set $\mathcal{S}^{l,0} = \{\mathbf{A}^l, \mathbf{B}^l, \mathbf{C}^l\}$, for a new tensor and the augmented tensor batch $\mathcal{T}^j, \tilde{\mathcal{T}}^j$, we first conduct the Cold Start and Auxiliary Step to obtain $\{\mathbf{X}^j, \tilde{\mathbf{X}}^j\}$. Then, there exist constants, $0 \leq C_{11}, C_{12} < \infty$, such that the gradient and the Newton step from the batch (e.g., a small scale of the objective in main text Equation (8)) are bounded,

$$\begin{aligned} \|\mathbf{G}_1(\mathcal{T}^j; \mathcal{S}^{l,0}) - \mathbf{G}_1(\mathcal{T}^k; \mathcal{S}^{l,0})\|_F &\leq C_{11}\eta^l. \\ \|\mathbf{G}_1(\mathcal{T}^j; \mathcal{S}^{l,0})\mathbf{H}_1^{-1}(\mathcal{T}^j; \mathcal{S}^{l,0}) - \mathbf{G}_1(\mathcal{T}^k; \mathcal{S}^{l,0})\mathbf{H}_1^{-1}(\mathcal{T}^k; \mathcal{S}^{l,0})\|_F &\leq C_{12}\eta^l. \end{aligned}$$

Proof. This bound states that given different batch data at the l -th batch, the gradient and the Newton step will be bounded by the learning rate. We only prove for \mathbf{A} . Similar derivations could be applied for \mathbf{B} (given $\mathcal{S}^{l,1}$) and \mathbf{C} (given $\mathcal{S}^{l,2}$).

Proof for the gradient. Following the moving average setting and Definition 2, the gradient is,

$$\begin{aligned} \mathbf{G}_1(\mathcal{T}^j; \mathcal{S}^{l,0}) &= \mathbf{A}^l \left[\Pi(\mathbf{X}^j, \mathbf{B}^l, \mathbf{C}^l) + \Pi(\tilde{\mathbf{X}}^j, \mathbf{B}^l, \mathbf{C}^l) + \alpha \mathbf{I} \right] - \left[\left(\eta^l * \mathbf{T}_2^j + (1 - \eta^l) * \mathbf{T}_2^l \right) \text{KR}(\mathbf{X}^j, \mathbf{B}^l, \mathbf{C}^l) \right. \\ &\quad \left. + \left(\eta^l * \tilde{\mathbf{T}}_2^j + (1 - \eta^l) * \tilde{\mathbf{T}}_2^l \right) \text{KR}(\tilde{\mathbf{X}}^j, \mathbf{B}^l, \mathbf{C}^l) \right]. \end{aligned}$$

where $\{\mathbf{X}^j, \tilde{\mathbf{X}}^j\}$ are the outputs of the *Auxiliary Step* from $\mathcal{T}^j, \tilde{\mathcal{T}}^j, \mathcal{S}^{l,0}$.

We can bound the difference of the first order derivatives by (using triangular inequality)

$$\begin{aligned} &\|\mathbf{G}_1(\mathcal{T}^j; \mathcal{S}^{l,0}) - \mathbf{G}_1(\mathcal{T}^k; \mathcal{S}^{l,0})\|_F \\ &= \left\| \mathbf{A}^l \left(\Pi(\mathbf{X}^j, \mathbf{B}^l, \mathbf{C}^l) - \Pi(\mathbf{X}^k, \mathbf{B}^l, \mathbf{C}^l) + \Pi(\tilde{\mathbf{X}}^j, \mathbf{B}^l, \mathbf{C}^l) - \Pi(\tilde{\mathbf{X}}^k, \mathbf{B}^l, \mathbf{C}^l) \right) \right. \\ &\quad + \eta^l \left(\mathbf{T}_2^k - \mathbf{T}_2^j \right) \text{KR}(\mathbf{X}^j, \mathbf{B}^l, \mathbf{C}^l) + \left(\eta^l * \mathbf{T}_2^k + (1 - \eta^l) * \mathbf{T}_2^l \right) \text{KR}(\mathbf{X}^k - \mathbf{X}^j, \mathbf{B}^l, \mathbf{C}^l) \\ &\quad \left. + \eta^l \left(\tilde{\mathbf{T}}_2^k - \tilde{\mathbf{T}}_2^j \right) \text{KR}(\tilde{\mathbf{X}}^j, \mathbf{B}^l, \mathbf{C}^l) + \left(\eta^l * \tilde{\mathbf{T}}_2^k + (1 - \eta^l) * \tilde{\mathbf{T}}_2^l \right) \text{KR}(\tilde{\mathbf{X}}^k - \tilde{\mathbf{X}}^j, \mathbf{B}^l, \mathbf{C}^l) \right\|_F \\ &\leq \|\mathbf{A}^l\|_F \left(\left\| \Pi(\mathbf{X}^j, \mathbf{B}^l, \mathbf{C}^l) - \Pi(\mathbf{X}^k, \mathbf{B}^l, \mathbf{C}^l) \right\|_F + \left\| \Pi(\tilde{\mathbf{X}}^j, \mathbf{B}^l, \mathbf{C}^l) - \Pi(\tilde{\mathbf{X}}^k, \mathbf{B}^l, \mathbf{C}^l) \right\|_F \right) \\ &\quad + \eta^l \left\| \mathcal{T}^k - \mathcal{T}^j \right\|_F \left\| \text{KR}(\mathbf{X}^j, \mathbf{B}^l, \mathbf{C}^l) \right\|_F + \left\| \eta^l * \mathcal{T}^k + (1 - \eta^l) * \mathcal{T}^l \right\|_F \left\| \text{KR}(\mathbf{X}^k - \mathbf{X}^j, \mathbf{B}^l, \mathbf{C}^l) \right\|_F \\ &\quad + \eta^l \left\| \tilde{\mathcal{T}}^k - \tilde{\mathcal{T}}^j \right\|_F \left\| \text{KR}(\tilde{\mathbf{X}}^j, \mathbf{B}^l, \mathbf{C}^l) \right\|_F + \left\| \eta^l * \tilde{\mathcal{T}}^k + (1 - \eta^l) * \tilde{\mathcal{T}}^l \right\|_F \left\| \text{KR}(\tilde{\mathbf{X}}^k - \tilde{\mathbf{X}}^j, \mathbf{B}^l, \mathbf{C}^l) \right\|_F. \end{aligned}$$

For the first term, we use the results from Lemma 4 and Lemma 5, which yields,

$$\begin{aligned} \left\| \Pi(\mathbf{X}^j, \mathbf{B}^l, \mathbf{C}^l) - \Pi(\mathbf{X}^k, \mathbf{B}^l, \mathbf{C}^l) \right\|_F &\leq C_4 \|\mathbf{X}^j - \mathbf{X}^k\|_F \leq C_4 C_5 \eta^l, \\ \left\| \Pi(\tilde{\mathbf{X}}^j, \mathbf{B}^l, \mathbf{C}^l) - \Pi(\tilde{\mathbf{X}}^k, \mathbf{B}^l, \mathbf{C}^l) \right\|_F &\leq C_4 \|\tilde{\mathbf{X}}^j - \tilde{\mathbf{X}}^k\|_F \leq C_4 C_6 \eta^l. \end{aligned}$$

For the third and fifth term, we use the results from Lemma 3 and Lemma 5, which yields,

$$\begin{aligned} \left\| \text{KR}(\mathbf{X}^k - \mathbf{X}^j, \mathbf{B}^l, \mathbf{C}^l) \right\|_F &\leq C_3 \|\mathbf{X}^k - \mathbf{X}^j\|_F \leq C_3 C_5 \eta^l \\ \left\| \text{KR}(\tilde{\mathbf{X}}^k - \tilde{\mathbf{X}}^j, \mathbf{B}^l, \mathbf{C}^l) \right\|_F &\leq C_3 \|\tilde{\mathbf{X}}^k - \tilde{\mathbf{X}}^j\|_F \leq C_3 C_6 \eta^l \end{aligned}$$

We combine the results and get the following for some constant

$$C_{11} = C_4(C_5 + C_6) \max_l \{\|\mathbf{A}^l\|_F\} + \max_j \{\|\mathcal{T}^j\|_F, \|\tilde{\mathcal{T}}^j\|_F\} \left(2 \max_{j,l} \left\{ \left\| \text{KR}(\tilde{\mathbf{X}}^j, \mathbf{B}^l, \mathbf{C}^l) \right\|_F \right\} + C_3(C_5 + C_6) \right),$$

such that,

$$\|\mathbf{G}_1(\mathcal{T}^j; \mathcal{S}^{l,0}) - \mathbf{G}_1(\mathcal{T}^k; \mathcal{S}^{l,0})\|_F \leq C_{11}\eta^l. \quad (67)$$

Proof for the Newton Step. The proof of the Newton step is built on the bound of gradient (we add and subtract terms and use triangular inequality),

$$\begin{aligned} &\|\mathbf{G}_1(\mathcal{T}^j; \mathcal{S}^{l,0})\mathbf{H}_1^{-1}(\mathcal{T}^j; \mathcal{S}^{l,0}) - \mathbf{G}_1(\mathcal{T}^k; \mathcal{S}^{l,0})\mathbf{H}_1^{-1}(\mathcal{T}^k; \mathcal{S}^{l,0})\|_F \\ &= \|\mathbf{G}_1(\mathcal{T}^j; \mathcal{S}^{l,0})\mathbf{H}_1^{-1}(\mathcal{T}^j; \mathcal{S}^{l,0}) - \mathbf{G}_1(\mathcal{T}^k; \mathcal{S}^{l,0})\mathbf{H}_1^{-1}(\mathcal{T}^j; \mathcal{S}^{l,0}) + \mathbf{G}_1(\mathcal{T}^k; \mathcal{S}^{l,0})\mathbf{H}_1^{-1}(\mathcal{T}^j; \mathcal{S}^{l,0}) - \mathbf{G}_1(\mathcal{T}^k; \mathcal{S}^{l,0})\mathbf{H}_1^{-1}(\mathcal{T}^k; \mathcal{S}^{l,0})\|_F \\ &\leq \|\mathbf{G}_1(\mathcal{T}^j; \mathcal{S}^{l,0}) - \mathbf{G}_1(\mathcal{T}^k; \mathcal{S}^{l,0})\|_F \|\mathbf{H}_1^{-1}(\mathcal{T}^j; \mathcal{S}^{l,0})\|_F + \|\mathbf{G}_1(\mathcal{T}^k; \mathcal{S}^{l,0})\|_F \|\mathbf{H}_1^{-1}(\mathcal{T}^j; \mathcal{S}^{l,0}) - \mathbf{H}_1^{-1}(\mathcal{T}^k; \mathcal{S}^{l,0})\|_F. \end{aligned}$$

The first term is bounded by the gradient, and as for the second term, we have

$$\begin{aligned}
& \|\mathbf{H}_1^{-1}(\mathcal{T}^j; \mathcal{S}^{l,0}) - \mathbf{H}_1^{-1}(\mathcal{T}^k; \mathcal{S}^{l,0})\|_F \\
&= \|\mathbf{H}_1^{-1}(\mathcal{T}^j; \mathcal{S}^{l,0}) [\mathbf{H}(\mathcal{T}^k; \mathcal{S}^{l,0}) - \mathbf{H}_1(\mathcal{T}^j; \mathcal{S}^{l,0})] \mathbf{H}_1^{-1}(\mathcal{T}^k; \mathcal{S}^{l,0})\|_F \\
&= \|\mathbf{H}_1^{-1}(\mathcal{T}^j; \mathcal{S}^{l,0}) [\Pi(\mathbf{X}^k, \mathbf{B}^l, \mathbf{C}^l) + \Pi(\tilde{\mathbf{X}}^k, \mathbf{B}^l, \mathbf{C}^l) - \Pi(\mathbf{X}^j, \mathbf{B}^l, \mathbf{C}^l) - \Pi(\tilde{\mathbf{X}}^j, \mathbf{B}^l, \mathbf{C}^l)] \mathbf{H}_1^{-1}(\mathcal{T}^k; \mathcal{S}^{l,0})\|_F \\
&\leq \|\mathbf{H}_1^{-1}(\mathcal{T}^j; \mathcal{S}^{l,0})\|_F \left(\|\Pi(\mathbf{X}^k, \mathbf{B}^l, \mathbf{C}^l) - \Pi(\mathbf{X}^j, \mathbf{B}^l, \mathbf{C}^l)\|_F + \|\Pi(\tilde{\mathbf{X}}^k, \mathbf{B}^l, \mathbf{C}^l) - \Pi(\tilde{\mathbf{X}}^j, \mathbf{B}^l, \mathbf{C}^l)\|_F \right) \|\mathbf{H}_1^{-1}(\mathcal{T}^k; \mathcal{S}^{l,0})\|_F.
\end{aligned}$$

By using the results from Lemma 4 and Lemma 5, we have,

$$\begin{aligned}
& \|\mathbf{H}_1^{-1}(\mathcal{T}^j; \mathcal{S}^{l,0}) - \mathbf{H}_1^{-1}(\mathcal{T}^k; \mathcal{S}^{l,0})\|_F \\
&\leq C_4 \max_{j,l} \left\{ \|\mathbf{H}_1^{-1}(\mathcal{T}^j; \mathcal{S}^{l,0})\|_F^2 \right\} \left(\|\mathbf{X}^j - \mathbf{X}^k\|_F + \|\tilde{\mathbf{X}}^j - \tilde{\mathbf{X}}^k\|_F \right) \\
&\leq C_4(C_5 + C_6) \max_{j,l} \left\{ \|\mathbf{H}_1^{-1}(\mathcal{T}^j; \mathcal{S}^{l,0})\|_F^2 \right\} \eta^l. \tag{68}
\end{aligned}$$

Therefore, by inserting the results of Equation (67) and Equation (68), we can find the constant,

$$C_{12} = C_{11} \max_{j,l} \left\{ \|\mathbf{H}_1^{-1}(\mathcal{T}^j; \mathcal{S}^{l,0})\|_F \right\} + C_4(C_5 + C_6) \max_{k,l} \left\{ \|\mathbf{G}_1(\mathcal{T}^k; \mathcal{S}^{l,0})\|_F \right\} \max_{j,l} \left\{ \|\mathbf{H}_1^{-1}(\mathcal{T}^j; \mathcal{S}^{l,0})\|_F^2 \right\},$$

such that,

$$\|\mathbf{G}_1(\mathcal{T}^j; \mathcal{S}^{l,0}) \mathbf{H}_1^{-1}(\mathcal{T}^j; \mathcal{S}^{l,0}) - \mathbf{G}_1(\mathcal{T}^k; \mathcal{S}^{l,0}) \mathbf{H}_1^{-1}(\mathcal{T}^k; \mathcal{S}^{l,0})\|_F \leq C_{12} \eta^l.$$

□

Lemma 9. (Adopted from Lemma 3.12 in (Cao et al., 2020)) Assume $\mathcal{S}^{l,0} = \{\mathbf{A}^l, \mathbf{B}^l, \mathbf{C}^l\}$ is up-to-date base set, given $\mathcal{H}^l = \{\mathcal{T}^1, \dots, \mathcal{T}^{l-1}\} \cup \{\tilde{\mathcal{T}}^1, \dots, \tilde{\mathcal{T}}^{l-1}\}$ is the notation to represent historical information up to the $(l-1)$ -th batch. $\{\mathbf{X}^j, \tilde{\mathbf{X}}^j\}$ and $\{\mathbf{X}, \tilde{\mathbf{X}}\}$ are the outputs of the Auxiliary Step given a new batch $\mathcal{T}^j, \tilde{\mathcal{T}}^j$ or the whole tensor and the augmented tensor $\mathcal{T}, \tilde{\mathcal{T}}$, separately, and the batch size is b , the size of the dataset is N . Then, there exists a constant $0 \leq C_{13} < \infty$, given \mathcal{H}^l ,

$$\mathbb{E} \left[\left\| \left(\mathbf{G}_1(\mathcal{T}^j; \mathcal{S}^{l,0}) - \frac{b}{N} \mathbf{G}_1(\mathcal{T}; \mathcal{S}^{l,0}) \right) \mathbf{H}_1^{-1}(\mathcal{T}^j; \mathcal{S}^{l,0}) \right\|_F^2 \right] \leq C_{13} \eta^l. \tag{69}$$

Proof. We show the proof for \mathbf{A} , while similar derivations can be applied to \mathbf{B} (given $\mathcal{S}^{l,1}$) and \mathbf{C} (given $\mathcal{S}^{l,2}$). We have

$$\mathbb{E} \left[\left\| \left(\mathbf{G}_1(\mathcal{T}^j; \mathcal{S}^{l,0}) - \frac{b}{N} \mathbf{G}_1(\mathcal{T}; \mathcal{S}^{l,0}) \right) \mathbf{H}_1^{-1}(\mathcal{T}^j; \mathcal{S}^{l,0}) \right\|_F^2 \right] \tag{70}$$

$$= \mathbb{E}_j \left[\left\| (\mathbf{G}_1(\mathcal{T}^j; \mathcal{S}^{l,0}) - \mathbb{E}_k [\mathbf{G}_1(\mathcal{T}^k; \mathcal{S}^{l,0})]) \mathbf{H}_1^{-1}(\mathcal{T}^j; \mathcal{S}^{l,0}) \right\|_F^2 \right] \tag{71}$$

$$\leq \mathbb{E}_j \left[\left\| \mathbf{G}_1(\mathcal{T}^j; \mathcal{S}^{l,0}) - \mathbb{E}_k [\mathbf{G}_1(\mathcal{T}^k; \mathcal{S}^{l,0})] \right\|_F^2 \left\| \mathbf{H}_1^{-1}(\mathcal{T}^j; \mathcal{S}^{l,0}) \right\|_F^2 \right] \tag{72}$$

$$\leq \mathbb{E}_j \left[\left\| \mathbf{G}_1(\mathcal{T}^j; \mathcal{S}^{l,0}) - \mathbb{E}_k [\mathbf{G}_1(\mathcal{T}^k; \mathcal{S}^{l,0})] \right\|_F^2 \right] \max_j \left\{ \left\| \mathbf{H}_1^{-1}(\mathcal{T}^j; \mathcal{S}^{l,0}) \right\|_F^2 \right\} \tag{73}$$

$$\leq \mathbb{E}_j \left[\mathbb{E}_k \left[\left\| \mathbf{G}_1(\mathcal{T}^j; \mathcal{S}^{l,0}) - \mathbf{G}_1(\mathcal{T}^k; \mathcal{S}^{l,0}) \right\|_F^2 \right] \right] \max_j \left\{ \left\| \mathbf{H}_1^{-1}(\mathcal{T}^j; \mathcal{S}^{l,0}) \right\|_F^2 \right\} \tag{74}$$

$$\leq \mathbb{E}_j \left[\mathbb{E}_k [(C_{11} \eta^l)^2] \right] \max_j \left\{ \left\| \mathbf{H}_1^{-1}(\mathcal{T}^j; \mathcal{S}^{l,0}) \right\|_F^2 \right\} = C_{11}^2 \max_j \left\{ \left\| \mathbf{H}_1^{-1}(\mathcal{T}^j; \mathcal{S}^{l,0}) \right\|_F^2 \right\} (\eta^l)^2, \tag{75}$$

where from Equation (74) to Equation (75), we use Lemma 8, from Equation (70) to Equation (71), we replace $\mathbf{G}_1(\mathcal{T}^j; \mathcal{S}^{l,0})$ with the expected gradient over the batch, from Equation (73) to Equation (74), we use Jensen's inequality (square function being a convex function).

To this end, we achieve Equation (69) using the above bound,

$$\begin{aligned}
& \mathbb{E} \left[\left\| \left(\mathbf{G}_1(\mathcal{T}^j; \mathcal{S}^{l,0}) - \frac{b}{N} \mathbf{G}_1(\mathcal{T}; \mathcal{S}^{l,0}) \right) \mathbf{H}_1^{-1}(\mathcal{T}^j; \mathcal{S}^{l,0}) \right\|_F \right] \\
&= \mathbb{E} \left[\sqrt{\left\| \left(\mathbf{G}_1(\mathcal{T}^j; \mathcal{S}^{l,0}) - \frac{b}{N} \mathbf{G}_1(\mathcal{T}; \mathcal{S}^{l,0}) \right) \mathbf{H}_1^{-1}(\mathcal{T}^j; \mathcal{S}^{l,0}) \right\|_F^2} \right] \\
&\leq \sqrt{\mathbb{E} \left[\left\| \left(\mathbf{G}_1(\mathcal{T}^j; \mathcal{S}^{l,0}) - \frac{b}{N} \mathbf{G}_1(\mathcal{T}; \mathcal{S}^{l,0}) \right) \mathbf{H}_1^{-1}(\mathcal{T}^j; \mathcal{S}^{l,0}) \right\|_F^2 \right]} \\
&\leq C_{11} \sqrt{\max_j \left\{ \left\| \mathbf{H}_1^{-1}(\mathcal{T}^j; \mathcal{S}^{l,0}) \right\|_F^2 \right\}} \eta^l.
\end{aligned}$$

The above inequality holds due to the Jensen's inequality (square root being a concave function). The lemma completes with

$$C_{13} = C_{11} \sqrt{\max_j \left\{ \left\| \mathbf{H}_1^{-1}(\mathcal{T}^j; \mathcal{S}^{l,0}) \right\|_F^2 \right\}}.$$

□

Lemma 10 (Lemma A.5 in (Mairal, 2013)). *Let $(a^l)_{l \geq 1}$ and $(b^l)_{l \geq 1}$ be two non-negative real sequences such that the series $\sum_{l=1}^{\infty} a^l$ diverges, the series $\sum_{l=1}^{\infty} a^l b^l$ converges, and there exists $K > 0$ such that $|b^{l+1} - b^l| \leq K a^l$. Then, the sequence $(b^l)_{l \geq 1}$ converges to 0.*

F.4 Proof of the Main Theorem

We now prove the convergence of \mathbf{A} in the main theorem, and similar derivations can be applied to \mathbf{B}, \mathbf{C} . We let $a^l = \eta^l$ and $b^l = \mathbb{E} [\|\mathbf{G}_1(\mathcal{T}; \mathcal{S}^{l,0})\|_F^2]$, which is the short-hand quantity of gradient defined in Definition 2.

Proof of the first condition. First, we know that the harmonic sequence $\{\frac{1}{l}\}_{l \geq 1}$ diverges, which satisfies the first condition,

$$\sum_{l=1}^{\infty} a^l \geq C_{min} \sum_{l=1}^{\infty} \frac{1}{l} \rightarrow \infty. \quad (76)$$

Proof of the second condition. Second, we prove that $\sum_{l=1}^{\infty} a^l b^l$ converges. According to the main paper, the update rule of \mathbf{A} follows,

$$\mathbf{A}^{l+1} = \eta^l \mathbf{A}^l + (1 - \eta^l) \mathbf{A}^*,$$

where \mathbf{A}^* is the closed-form solution of the least square problem. In fact, our update is one Newton step with learning rate η^l , where the original form is,

$$\mathbf{A}^{l+1} = \mathbf{A}^l - \eta^l \mathbf{G}_1(\mathcal{T}^l; \mathcal{S}^{l,0}) \mathbf{H}_1^{-1}(\mathcal{T}^l; \mathcal{S}^{l,0}), \quad (77)$$

and \mathbf{A}^* happens to be,

$$\mathbf{A}^* = \mathbf{A}^l - \mathbf{G}_1(\mathcal{T}^l; \mathcal{S}^{l,0}) \mathbf{H}_1^{-1}(\mathcal{T}^l; \mathcal{S}^{l,0}).$$

Taylor Expansion. We have for any quadratic function f ,

$$f(\mathbf{x}_1, \dots, \mathbf{x}_k + \Delta \mathbf{x}_k, \dots, \mathbf{x}_n) = f(\mathbf{x}_1, \dots, \mathbf{x}_k, \dots, \mathbf{x}_n) + \Delta \mathbf{x}_k^T \nabla_{\mathbf{x}_k} f + \frac{1}{2} \Delta \mathbf{x}_k^T \mathbf{H}_f(\mathbf{x}_k) \Delta \mathbf{x}_k,$$

where $\nabla_{\mathbf{x}_k} f$ is the gradient vector and $\mathbf{H}_f(\mathbf{x}_k)$ is the Hessian matrix.

Using the above Taylor expansion and using the matrix form we get,

$$\begin{aligned}
& \mathcal{L}(\mathcal{T}, \tilde{\mathcal{T}}; \mathcal{S}^{l,1}) - \mathcal{L}(\mathcal{T}, \tilde{\mathcal{T}}; \mathcal{S}^{l,0}) \\
&= -\eta^l \text{Tr} \left(\mathbf{G}_1(\mathcal{T}^l; \mathcal{S}^{l,0}) \mathbf{H}_1^{-1}(\mathcal{T}^l; \mathcal{S}^{l,0}) \mathbf{G}_1^{\top}(\mathcal{T}; \mathcal{S}^{l,0}) \right) \\
&\quad + \frac{(\eta^l)^2}{2} \text{Tr} \left(\mathbf{G}_1(\mathcal{T}^l; \mathcal{S}^{l,0}) \mathbf{H}_1^{-1}(\mathcal{T}^l; \mathcal{S}^{l,0}) \mathbf{H}_1(\mathcal{T}; \mathcal{S}^{l,0}) \mathbf{H}_1^{-1}(\mathcal{T}^l; \mathcal{S}^{l,0}) \mathbf{G}_1^{\top}(\mathcal{T}^l; \mathcal{S}^{l,0}) \right). \quad (78)
\end{aligned}$$

Follow the Definition 2, we sum these three results and get Equation (78).

By re-arranging the terms in Equation (78), we have

$$\begin{aligned}
& \eta^l \text{Tr} \left(\frac{b}{N} \mathbf{G}_1(\mathcal{T}; \mathcal{S}^{l,0}) \mathbf{H}_1^{-1}(\mathcal{T}^l; \mathcal{S}^{l,0}) \mathbf{G}_1^\top(\mathcal{T}; \mathcal{S}^{l,0}) \right) \\
&= -\eta^l \text{Tr} \left(\mathbf{G}_1(\mathcal{T}; \mathcal{S}^{l,0}) \mathbf{H}_1^{-1}(\mathcal{T}^l; \mathcal{S}^{l,0}) \left(\mathbf{G}_1^\top(\mathcal{T}^l; \mathcal{S}^{l,0}) - \frac{b}{N} \mathbf{G}_1^\top(\mathcal{T}; \mathcal{S}^{l,0}) \right) \right) \\
&+ \mathcal{L}(\mathcal{T}, \tilde{\mathcal{T}}; \mathcal{S}^{l,0}) - \mathcal{L}(\mathcal{T}, \tilde{\mathcal{T}}; \mathcal{S}^{l,1}) \\
&+ \frac{(\eta^l)^2}{2} \text{Tr} \left(\mathbf{G}_1(\mathcal{T}^l; \mathcal{S}^{l,0}) \mathbf{H}_1^{-1}(\mathcal{T}^l; \mathcal{S}^{l,0}) \mathbf{H}_1(\mathcal{T}; \mathcal{S}^{l,0}) \mathbf{H}_1^{-1}(\mathcal{T}^l; \mathcal{S}^{l,0}) \mathbf{G}_1^\top(\mathcal{T}^l; \mathcal{S}^{l,0}) \right). \quad (79)
\end{aligned}$$

F-Norm Inequality. For now, let us consider the following problem: given a symmetric positive-definite matrix, $\Sigma \in \mathbb{R}^{d \times d}$, its inverse is also symmetric positive-definite. Suppose $\Sigma^{-1} \succ a > 0$, given any non-zero matrix $\mathbf{Y} \in \mathbb{R}^{s \times d}$, we have the following trace inequality,

$$\text{Tr}(\mathbf{Y}(\Sigma^{-1} - a)\mathbf{Y}^\top) > 0 \quad \Rightarrow \quad \text{Tr}(\mathbf{Y}\Sigma^{-1}\mathbf{Y}^\top) > a\|\mathbf{Y}\|_F^2. \quad (80)$$

We use the result of this F-norm Inequality. By Definition 2, $\mathbf{H}_1(\mathcal{T}^l; \mathcal{S}^{l,0})$ is a positive-definite matrix. We let

$$\begin{aligned}
\Sigma &= \mathbf{H}_1(\mathcal{T}^l; \mathcal{S}^{l,0}) \\
Y &= \mathbf{G}_1(\mathcal{T}; \mathcal{S}^{l,0})
\end{aligned}$$

Then, we have, with some constant $C_{14} > 0$,

$$\eta^l \text{Tr} \left(\frac{b}{N} \mathbf{G}_1(\mathcal{T}; \mathcal{S}^{l,0}) \mathbf{H}_1^{-1}(\mathcal{T}^l; \mathcal{S}^{l,0}) \mathbf{G}_1^\top(\mathcal{T}; \mathcal{S}^{l,0}) \right) > \frac{1}{C_{14}} \eta^l \|\mathbf{G}_1(\mathcal{T}; \mathcal{S}^{l,0})\|_F^2.$$

The LHS can be replaced by using the results in Equation (79), and the expectation of the RHS is $a^l b^l$ scaled by a constant. We thus take the expectation on both side for the above inequality and let

$$\begin{aligned}
Q_1^l &= \mathbb{E} \left[-\eta^l \text{Tr} \left(\mathbf{G}_1(\mathcal{T}; \mathcal{S}^{l,0}) \mathbf{H}_1^{-1}(\mathcal{T}^l; \mathcal{S}^{l,0}) \left(\mathbf{G}_1^\top(\mathcal{T}^l; \mathcal{S}^{l,0}) - \frac{b}{N} \mathbf{G}_1^\top(\mathcal{T}; \mathcal{S}^{l,0}) \right) \right) \right], \\
Q_2^l &= \mathbb{E} \left[\mathcal{L}(\mathcal{T}, \tilde{\mathcal{T}}; \mathcal{S}^{l,0}) - \mathcal{L}(\mathcal{T}, \tilde{\mathcal{T}}; \mathcal{S}^{l,1}) \right], \\
Q_3^l &= \mathbb{E} \left[\frac{(\eta^l)^2}{2} \text{Tr} \left(\mathbf{G}_1(\mathcal{T}^l; \mathcal{S}^{l,0}) \mathbf{H}_1^{-1}(\mathcal{T}^l; \mathcal{S}^{l,0}) \mathbf{H}_1(\mathcal{T}; \mathcal{S}^{l,0}) \mathbf{H}_1^{-1}(\mathcal{T}^l; \mathcal{S}^{l,0}) \mathbf{G}_1^\top(\mathcal{T}^l; \mathcal{S}^{l,0}) \right) \right].
\end{aligned}$$

Since $a^l b^l = \mathbb{E} \left[\eta^l \|\mathbf{G}_1(\mathcal{T}; \mathcal{S}^{l,0})\|_F^2 \right]$, if we can bound $\sum_{l=1}^{\infty} Q_1^l$, $\sum_{l=1}^{\infty} Q_2^l$, $\sum_{l=1}^{\infty} Q_3^l$, then, the second condition will be satisfied: $\sum_{l=1}^{\infty} a^l b^l$ converges. Now, let us show how to bound three summation terms.

For $\sum_{l=1}^{\infty} Q_1^l$, we have,

$$\begin{aligned}
\sum_{l=1}^{\infty} Q_1^l &= \sum_{l=1}^{\infty} \mathbb{E} \left[-\eta^l \text{Tr} \left(\mathbf{G}_1(\mathcal{T}; \mathcal{S}^{l,0}) \mathbf{H}_1^{-1}(\mathcal{T}^l; \mathcal{S}^{l,0}) \left(\mathbf{G}_1^\top(\mathcal{T}^l; \mathcal{S}^{l,0}) - \frac{b}{N} \mathbf{G}_1^\top(\mathcal{T}; \mathcal{S}^{l,0}) \right) \right) \right] \\
&\leq \sum_{l=1}^{\infty} \eta^l \mathbb{E} \left[\left\| \mathbf{G}_1(\mathcal{T}; \mathcal{S}^{l,0}) \right\|_F \left\| \mathbf{H}_1^{-1}(\mathcal{T}^l; \mathcal{S}^{l,0}) \left(\mathbf{G}_1^\top(\mathcal{T}^l; \mathcal{S}^{l,0}) - \frac{b}{N} \mathbf{G}_1^\top(\mathcal{T}; \mathcal{S}^{l,0}) \right) \right\|_F \right] \\
&\leq \sum_{l=1}^{\infty} \eta^l \max_l \{ \left\| \mathbf{G}_1(\mathcal{T}; \mathcal{S}^{l,0}) \right\|_F \} \mathbb{E} \left[\left\| \mathbf{H}_1^{-1}(\mathcal{T}^l; \mathcal{S}^{l,0}) \left(\mathbf{G}_1^\top(\mathcal{T}^l; \mathcal{S}^{l,0}) - \frac{b}{N} \mathbf{G}_1^\top(\mathcal{T}; \mathcal{S}^{l,0}) \right) \right\|_F \right] \quad (81)
\end{aligned}$$

$$\leq \sum_{l=1}^{\infty} C_{13} (\eta^l)^2 \max_l \{ \left\| \mathbf{G}_1(\mathcal{T}; \mathcal{S}^{l,0}) \right\|_F \} < \infty, \quad (82)$$

where from Equation (81) to Equation (82), we use the results from Lemma 9.

For $\sum_{l=1}^{\infty} Q_2^l$, we have,

$$\begin{aligned}
\sum_{l=1}^{\infty} Q_2^l &= \sum_{l=1}^{\infty} \mathbb{E} \left[\mathcal{L}(\mathcal{T}, \tilde{\mathcal{T}}; \mathcal{S}^{l,0}) - \mathcal{L}(\mathcal{T}, \tilde{\mathcal{T}}; \mathcal{S}^{l,1}) \right] \\
&= \mathcal{L}(\mathcal{T}, \tilde{\mathcal{T}}; \mathcal{S}^{l,0}) + \sum_{l=1}^{\infty} \mathbb{E} \left[\mathcal{L}(\mathcal{T}, \tilde{\mathcal{T}}; \mathcal{S}^{l+1,0}) - \mathcal{L}(\mathcal{T}, \tilde{\mathcal{T}}; \mathcal{S}^{l,1}) \right] \\
&= \mathcal{L}(\mathcal{T}, \tilde{\mathcal{T}}; \mathcal{S}^{l,0}) + \sum_{l=1}^{\infty} \mathbb{E} \left[\mathcal{L}(\mathcal{T}, \tilde{\mathcal{T}}; \mathcal{S}^{l+1,0}) - \mathcal{L}(\mathcal{T}, \tilde{\mathcal{T}}; \mathcal{S}^{l,2}) + \mathcal{L}(\mathcal{T}, \tilde{\mathcal{T}}; \mathcal{S}^{l,2}) - \mathcal{L}(\mathcal{T}, \tilde{\mathcal{T}}; \mathcal{S}^{l,1}) \right] \tag{83}
\end{aligned}$$

$$\leq \mathcal{L}(\mathcal{T}, \tilde{\mathcal{T}}; \mathcal{S}^{l,0}) + \sum_{l=1}^{\infty} \mathbb{E} \left[\mathcal{L}(\mathcal{T}, \tilde{\mathcal{T}}; \mathcal{S}^{l,3}) - \mathcal{L}(\mathcal{T}, \tilde{\mathcal{T}}; \mathcal{S}^{l,2}) + \mathcal{L}(\mathcal{T}, \tilde{\mathcal{T}}; \mathcal{S}^{l,2}) - \mathcal{L}(\mathcal{T}, \tilde{\mathcal{T}}; \mathcal{S}^{l,1}) \right] \tag{84}$$

$$= \mathcal{L}(\mathcal{T}, \tilde{\mathcal{T}}; \mathcal{S}^{l,0}) + \sum_{l=1}^{\infty} \mathbb{E} \left[\mathcal{L}(\mathcal{T}, \tilde{\mathcal{T}}; \mathcal{S}^{l,3}) - \mathcal{L}(\mathcal{T}, \tilde{\mathcal{T}}; \mathcal{S}^{l,2}) \right] + \sum_{l=1}^{\infty} \mathbb{E} \left[\mathcal{L}(\mathcal{T}, \tilde{\mathcal{T}}; \mathcal{S}^{l,2}) - \mathcal{L}(\mathcal{T}, \tilde{\mathcal{T}}; \mathcal{S}^{l,1}) \right] \tag{85}$$

$$\leq \mathcal{L}(\mathcal{T}, \tilde{\mathcal{T}}; \mathcal{S}^{l,0}) + 2M_9. \tag{86}$$

From Equation (83) to Equation (84), $\mathcal{S}^{l+1,0} = \mathcal{S}^{l,3} = \{\mathbf{A}^{l+1}, \mathbf{B}^{l+1}, \mathbf{C}^{l+1}\}$, however, the loss $\mathcal{L}(\mathcal{T}, \tilde{\mathcal{T}}; \mathcal{S}^{l+1,0})$ is calculated based on the updated coefficient matrices $\{\mathbf{X}^{l+2}, \tilde{\mathbf{X}}^{l+2}\}$, which is optimized w.r.t. $\{\mathbf{A}^{l+1}, \mathbf{B}^{l+1}, \mathbf{C}^{l+1}\}$, while $\mathcal{L}(\mathcal{T}, \tilde{\mathcal{T}}; \mathcal{S}^{l,3})$ uses old coefficient set $\{\mathbf{X}^{l+1}, \tilde{\mathbf{X}}^{l+1}\}$. Thus,

$$\mathbb{E} \left[\mathcal{L}(\mathcal{T}, \tilde{\mathcal{T}}; \mathcal{S}^{l+1,0}) \right] < \mathbb{E} \left[\mathcal{L}(\mathcal{T}, \tilde{\mathcal{T}}; \mathcal{S}^{l,3}) \right].$$

From Equation (85) to Equation (86), we show that,

$$\begin{aligned}
&\mathbb{E} \left[\mathcal{L}(\mathcal{T}, \tilde{\mathcal{T}}; \mathcal{S}^{l,3}) - \mathcal{L}(\mathcal{T}, \tilde{\mathcal{T}}; \mathcal{S}^{l,2}) \right] \\
&= -\eta^l \mathbb{E} \left[\text{Tr} \left(\mathbf{G}_3(\mathcal{T}^l; \mathcal{S}^{l,2}) \mathbf{H}_3^{-1}(\mathcal{T}^l; \mathcal{S}^{l,2}) \mathbf{G}_3^\top(\mathcal{T}; \mathcal{S}^{l,2}) \right) \right] \tag{87}
\end{aligned}$$

$$+ \frac{(\eta^l)^2}{2} \mathbb{E} \left[\text{Tr} \left(\mathbf{G}_3(\mathcal{T}^l; \mathcal{S}^{l,2}) \mathbf{H}_3^{-1}(\mathcal{T}^l; \mathcal{S}^{l,2}) \mathbf{H}_3(\mathcal{T}; \mathcal{S}^{l,2}) \mathbf{H}_3^{-1}(\mathcal{T}^l; \mathcal{S}^{l,2}) \mathbf{G}_3^\top(\mathcal{T}^l; \mathcal{S}^{l,2}) \right) \right] \tag{88}$$

$$= -\eta^l \mathbb{E} \left[\text{Tr} \left(\left(\mathbf{G}_3(\mathcal{T}^l; \mathcal{S}^{l,2}) - \frac{b}{N} \mathbf{G}_3(\mathcal{T}; \mathcal{S}^{l,2}) \right) \mathbf{H}_3^{-1}(\mathcal{T}^l; \mathcal{S}^{l,2}) \mathbf{G}_3^\top(\mathcal{T}; \mathcal{S}^{l,2}) \right) \right] \tag{89}$$

$$- \eta^l \frac{b}{N} \mathbb{E} \left[\text{Tr} \left(\mathbf{G}_3(\mathcal{T}; \mathcal{S}^{l,2}) \mathbf{H}_3^{-1}(\mathcal{T}^l; \mathcal{S}^{l,2}) \mathbf{G}_3^\top(\mathcal{T}; \mathcal{S}^{l,2}) \right) \right] \tag{90}$$

$$+ \frac{(\eta^l)^2}{2} \mathbb{E} \left[\text{Tr} \left(\mathbf{G}_3(\mathcal{T}^l; \mathcal{S}^{l,2}) \mathbf{H}_3^{-1}(\mathcal{T}^l; \mathcal{S}^{l,2}) \mathbf{H}_3(\mathcal{T}; \mathcal{S}^{l,2}) \mathbf{H}_3^{-1}(\mathcal{T}^l; \mathcal{S}^{l,2}) \mathbf{G}_3^\top(\mathcal{T}^l; \mathcal{S}^{l,2}) \right) \right]$$

$$\leq C_{13}(\eta^l)^2 \max_l \{ \|\mathbf{G}_3(\mathcal{T}; \mathcal{S}^{l,2})\|_F \} \tag{91}$$

$$+ \frac{(\eta^l)^2}{2} \max_l \{ \text{Tr} \left(\mathbf{G}_3(\mathcal{T}^l; \mathcal{S}^{l,2}) \mathbf{H}_3^{-1}(\mathcal{T}^l; \mathcal{S}^{l,2}) \mathbf{H}_3(\mathcal{T}; \mathcal{S}^{l,2}) \mathbf{H}_3^{-1}(\mathcal{T}^l; \mathcal{S}^{l,2}) \mathbf{G}_3^\top(\mathcal{T}^l; \mathcal{S}^{l,2}) \right) \}.$$

From Equation (87) to Equation (89)(90), we add and subtract one term. From Equation (89) to Equation (91), we apply Lemma (9). For Equation (90), since the term is always negative (refer to Equation (80)), we directly throw it away. Similar analysis can be applied for $\sum_{l=1}^{\infty} \mathbb{E} \left[\mathcal{L}(\mathcal{T}, \tilde{\mathcal{T}}; \mathcal{S}^{l,2}) - \mathcal{L}(\mathcal{T}, \tilde{\mathcal{T}}; \mathcal{S}^{l,1}) \right]$, so we have with some constant, $M_9 > 0$,

$$\begin{aligned}
\sum_{l=1}^{\infty} \mathbb{E} \left[\mathcal{L}(\mathcal{T}, \tilde{\mathcal{T}}; \mathcal{S}^{l,3}) - \mathcal{L}(\mathcal{T}, \tilde{\mathcal{T}}; \mathcal{S}^{l,2}) \right] &\leq M_9, \\
\sum_{l=1}^{\infty} \mathbb{E} \left[\mathcal{L}(\mathcal{T}, \tilde{\mathcal{T}}; \mathcal{S}^{l,2}) - \mathcal{L}(\mathcal{T}, \tilde{\mathcal{T}}; \mathcal{S}^{l,1}) \right] &\leq M_9.
\end{aligned}$$

For $\sum_{l=1}^{\infty} Q_3^l$, we have

$$\begin{aligned} \sum_{l=1}^{\infty} Q_3^l &= \sum_{l=1}^{\infty} \mathbb{E} \left[\frac{(\eta^l)^2}{2} \text{Tr} (\mathbf{G}_1(\mathcal{T}^l; \mathcal{S}^{l,0}) \mathbf{H}_1^{-1}(\mathcal{T}^l; \mathcal{S}^{l,0}) \mathbf{H}_1(\mathcal{T}; \mathcal{S}^{l,0}) \mathbf{H}_1^{-1}(\mathcal{T}^l; \mathcal{S}^{l,0}) \mathbf{G}_1^{\top}(\mathcal{T}^l; \mathcal{S}^{l,0})) \right] \\ &\leq \sum_{l=1}^{\infty} \frac{(\eta^l)^2}{2} \max \{ \|\mathbf{G}_1(\mathcal{T}^l; \mathcal{S}^{l,0}) \mathbf{H}_1^{-1}(\mathcal{T}^l; \mathcal{S}^{l,0}) \mathbf{H}_1(\mathcal{T}; \mathcal{S}^{l,0}) \mathbf{H}_1^{-1}(\mathcal{T}^l; \mathcal{S}^{l,0}) \mathbf{G}_1^{\top}(\mathcal{T}^l; \mathcal{S}^{l,0})\|_F \} < \infty. \end{aligned}$$

Proof of the third condition. Third, we prove that $|b^{l+1} - b^l|$ is bounded by a^l ,

$$\begin{aligned} &|\mathbb{E} [\|\mathbf{G}_1(\mathcal{T}; \mathcal{S}^{l+1,0})\|_F^2] - \mathbb{E} [\|\mathbf{G}_1(\mathcal{T}; \mathcal{S}^{l,0})\|_F^2]| \\ &= |\mathbb{E} [\|\mathbf{G}_1(\mathcal{T}; \mathcal{S}^{l+1,0})\|_F^2 - \|\mathbf{G}_1(\mathcal{T}; \mathcal{S}^{l,0})\|_F^2]| \\ &= \mathbb{E} [\text{Tr} (\mathbf{G}_1(\mathcal{T}; \mathcal{S}^{l+1,0})^{\top} \mathbf{G}_1(\mathcal{T}; \mathcal{S}^{l+1,0}) - \mathbf{G}_1(\mathcal{T}; \mathcal{S}^{l,0})^{\top} \mathbf{G}_1(\mathcal{T}; \mathcal{S}^{l,0}))] \\ &= \mathbb{E} [\text{Tr} (\mathbf{G}_1(\mathcal{T}; \mathcal{S}^{l+1,0}) + \mathbf{G}_1(\mathcal{T}; \mathcal{S}^{l,0}))^{\top} (\mathbf{G}_1(\mathcal{T}; \mathcal{S}^{l+1,0}) - \mathbf{G}_1(\mathcal{T}; \mathcal{S}^{l,0}))] \\ &\leq 2 \max_l \{ \|\mathbf{G}_1(\mathcal{T}; \mathcal{S}^{l,0})\|_F \} \mathbb{E} [\|\mathbf{G}_1(\mathcal{T}; \mathcal{S}^{l+1,0}) - \mathbf{G}_1(\mathcal{T}; \mathcal{S}^{l,0})\|_F] \quad (92) \end{aligned}$$

$$\leq 2 \max_l \{ \|\mathbf{G}_1(\mathcal{T}; \mathcal{S}^{l,0})\|_F \} C_7 \mathbb{E} [\|\mathbf{A}^{l+1} - \mathbf{A}^l, \mathbf{B}^{l+1} - \mathbf{B}^l, \mathbf{C}^{l+1} - \mathbf{C}^l\|_F], \quad (93)$$

where from Equation (92) to Equation (93), we use Lemma 7.

Finally, by the (Newton step based) update rule of the factors in Equation (77), we have that

$$\begin{aligned} \mathbf{A}^{l+1} - \mathbf{A}^l &= -\eta^l \mathbf{G}_1 \mathcal{L}(\mathcal{T}; \mathcal{S}^{l,0}) \mathbf{H}_1^{-1}(\mathcal{T}; \mathcal{S}^{l,0}), \\ \mathbf{B}^{l+1} - \mathbf{B}^l &= -\eta^l \mathbf{G}_2 \mathcal{L}(\mathcal{T}; \mathcal{S}^{l,1}) \mathbf{H}_2^{-1}(\mathcal{T}; \mathcal{S}^{l,1}), \\ \mathbf{C}^{l+1} - \mathbf{C}^l &= -\eta^l \mathbf{G}_3 \mathcal{L}(\mathcal{T}; \mathcal{S}^{l,2}) \mathbf{H}_3^{-1}(\mathcal{T}; \mathcal{S}^{l,2}). \end{aligned}$$

We plug the results into Equation (93), we can find,

$$K = 2\sqrt{3}C_7 \max_l \{ \|\mathbf{G}_1(\mathcal{T}; \mathcal{S}^{l,0})\|_F \} \max_{i \in [0,1,2], l} \{ \|\mathbf{G}_i \mathcal{L}(\mathcal{T}; \mathcal{S}^{l,i}) \mathbf{H}_i^{-1}(\mathcal{T}; \mathcal{S}^{l,i})\|_F \},$$

such that,

$$|b^{l+1} - b^l| = |\mathbb{E} [\|\mathbf{G}_1(\mathcal{T}; \mathcal{S}^{l+1,0})\|_F^2] - \mathbb{E} [\|\mathbf{G}_1(\mathcal{T}; \mathcal{S}^{l,0})\|_F^2]| \leq K\eta^l = Ka^l. \quad (94)$$

To this end, we prove that three conditions of Lemma 10 are satisfied. We complete the proof of the main convergence theorem.